

Photobiocatalytic Strategies for Organic Synthesis

Megan A. Emmanuel, Sophie G. Bender, Catherine Bilodeau, Jose M. Carceller, Jacob S. DeHovitz, Haigen Fu, Yi Liu, Bryce T. Nicholls, Yao Ouyang, Claire G. Page, Tianzhang Qiao, Felix C. Raps, Damien R. Sorigué, Shang-Zheng Sun, Joshua Turek-Herman, Yuxuan Ye, Ariadna Rivas-Souchet, Jingzhe Cao, and Todd K. Hyster*



Cite This: *Chem. Rev.* 2023, 123, 5459–5520



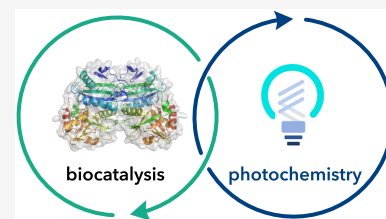
Read Online

ACCESS |

Metrics & More

Article Recommendations

ABSTRACT: Biocatalysis has revolutionized chemical synthesis, providing sustainable methods for preparing various organic molecules. In enzyme-mediated organic synthesis, most reactions involve molecules operating from their ground states. Over the past 25 years, there has been an increased interest in enzymatic processes that utilize electronically excited states accessed through photoexcitation. These photobiocatalytic processes involve a diverse array of reaction mechanisms that are complementary to one another. This comprehensive review will describe the state-of-the-art strategies in photobiocatalysis for organic synthesis until December 2022. Apart from reviewing the relevant literature, a central goal of this review is to delineate the mechanistic differences between the general strategies employed in the field. We will organize this review based on the relationship between the photochemical step and the enzymatic transformations. The review will include mechanistic studies, substrate scopes, and protein optimization strategies. By clearly defining mechanistically-distinct strategies in photobiocatalytic chemistry, we hope to illuminate future synthetic opportunities in the area.



CONTENTS

1. Introduction	5460	3.1. Synergistic Reactions Involving Native Reactivity	5488
2. Photoenzymatic Catalysis	5460	3.1.1. Cytochromes P450	5488
2.1. Fatty Acid Photodecarboxylase	5461	3.1.2. Rieske-type Non-heme Iron Enzymes	5490
2.1.1. Reaction Mechanism and Substrate Scope	5461	3.2. Synergistic Reactions Involving Non-natural Reactivity	5490
2.1.2. Reaction Condition Engineering	5462	3.2.1. Nicotinamide-Dependent Enzymes	5490
2.1.3. Synthetic Applications of Wild-Type FAP	5464	3.2.2. Flavin-Dependent Enzymes	5490
2.1.4. Synthetic Applications with Engineered FAP Variants	5467	4. Tandem Photocatalyst/Enzyme Reactions	5493
2.1.5. Outlook	5470	4.1. Light-Driven Cofactor Regeneration	5493
2.2. Nicotinamide-Dependent Ketoreductase Photochemistry	5470	4.1.1. "Ene"-Reductases	5493
2.3. Flavin-Dependent "Ene"-Reductase Photochemistry	5471	4.1.2. Baeyer–Villiger Monooxygenases	5495
2.4. Flavin-Dependent Baeyer–Villiger Monooxygenase Photochemistry	5482	4.1.3. FAD-Dependent Halogenases	5496
2.5. Flavin-Dependent Photoenzymes for Radical Polymerization	5483	4.1.4. Ketoreductases	5496
2.5.1. Outlook for Flavin-Dependent Photoenzymes	5483	4.1.5. Cytochromes P450	5498
2.6. Photoenzymes Using Non-natural Cofactors and Amino Acids	5484	4.1.6. Peroxygenases	5500
2.6.1. Outlook for Photoenzymes with Non-natural Cofactors	5487	4.2. Synthetic Photochemical/Enzyme Cascades	5502
3. Synergistic Photoenzymatic Catalysis	5488	4.2.1. One-Pot/One-Step Cascades	5502
		4.2.2. One-Pot/Two-Step Photobiocatalytic Cascades	5506
		4.2.3. Outlook	5507

Special Issue: Bridging the Gaps: Learning from Catalysis across Boundaries

Received: November 2, 2022

Published: April 28, 2023



5. Enzymatic Reactions Coupled to Natural Photosynthesis	5507
5.1. Biocatalysts Native to Cyanobacteria	5507
5.2. Heterologously Expressed Biocatalysts in Cyanobacteria	5508
5.3. Transmembrane Shuttling	5509
6. Conclusion	5511
Author Information	5511
Corresponding Author	5511
Authors	5511
Author Contributions	5512
Notes	5512
Biographies	5512
Acknowledgments	5513
References	5513

1. INTRODUCTION

Enzymes are attractive catalysts for chemical synthesis because they carry out transformations with unparalleled catalytic efficiencies and reaction selectivity.^{1–3} The advent of sophisticated techniques for generating mutant libraries and advances in analytical chemistry has accelerated protein engineering to the point where biocatalysts are now considered competitive alternatives to traditional small molecule catalysts,^{4,5} leading to their increased use in the chemical manufacturing of pharmaceuticals.^{6–10} An ongoing goal in the field has been to identify new activation modes that would enable enzymes to catalyze new types of reactions.^{11,12} As the *in-silico* design of enzymes remains challenging,^{13,14} new biocatalytic reactions are typically developed by mining natural product pathways to discover enzymes that catalyze new types of transformations. Researchers often focus on the reactivity available to proteins in their ground state when searching for new enzyme functions. However, recent advances in small-molecule catalysis suggest that new functions can be unlocked by looking at the electronically excited states of catalysts.

Over the past 15 years, visible light photocatalysis has reemerged as a powerful platform in chemical synthesis.^{15,16} In these reactions, a photocatalyst, typically an organic dye or transition metal complex, is photoexcited to access an electronically excited state which can engage in electron or energy-transfer events to form radical intermediates. This activation mode has enabled countless synthetic reactions. Moreover, merging photocatalysis with transition metal catalysis or organocatalysis allows for reactions that are inaccessible to either catalyst individually.^{17,18} These reports have spurred interest in using light with enzymes. Nature uses light in many different contexts. In photosynthesis, large multiprotein complexes convert photonic energy to chemical energy to sustain life. Alternatively, light–oxygen–voltage (LOV) domains use light to induce conformation changes to regulate proteins and enzymes. Interestingly, only three enzymes are known in Nature to absorb sunlight to promote a chemical reaction: DNA photolyase,¹⁹ fatty acid photodecarboxylase,²⁰ and protochlorophyllide reductase.²¹ While this activation mode is rare, these enzymes showcase how enzymes use light to facilitate biologically-essential transformations.

The burgeoning area of photobiocatalysis is focused on developing new biocatalytic reactions that involve light.^{22–25} This review will organize reports based on the relationship between the photochemical step and enzymatic transforma-

tion. We will define key concepts and focus on mechanistic nuances that make strategies distinct from one another. By clearly defining the mechanistic differences between various approaches, we hope to contribute to understanding how light can be used in biocatalytic synthesis.

The first section will focus on photoenzymatic catalysis. We define photoenzymatic catalysis as reactions where a cofactor within the protein active site is photoexcited to promote electron or energy transfer required to convert starting material to product (Figure 1A). This topic will focus on enzymes of value for synthetic organic chemistry. The second section will explore synergistic photoenzymatic catalysis (Figure 1B). These reactions involve the excitation of an exogenous cofactor to enable a chemical transformation within a protein active site. The third section will focus on tandem photocatalyst/enzyme reactions (Figure 1C). In these transformations, the photochemical reaction occurs in the presence of the enzyme but is not involved in the enzyme's mechanism for converting starting material to product. This section will contain two subsections: (i) reactions where light is used for cofactor regeneration and (ii) reactions where photoexcitation is involved in modifying the substrate of the enzyme. The final section will discuss enzymatic reactions coupled to natural photosynthesis. These systems use cyanobacteria to produce NADPH that enzymes can consume to reduce substrates (Figure 1D). In clearly defining these terms, we hope to provide precise language for discussing photobiocatalysis and can help researchers understand the current limits of the technology to drive new areas.

2. PHOTOENZYMATIC CATALYSIS

Photoenzymatic processes are reactions where a cofactor or amino acid side chain within an enzyme absorbs light and uses the photonic energy to convert starting material to product.²⁶ While this general mechanism is ubiquitous in small molecule photoredox catalysis,^{27,28} photoenzymes are relatively rare, with only three currently known in Nature. The oldest photoenzyme is DNA photolyase, a flavin-dependent enzyme responsible for repairing pyrimidine cyclobutane dimers in DNA.¹⁹ These dimeric lesions are formed when DNA is irradiated with UV light. In this enzyme, the reduced flavin adenine dinucleotide (FAD) cofactor (FAD_{hq}[−]) serves as the photocatalyst, initially reducing the pyrimidine dimer to initiate a retro [2 + 2] reaction followed by oxidation of the resulting radical anion by FAD semiquinone (FAD_{sq}).^{29,30} Many homologues of this enzyme have additional deazaflavin or pterin cofactors to expand the wavelengths of light that can promote this reactivity. Another well-studied natural photoenzyme is light-dependent protochlorophyllide reductase (LPOR), a nicotinamide adenine dinucleotide phosphate (NADPH)-dependent enzyme responsible for reducing protochlorophyllide (PChlide) to chlorophyllide.^{31,32} Among natural photoenzymes, LPOR remains unique because the reduction occurs via photoexcitation of the PChlide substrate rather than the NADPH cofactor. This excited state can oxidize NADPH via single-electron transfer to form NADPH^{•+} and PChlide radical anion. Proton transfer from a conserved tyrosine and hydrogen atom abstraction from NADPH^{•+} produces the product. As these enzymes hold little value to synthetic chemists and have been recently reviewed, we will not elaborate on their function or mechanism in this review.

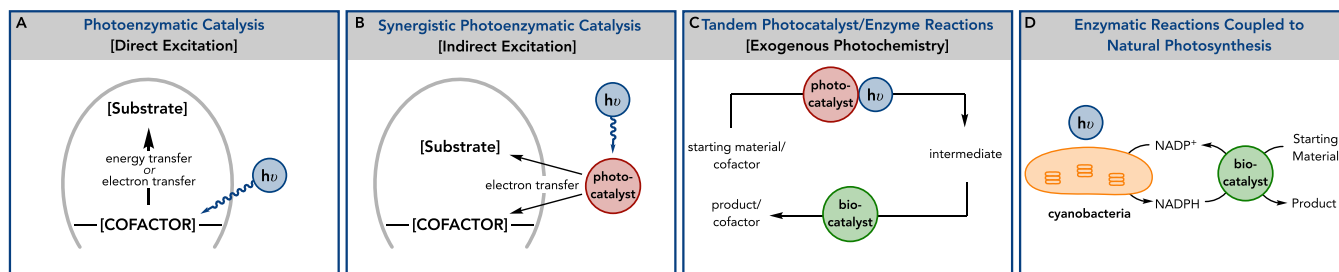


Figure 1. Types of photobiocatalysis in organic synthesis.

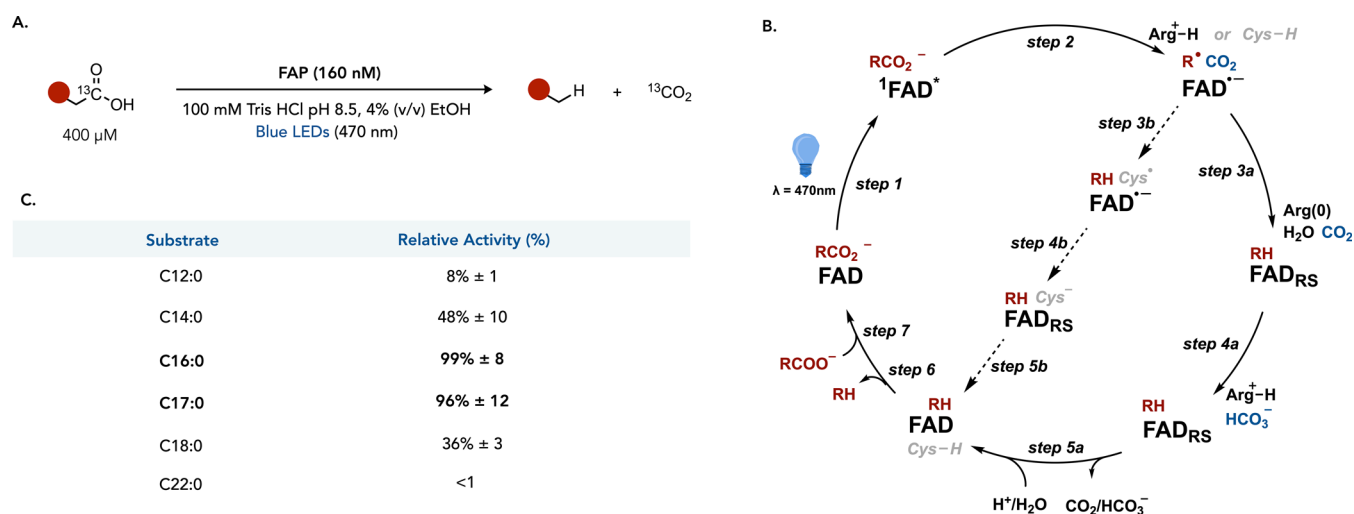


Figure 2. Mechanism and substrate scope of fatty acid photodecarboxylase. (A) Discovery of fatty acid photodecarboxylase (FAP) and initial substrate scope. (B) Proposed mechanisms for FAP. (C) Activity with fatty acids of different lengths.

2.1. Fatty Acid Photodecarboxylase

The third natural photoenzyme is fatty acid photodecarboxylase (FAP). As reported in 2017 by Beisson and coworkers, this is a natural photoenzyme that catalyzes the hydrodecarboxylation of fatty acids, a reaction with potential synthetic value (Figure 2A).³³ In contrast to previously known fatty acid decarboxylases, which catalyze oxidative decarboxylation to afford a terminal alkene, FAPs facilitate a redox-neutral reaction to form an alkane.^{34,35} The first member of this family was found in the microalgae *Chlorella variabilis* NC64A (EC 4.1.1.106) (CvFAP), although putative FAPs are found in many algal species, suggesting this enzyme family is ancient.³⁶ This flavoprotein is in the glucose-methanol-choline (GMC) family of oxidoreductases. Like other GMC oxidoreductases, FAP is a two-domain protein where the first domain contains the N-terminal residues and is responsible for flavin binding and stabilization, while the second domain is involved in substrate and product binding and trafficking.³³ The conserved residues in the FAD binding domain interact with the FAD cofactor, causing it to adopt a butterfly conformation bent 14 degrees from planarity. This structural feature red-shifts the ground state FAD absorption spectrum, which could aid in light absorption.³⁷

2.1.1. Reaction Mechanism and Substrate Scope.

Mechanistically, the reaction begins with the carboxylic acid binding close to the FAD cofactor within the protein active site (Figure 2B). Photoexcitation of the FAD cofactor with visible light ($\lambda = 325\text{--}530\text{ nm}$ with $\lambda_{\text{max}} = 467\text{ nm}$) affords the singlet excited state $^1\text{FAD}^*$ (Figure 2B, step 1), which rapidly oxidizes the carboxylate ($\sim 300\text{ ps}$) and, upon decarboxylation, affords

an alkyl radical and $\text{FAD}^{\bullet-}$ (Figure 2B, step 2). The quantum efficiency of this step is 80%, indicating that decarboxylation is favored by comparison to back-electron transfer. Radical termination occurs to provide a red-shifted FAD intermediate attributed to the cofactor interacting with a negatively charged species.³³ There are two proposed mechanisms for the termination step. Heyes et al. suggest that termination occurs via hydrogen atom transfer (HAT) from Cys432 to form the alkane product and cysteinyl radical (Figure 2B, step 3b), which is reduced by $\text{FAD}^{\bullet-}$ to afford a red-shifted thiolate–FAD complex ($\sim 170\text{ ns}$) (Figure 2B, step 4b).³⁸ Beisson previously observed basal activity when this residue is mutated to serine (C432S), suggesting a different mechanism could be responsible for radical termination. Sorigué et al. propose that termination occurs via a proton-coupled electron transfer involving a protonated arginine (R451) as a proton source and $\text{FAD}^{\bullet-}$ as the reductant (Figure 2B, step 3a).³⁷ In this mechanism, the red-shifted feature could be attributed to bicarbonate interacting with FAD ($\ll 100\text{ ns}$) (Figure 2B, step 4a). The red-shifted flavin quinone (FAD_{RS}) then disappears ($\sim 3\text{ ms}$) to regenerate FAD, while $\text{CO}_2/\text{HCO}_3^-$ leaves the active site (Figure 2B, step 5a). Without a substrate, the flavin cofactor can oxidize the protein scaffold, leading to deactivation. Electron paramagnetic resonance spectroscopy studies by Lakavath et al. suggest oxidation of amino acids, such as cysteine, tyrosine, and tryptophan, is responsible for the deactivation.³⁹

In the context of synthetic utility, FAPs catalyze the decarboxylation of C_{12} to C_{22} fatty acids to form C_{n-1} alkanes, with CvFAP displaying the highest activity on C_{16} to C_{17} fatty

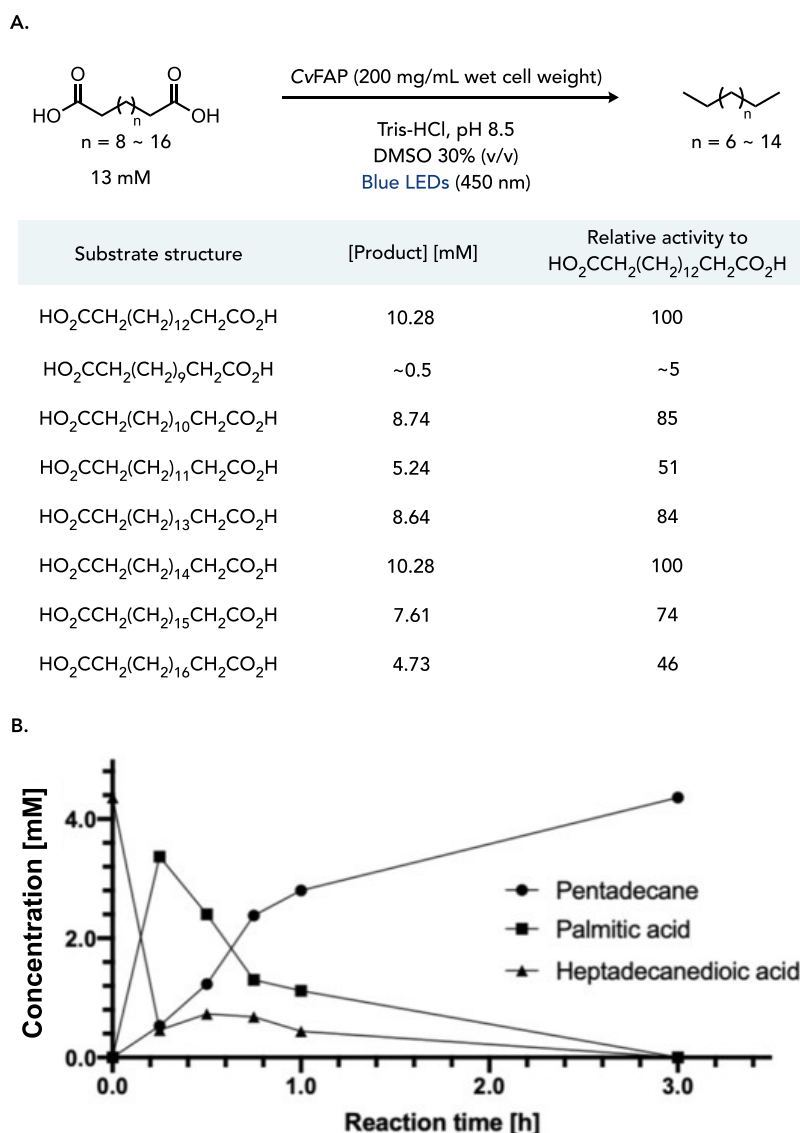


Figure 3. CvFAP reactivity with dicarboxylic acids. (A) Scope of CvFAP with dicarboxylic acids. (B) Concentrations of starting material, intermediates, and products over 3 h. Adapted with permission from *ChemistryOpen* 2021, 10, 553–559. Copyright 2021 The Authors. Published by Wiley-VCH GmbH.

acids (Figure 2C).³³ At higher substrate loadings with 30% DMSO, Hollmann observed decarboxylation of C₁₂ to C₂₀ fatty acids.⁴⁰ Zhang and co-workers reported that CvFAP could catalyze the decarboxylation of long-chain dicarboxylic acids.⁴¹ The dicarboxylic acids display a similar reactivity trend to monocarboxylic acids, with C₁₄ to C₁₆ diacids being the most reactive. These reactions can be run on a multigram scale, with hexadecanedioic acid being doubly decarboxylated in 81% yield (Figure 3A). When following the reaction progress, the authors found that CvFAP decarboxylated 90% of the heptadecanoic acid to palmitic acid in 15 min, while complete conversion to pentadecane required 3 h, indicating that dicarboxylic acids are converted into hydrocarbon via a two-step process. The authors hypothesize that the monocarboxylic acid must leave the enzyme's active site and rebind for the second decarboxylation (Figure 3B).

2.1.2. Reaction Condition Engineering. As CvFAP has a relatively narrow substrate scope and is prone to decomposition, researchers have engineered the reaction conditions to address these limitations. In two recent studies, CvFAP was

immobilized to increase its stability and reusability. Chanquia et al. tested the activity of CvFAP when immobilized on EziG beads. These resins contain Fe(III) cations, enabling them to selectively trap proteins possessing His-tags.⁴² The semi-hydrophilic Amber resin gave the highest degree of immobilization (84%) but provided low yields for decarboxylating C₁₇ fatty acid (4.8% yield). The immobilized enzyme could be reused up to three times in aqueous media. While the overall activity of immobilized CvFAP is lower than when used in a whole-cell formulation, the enzyme displays superior photostability. This study suggests that photon penetration of the solid support is poor. Developing optically transparent solid supports could lead to more active immobilized catalysts.

In the second study, Simić et al. explored enzyme immobilization to enable the use of CvFAP in flow.⁴³ They found that immobilization of CvFAP on EziG Opal provided the highest conversions at 4.2%. When tested in flow, the enzyme desorbed from the solid support due, in part, to the Ammoeng 102 surfactant required to solubilize the substrate. As modifications to the reaction conditions did not eliminate

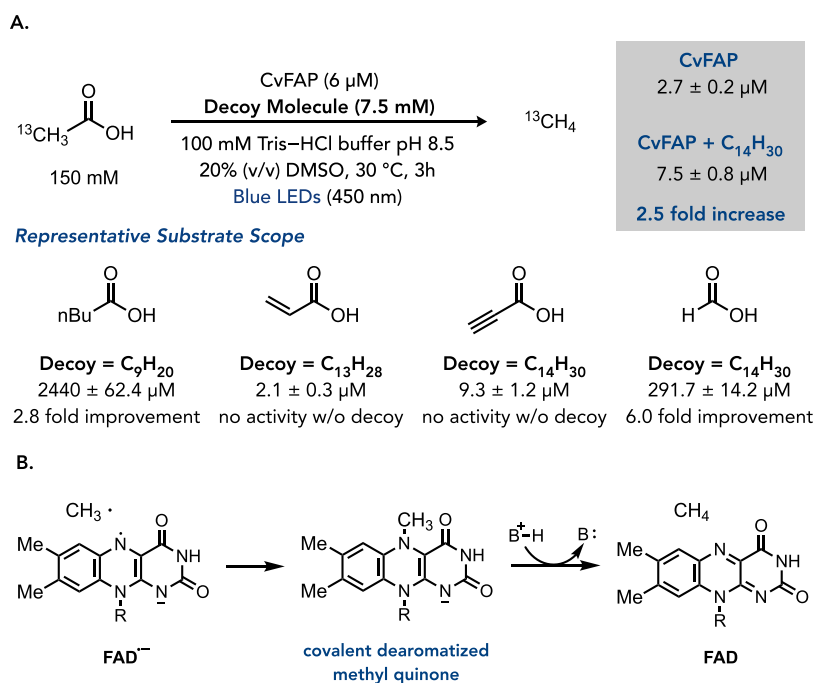


Figure 4. Decoy molecules used with CvFAP to expand the substrate scope. (A) Examples of decoy molecules enhancing the activity of CvFAP on short-chain carboxylic acids. (B) Alternative mechanism for radical termination when decarboxylating acetic acid.

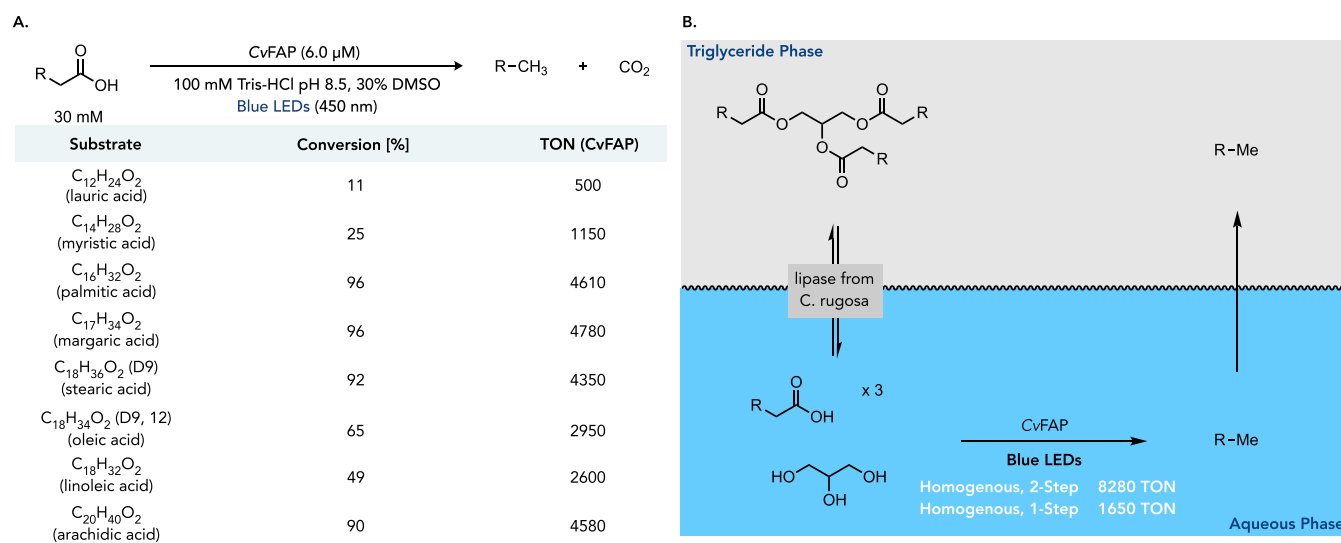


Figure 5. Conversion of triglycerides to alkanes using a photobiocatalytic cascade. (A) Scope of CvFAP with carboxylic acids found in triglycerides. (B) Schematic of a photoenzymatic cascade involving a lipase for triglyceride hydrolysis and CvFAP for acid decarboxylation.

desorption, the researchers switched to a flow reaction without an immobilized enzyme. Ultimately, they found that Tris buffer with Ammoeng 102 surfactant could be run in flow to achieve a space-time yield of 5.7 g L⁻¹ h⁻¹ for producing pentadecane from palmitic acid. This is the highest productivity of CvFAP reported to date.

Hollmann and coworkers found that FAP decarboxylation activity on short and medium carboxylic acids (C₁–C₆) could be enhanced by adding simple alkanes, ranging in size from nonane to pentadecane, as molecular decoys (Figure 4A).⁴⁴ For instance, nearly six times as much methane can be generated from acetic acid using CvFAP with pentadecane as a molecular decoy. The general strategy was successful across C₁ to C₆ substrates. This strategy also broadened the scope to include unsaturated fatty acids (e.g., acrylic acid, propionic

acid) and short alkyl chains (e.g., propionic acid). Additionally, CvFAP catalyzed the decarboxylation of formic acid, releasing H₂ (Figure 4A).

The authors hypothesize that adding a decoy molecule induces the same conformational changes that occur when longer fatty acids bind to the protein, helping to activate the enzyme for photoexcitation. A kinetic study of ¹³CH₃-CO₂H decarboxylation supports this hypothesis to form ¹³CH₄. In this study, the authors found that the reaction rate was only dependent on acetic acid concentration, indicating that the additive does not facilitate substrate binding but instead activates the enzyme for photoinduced electron transfer. While primary radicals are terminated using the mechanism outlined above, Hollmann proposed a different means of termination for the unstable methyl radical. DFT calculations suggest that

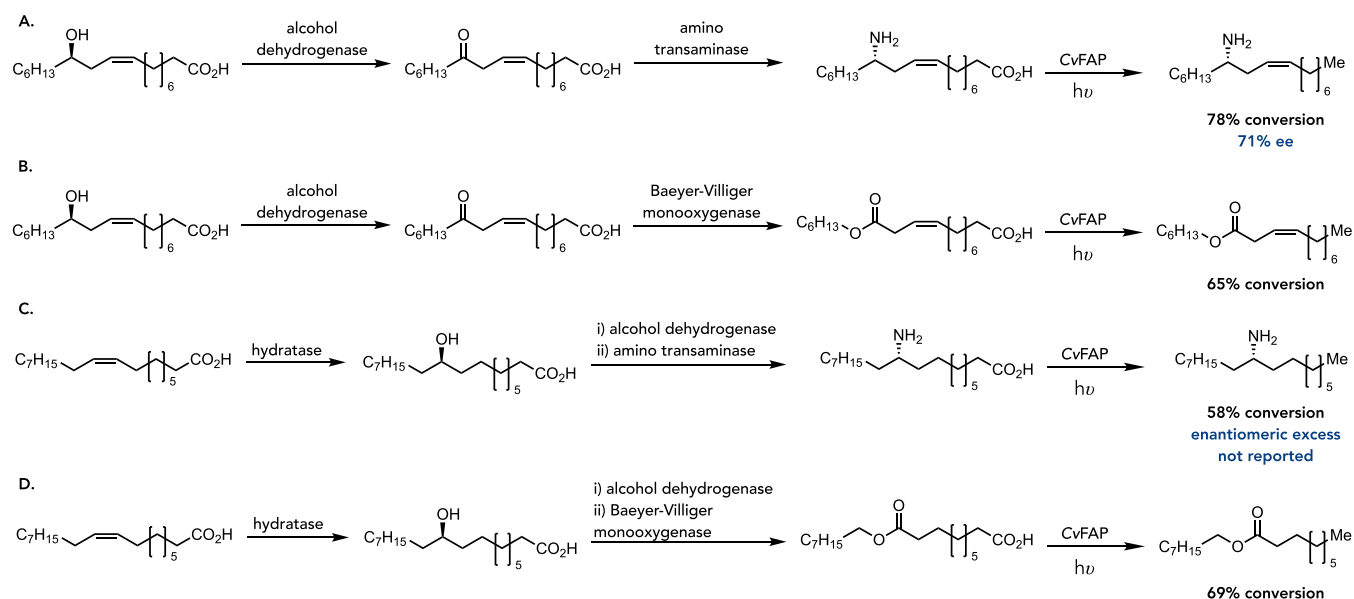


Figure 6. Enzyme cascades involving ricinoleic acid and oleic acid. (A) Enzyme cascade converting ricinoleic to a chiral amine. (B) Enzyme cascade converting ricinoleic to an achiral ester. (C) Enzyme cascade converting oleic acid to the corresponding amine. (D) Enzyme cascade to convert oleic acid to an ester.

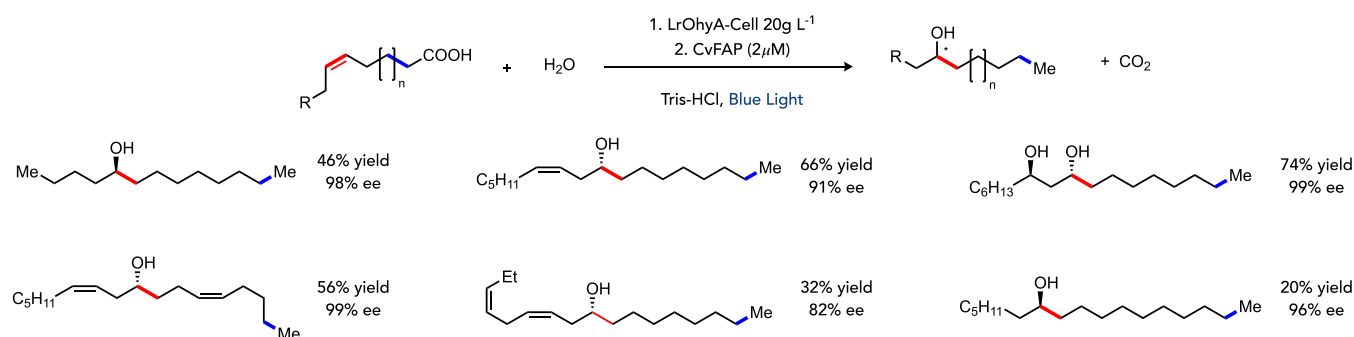


Figure 7. Enzyme cascades involving alkene hydratase.

radical termination occurs via alkylation of FAD^{•-} to form a covalent dearomatized methyl quinone flavin adduct, which upon protonation, forms methane and oxidized FAD quinone (Figure 4B).

2.1.3. Synthetic Applications of Wild-Type FAP.

Hollmann and coworkers have exploited the reactivity of CvFAP to synthesize biofuels from triglycerides.⁴⁰ In an initial study, the authors characterized the substrate preference for CvFAP. Consistent with the initial studies of this enzyme, the highest activity was shown to be for C₁₆ to C₂₀ fatty acids (Figure 5A). Next, they designed a two-enzyme cascade where a lipase initially hydrolyzes the triglyceride from *Candida rugosa*, followed by decarboxylation with CvFAP. In a two-step cascade, triolein is hydrolyzed by the lipase to oleic acid, followed by the addition of CvFAP and irradiation with blue light (450 nm) to afford (Z)-heptadec-8-ene in 83% conversion with 8280 TON for CvFAP. The same reaction can be run in a one-step protocol with lower catalyst efficiency (1650 TON) (Figure 5B).

In a related study, Hollmann and Wang found that CvFAP can remove free fatty acids from common oils.⁴⁵ A high degree of deacidification is observed in crude vegetable oils (83%–98%), soybean oil, rice bran oils, and palm oils. These contaminant acids negatively impact the flavor profiles of these

oils. The authors found that CvFAP in whole cells could effectively remove the free fatty acids in good yields. Molecular dynamics (MD) simulations suggest that at high concentrations, free fatty acids alter the binding orientation within the protein's active site and change the activity of the protein. These simulations also suggest that mixtures of oil and water, compared to pure water, increase the solvent-accessible surface area of the enzyme. This assessment agrees with a previous study by Aselmeyer et al. which shows that FAP displays its highest activity on ionized fatty acids present in organized lipid assemblies like microemulsions or large unilamellar vesicles compared to bulk fatty acids.⁴⁶ They also proposed an interfacial recognition site on FAP located at the entrance of the hydrophobic channel of the enzyme.

Cha et al. designed enzyme cascades involving CvFAP to synthesize long-chain aliphatic amines and esters from fatty acids.⁴⁷ The authors prepared recombinant *E. coli* cells expressing CvFAP. Different *E. coli* cells were prepared to express a fatty acid transporter, secondary alcohol dehydrogenase, and ketone-derivatizing enzymes (transaminase or Baeyer–Villiger monooxygenase (BVMO)). The first cascade involved converting ricinoleic acid to the corresponding amine (Figure 6A). Procedurally, the substrate was initially subjected to *E. coli* cells containing the alcohol dehydrogenase and

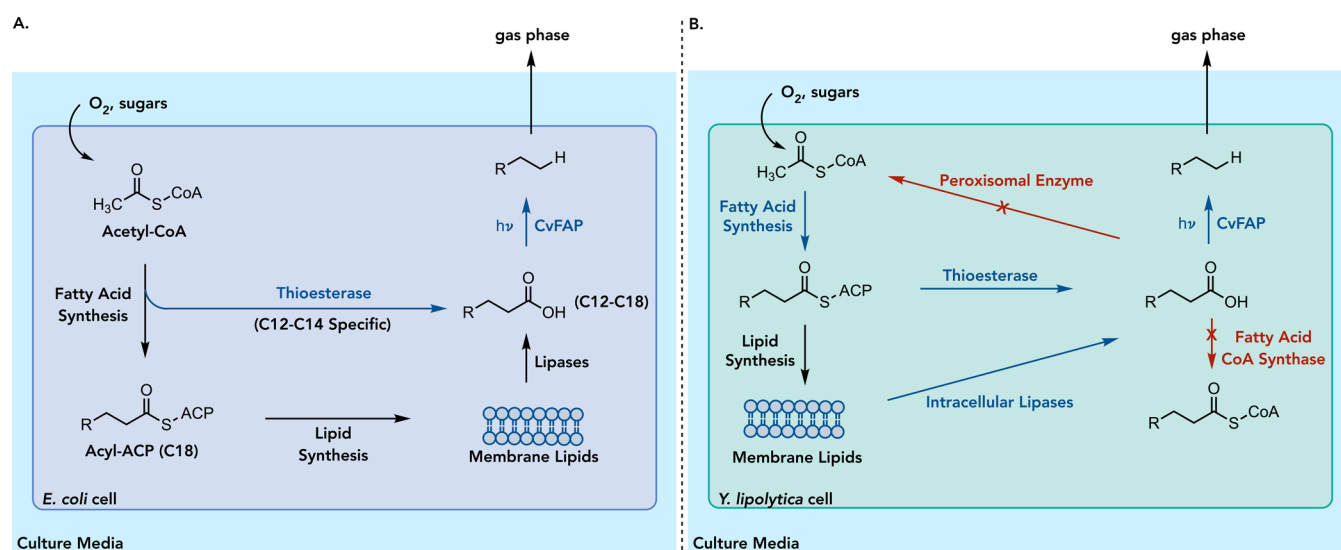


Figure 8. Whole-cell production of alkanes. (A) Hydrocarbon production in an *E. coli* cell expressing CvFAP to convert sugar to C11–C17 alkanes. (B) Hydrocarbon production in *Y. lipolytica* expressing CvFAP.

transaminase. After conversion to the amine was complete, *E. coli* cells encoding CvFAP were added to the reaction, and the whole system was irradiated with blue light. This protocol affords the amine product with 78% yield and 71% ee. An alternative cascade could convert ricinoleic acid to a fatty acid ester using an alcohol dehydrogenase and Baeyer–Villiger monooxygenase, followed by treatment with *E. coli* cells containing CvFAP to afford the product in 52% yield (Figure 6B). These cascades can also be merged with a fatty acid double-bond hydratase to convert oleic acid into the corresponding alcohol. In these reactions, the hydratase was coexpressed with the alcohol dehydrogenase, transaminase, and Baeyer–Villiger monooxygenase in the same *E. coli* cell. When using a hydratase, alcohol dehydrogenase, and transaminase followed by treatment with CvFAP, oleic acid was converted to 9-aminoheptadecane in 57% yield (Figure 6C). Alternatively, using the hydratase, alcohol dehydrogenase, Baeyer–Villiger monooxygenase, and CvFAP afforded octylnoate in 69% conversion (Figure 6D). These studies demonstrate how CvFAP can be used in enzyme cascades to afford elaborated products from simple fatty acids.

Park, Kourist, and Hollmann demonstrated that oleate hydratase from *Lactobacillus reuteri* (LrOhyA) could be used *in vitro* with CvFAP to access secondary alcohols in high yield and excellent enantioselectivity (Figure 7).⁴⁸ This family of secondary alcohols would be challenging to prepare stereoselectively because of the similar steric and electronic properties of functional groups off of the alcohol. The authors utilized a two-step protocol where the substrate was initially subjected to the hydratase and ran to high conversions. Subsequent addition of CvFAP and irradiation with visible light led to product formation. Alternatively, both enzymes could be coexpressed in *E. coli*, with irradiation only occurring after alkene hydration. Beyond hydratases, 5,8-diol synthase from *A. nidulans* (AnDS) was also used to transform oleic acid to (Z)-heptadec-8-ene-4,7-diol.

Building on these cascade reactions, Beisson and coworkers imagined developing a whole-cell biocatalytic cascade to produce undecane.⁴⁹ The researchers exploited the fact that hexadecanoic acid is the dominant component of the cell membrane of *E. coli*. To increase the concentration of fatty

acid, they coexpressed the thioesterase (Tes) from *Umbellularia californica* to produce lauric acid (C12) and myristic acid (C14) to be used by CvFAP (Figure 8A). By coexpressing these enzymes, the total hydrocarbon production was increased by a factor of 4 compared to the strain expressing only CvFAP. Moreover, the total amount of hydrocarbons in the gas phase increased by a factor of 6. When attempting to optimize hydrocarbon production, the authors observed a 50% reduction in hydrocarbon production after 48 h. Analysis of the soluble protein at different light intensities suggests that CvFAP degrades under high light conditions. This presumably occurs via the same mechanism described above, leading to the accumulation of free radicals and inactivation of the enzyme.

In a related study, researchers sought to produce biofuels in oleaginous yeast (*Yarrowia lipolytica*) expressing FAPs (Figure 8B). This model organism is known to accumulate large amounts of lipids (more than 20% of its cell dry weight), making it an ideal model organism for producing hydrocarbons. To optimize production, Bruder et al. modified the lipid metabolism of *Yarrowia lipolytica* to optimize fatty acid production.⁵⁰ Notable modifications include knocking out enzymes that consume free fatty acids, including a peroxisomal enzyme that converts fatty acids to Acetyl CoA and a Fatty acid CoA synthase. Additionally, they overexpressed diglycerol acyltransferase to synthesize more triacylglycerols (TAGs). These TAGs could be easily converted to fatty acids through the action of overexpressed intracellular lipases. The fatty acids produced through these mechanisms could be converted to hydrocarbon using CvFAP expressed in the cell. The authors optimize this hydrocarbon production by adjusting light and growth conditions, reaching a total hydrocarbon quantity of 58.69 mg/L after 60 h of fed-batch culture. As in the *E. coli* system, high photon flux decreased yeast growth and hydrocarbon production.⁴⁹

In a subsequent study, Li et al. modified the *Yarrowia lipolytica* strain developed by Bruder et al. to knock out genes encoding cytochromes P450 involved in *n*-alkane assimilation.⁵¹ To accelerate the rate of decarboxylation, they moved FAP to a high copy number plasmid, increasing its expression level. Hydrocarbons were produced at 1.47 g/L under fed-batch conditions over 18 days with these modifications.

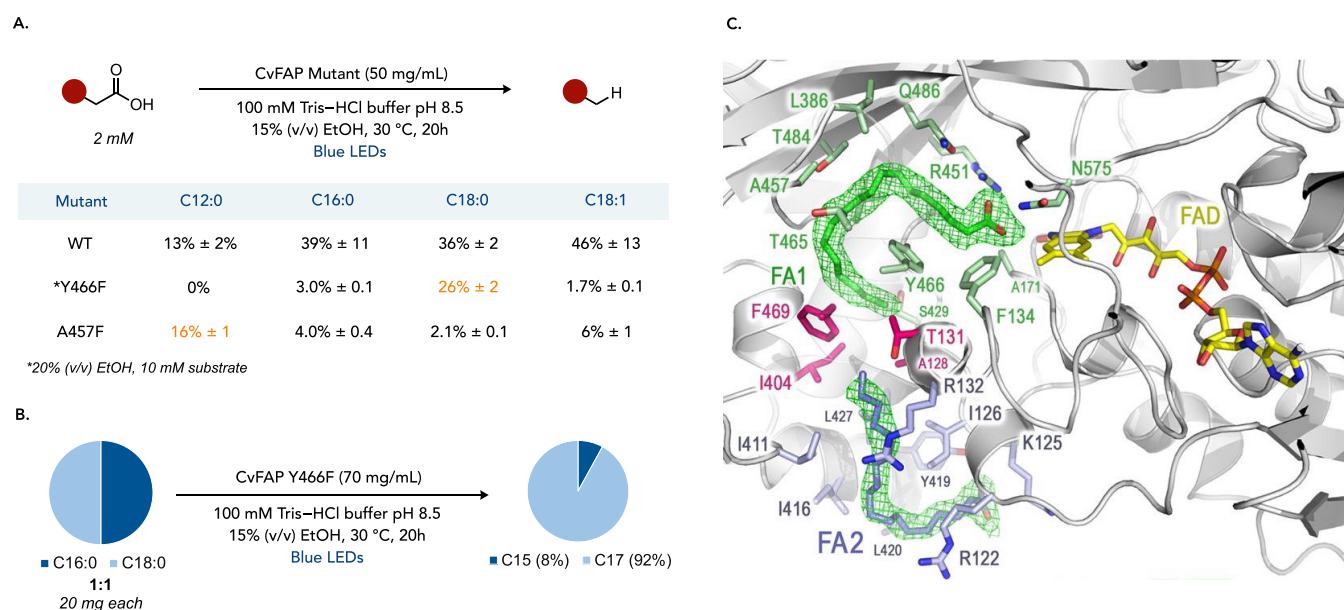


Figure 9. Engineering to alter the substrate specificity of CvFAP. (A) CvFAP mutant screening. (B) Selectivity with the CvFAP-Y466F variant on a preparative scale. (C) Image of the crystal structure of CvFAP with a fatty acid bound within its active site. Adapted with permission from *Science* 2021, 372, eabd5687. Copyright 2021 American Academy for the Advancement of Science.

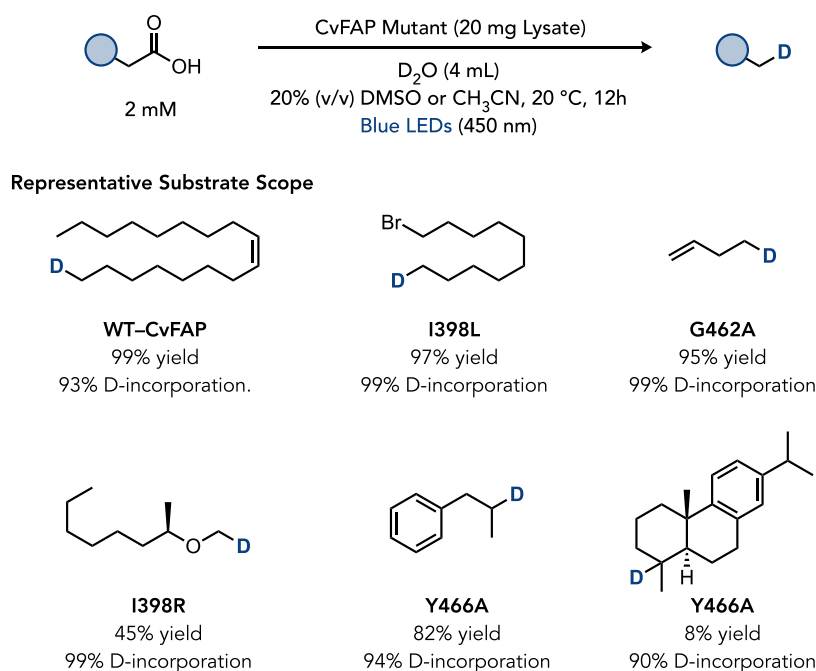


Figure 10. Engineered CvFAP variants for isotope incorporation experiments.

Although it is difficult to directly compare these two systems,⁵⁰ we can estimate that the latter strain has a 4-fold increase in production per unit time.

Yunus et al. were interested in producing hydrocarbons in photosynthetic chassis to directly use atmospheric or industrial CO_2 as a carbon source.⁵² In their initial study, they used *Synechocystis* sp. PCC 6803 as a model organism and coexpressed CrFAP with a thioesterase with activity for thioesters with chain lengths greater than ten carbons and maximum activity on C16 and C18. With this engineered strain, they increased the cellular hydrocarbon content of *Synechocystis* by nearly 19-fold over the cells lacking the FAP protein. In a second study, Yunus et al. changed the

thioesterase to one that was selective, either C8 fatty acids (CpFatB1) or C12 fatty acids (UcTES).⁵³ To increase the amount of decarboxylation, they modified the ribosome binding site upstream of FAP to increase the expression level. With UcTES, they produced 15 mg/L of undecane and 11 mg/L of tridecane. With CpFatB1, the cells produced about 10 mg/L of a mixture of heptane, nonane, undecane, and tridecane. However, due to the volatility of these shorter alkanes, the authors acknowledge that this yield might not accurately reflect the yield of these alkanes.

Guo et al. systematically compared hydrocarbon production using FAPs as cell-free lysates and in whole cells under different reaction conditions, substrate concentrations, stirring

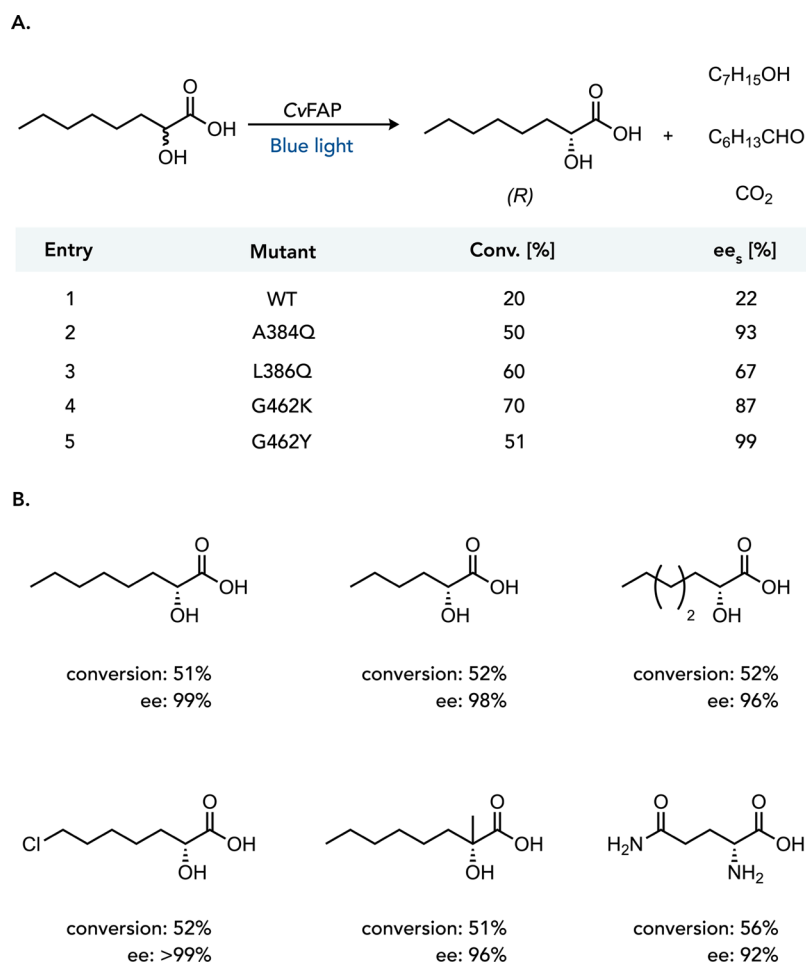


Figure 11. Engineered CvFAP for a kinetic resolution of α -hydrocarboxylic acids. (A) Protein engineering campaign to improve the stereoselectivity of CvFAP. (B) Representative substrate scope with the evolved enzyme.

rates, incubation times, and pH conditions.⁵⁴ When running the reactions in a transparent 5 mL vial with magnetic stirring, they found that with stirring at less than 200 rpm, the CvFAP activity in the whole cells was approximately 50% lower than that in the cell lysate. However, no other modification of the reaction conditions resulted in a statistically significant difference between the two formulations.

2.1.4. Synthetic Applications with Engineered FAP Variants. Ancestral reconstruction was used to identify FAPs with better reactivity profiles.⁵⁵ Kourist found that a collection of extant CvFAP homologues could be used to predict ancestral FAPs. One of the resurrected enzymes (ANC1) displayed improved decarboxylation activity. As is typical in ancestral reconstructions, ANC1 showed 15 °C enhanced thermal stability compared to CvFAP and displayed higher residual activity when the protein was preheated at 50 °C before the enzymatic assay. Moreover, there was a 12-fold improvement in protein expression using ANC1 compared to CvFAP.

Protein engineering via rational mutagenesis has been applied to improve the activity of CvFAP on medium- to long-chain (C₁₂ to C₁₈) fatty acids.⁵⁶ Sites were identified by selecting residues predicted to sit near the alkyl chain when bound within the protein active site but far enough from the FAD cofactor to ensure that the mutants retain catalytic function (Figure 9A). Specific mutations were selected to change the shape and hydrophobicity of the protein's active

site. Twenty-two mutants were prepared and tested on C12:0, C16:0, and C18:0 substrates and one unsaturated fatty acid (C18:1). Six mutants (Y466A, Y466F, Y466L, S429A, S429G, and W479A) showed increased specificity toward C18:0. Specifically, the Y466F mutant maintained similar activity for C18:0, with conversion levels for C16:0 and C18:1 decreasing 8-fold. Three mutants (A457F, T465R, and G455F) exhibited a higher preference for C12:0, with A457F and T465R showing a 10- to 20-fold decrease in activity for C₁₆ to C₁₈ fatty acids. To highlight the substrate selectivity of these mutants, Y466F was tested on a 1:1 mixture of C16:0 to C18:0 fatty acids, resulting in a 92% yield of the C17:0 product and an 8% yield of the C15 product in the final alkane mixture (Figure 9B).

In an independent study, Xu and Wu used CvFAP to selectively decarboxylate *trans*-fatty acids over *cis*-fatty acids (Figure 10).⁵⁷ Using “focused rational iterative site-specific mutagenesis” (FRISM), the authors prepared libraries around positions in the active site (T484, Y466, T465, A457, G455, and V453). They found that the mutation V453E displayed an almost exclusive preference for the *trans* fatty acid (elaidic acid) over the *cis* fatty acid (oleic acid). A similar engineering approach was used to increase the activity of shorter fatty acids and bulky substrates. On nonanoic acid, only one mutation (I398L) was beneficial, exhibiting a 10-fold improvement in activity. This strategy was also applied to decanoic acid, where CvFAP-I398L displayed an increased k_{cat} of 466.67 s⁻¹.⁵⁸ For

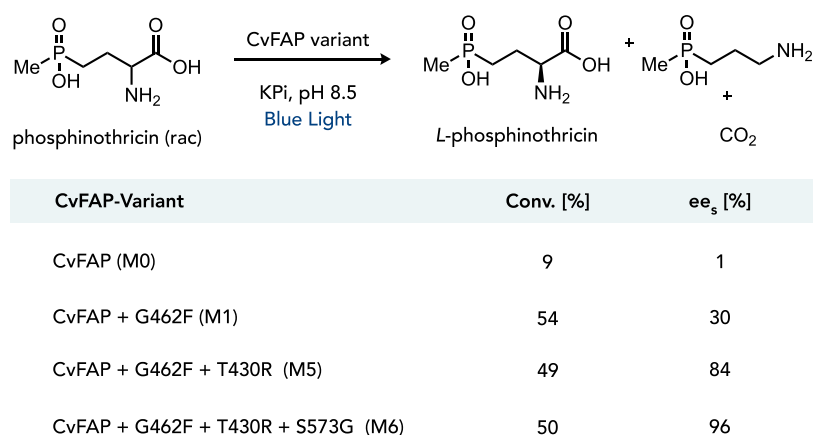


Figure 12. Kinetic resolution of phosphinothricin using a CvFAP variant.

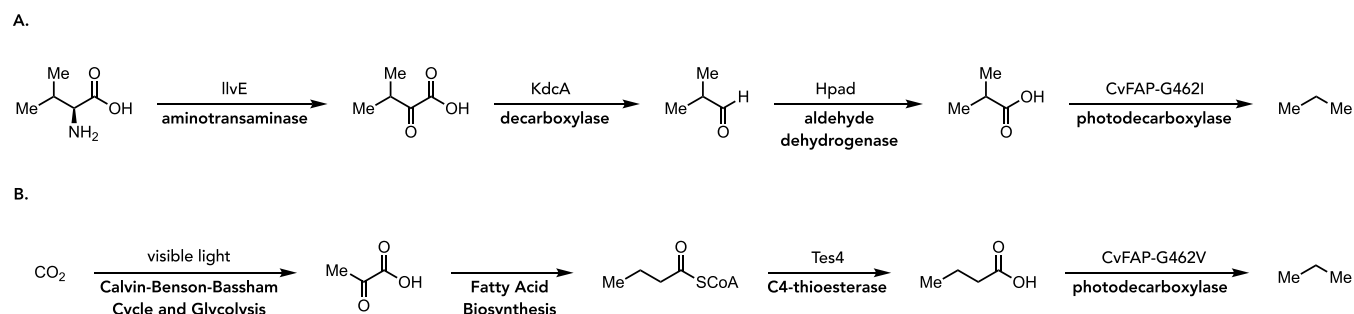


Figure 13. Whole cell strategies using engineered CvFAP variants for propane production. (A) *E. coli* and *Halomonas* pathway for converting valine to propane. (B) Cyanobacteria for propane production using *Synechocystis* PCC6803.

C3–C4 fatty acids, they identified a double mutant P460A/G462A whose k_{cat} was highly increased from 1.623×10^{-2} to 18.33 on butyric acid.

The same approach was used to optimize CvFAP for short-chain, racemic, and bulky fatty acid deuteration. They found that mutation of glycine at position 462 to alanine (G462A) provided improved yields across a range of substrates [propionic acid, 78% yield], I398R [(heptan-3-yloxy) acetic acid, 40% yield, $er = 94:6$], and Y466A [3-phenylbutanoic acid, 81% yield]. This mutation was previously found by Scrutton and co-workers to increase activity for propane production.⁵⁹ MD simulations showed the expanded binding tunnel in mutant Y466A (from 7.1 to 13.9 Å), which explains the higher binding efficiency of bulky substrates.⁶⁰ These mutants and the parent enzyme were used for deuteration experiments with D₂O. Using palmitic acid in D₂O gave the decarboxylated product a 99% yield and 93% deuterium incorporation. The researchers found that even 5% residual water decreased deuterium incorporation by ~20%. Consequently, the protein needed to be lyophilized to ensure a high degree of deuteration (Figure 10).

In 2019, Wu and co-workers demonstrated that these proteins could be applied to the asymmetric synthesis of α -functionalized carboxylic acids via kinetic resolution (Figure 11).⁶¹ Using 2-hydroxyoctanoic acid as a model substrate with wild-type CvFAP affords the unreacted starting material in 80% yield with 20% ee. The authors hypothesized mutating three small residues within the substrate binding pocket (A384, L386, and G462) to larger amino acids (phenylalanine, tyrosine, lysine, and glutamine) would narrow the binding channel and increase interactions between the substrate and

protein. Consistent with their hypothesis, many of the mutants provided improved selectivity, with G462Y being the most selective, furnishing unreacted starting material in 49% yield with 99% ee (Figure 11). The CvFAP-G462Y variant tolerates various α -hydroxy acids with C6 to C12 alkyl side chains. Besides acids with different lengths, this variant also accepts substrates with several functional groups, including α -substituted α -hydroxy acids and glutamine.

Zheng and co-workers applied this kinetic resolution strategy to prepare enantioenriched phosphinothricin.⁶² Phosphinothricin is a common herbicide that is typically distributed as a racemic mixture. As the D-enantiomer is inactive as an herbicide and harmful to the environment, there is interest in developing a synthetic strategy for preparing the enantioenriched L-enantiomer. The wild-type CvFAP gave only 9% conversion with 1% ee. Mirroring the strategy used with α -hydroxycarboxylic acids, three residues in the binding tunnel with small side chains (A384, L386, and G462) were mutated to residues with larger side chains to improve interactions with the substrate (Figure 12). This initial round of engineering revealed CvFAP-G462F to be the most active and selective (54% conversion, 30% ee). Next, using modeling, the authors identified two pairs of residues suspected to interact with the substrate (S573/S574 and T430/G431). Mutation of threonine at position 430 to arginine (T430R) increased activity and selectivity (49% conversion, 84% ee). Finally, decreasing the steric bulk at position 573 (S573G) led to the triple mutant (CvFAP-M6) that catalyzed the decarboxylation in 50% conversion with the unreacted carboxylate isolated with 95% ee. This reaction could be conducted on a preparative scale to isolate the unreacted starting material.

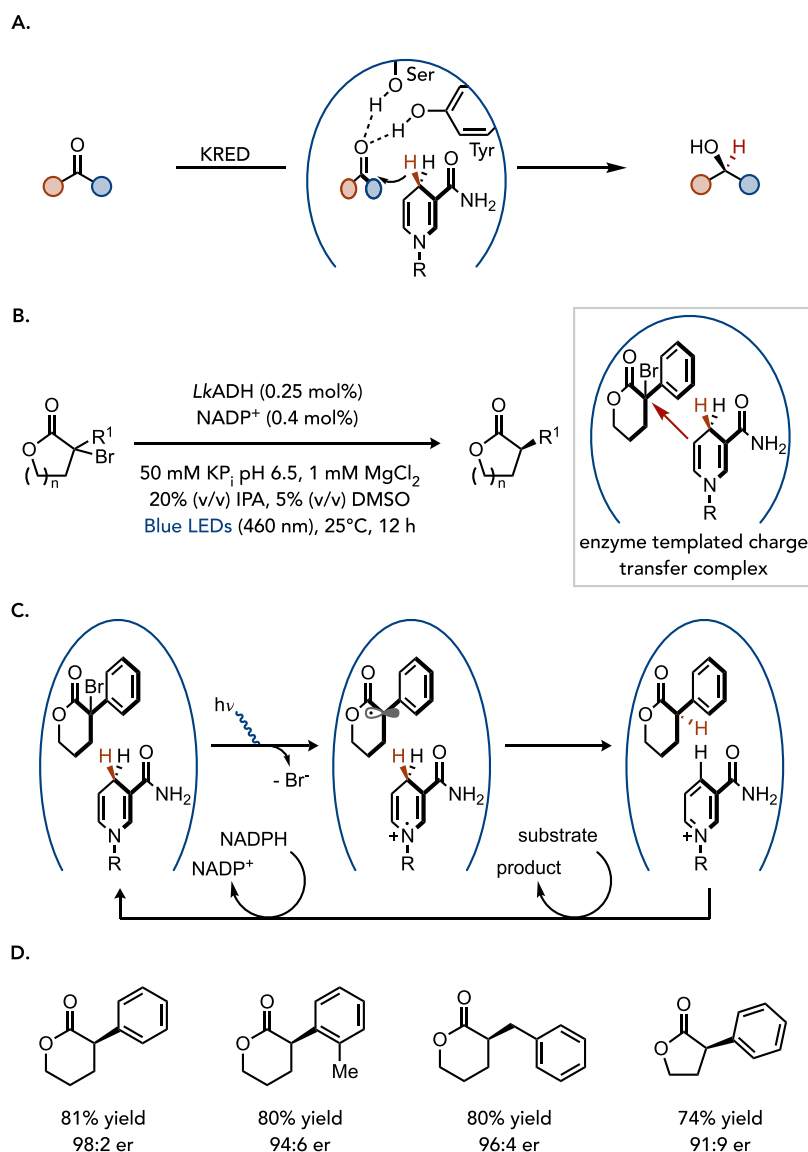


Figure 14. Photoenzymatic hydrodehalogenation of lactones using photoenzymatic catalysis. (A) Natural mechanisms for a short-chain ketoreductase. (B) General scheme for a KRED-catalyzed photoenzymatic hydrodehalogenation with the proposed charge-transfer complex. (C) Proposed mechanisms of hydrodehalogenation. (D) Representative substrate scope.

Using engineered FAP variants, researchers have focused on producing biogas, such as propane and butane.⁵⁹ Amer et al. analyzed the structure of CvFAP and surmised that mutation of glycine at position 462 (G462) could shrink the size of the active site to help favor the decarboxylation of small carboxylic acids. They found mutation to valine (G462V) or isoleucine (G462I) led to improved activity on C4 carboxylic acids. These mutants were selected for *in vivo* production of liquified petroleum gas. *E. coli* was selected as a model organism for this proof-of-concept (Figure 13A). The pathway for volatile hydrocarbon production starts with the transamination of valine to produce α -ketovalerate, which is decarboxylated using a thiamine-dependent ketoacid decarboxylase to form isobutyraldehyde. Finally, 3-hydroxypropionaldehyde dehydrogenase oxidizes the aldehyde to isobutyric acid, which can be decarboxylated using CvFAP-G462I. When run in *E. coli* that is supplied with 30 g/L valine, 110 mg/L of propane was produced.

Building on this work, the authors explored introducing the mutant CvFAP catalyst into *Halomonas*, an organism that grows in 20% NaCl at high pH, enabling seawater as a culture medium. By expressing CvFAP-G462V and adding butyric acid to the culture medium, the authors reported the production of nearly 157 mg/L of propane. When the valine to isobutyric acid pathway was introduced into *Halomonas* containing CvFAP-G462V, propane production was increased to 180 mg/g of cells/day.⁶³ Growing *Halomonas* under nonsterile conditions using renewable proteinaceous waste as an amino acid source could reduce the process cost for producing biosourced propane.⁶⁴

The same authors also explored cyanobacteria as a chassis for CvFAP-mediated propane production (Figure 13B).⁵⁹ By introducing CvFAP-G462V into *Synechocystis* PCC 6803 cyanobacteria and knocking out acyl ACP synthase and overexpressing a thioesterase to produce butanoic acid, CO₂ could be converted to propane. Under their optimized reaction

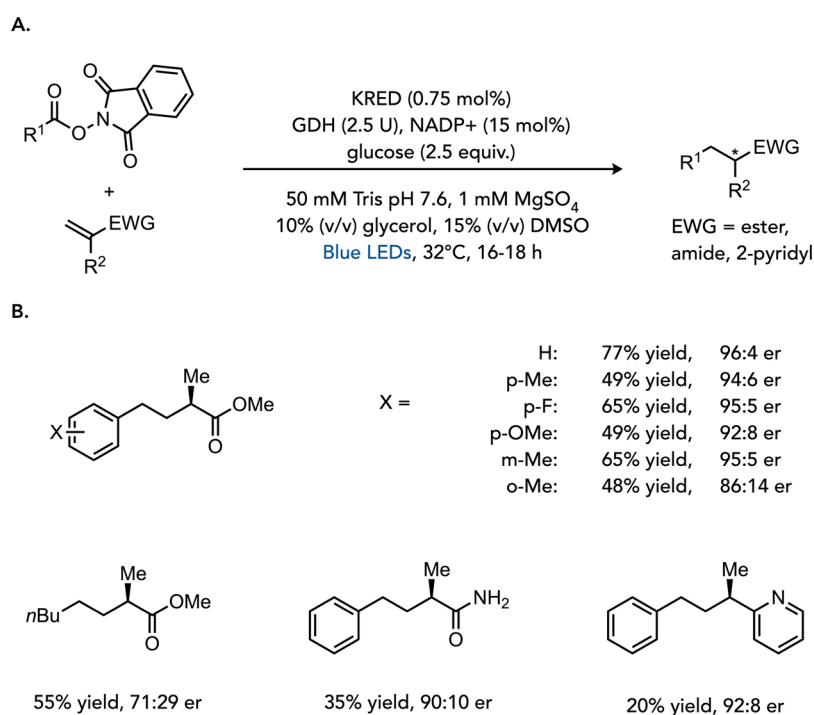


Figure 15. Intermolecular coupling with KREDs and redox-active esters. (A) KRED-catalyzed photoenzymatic Giese reaction between a Michael acceptor and redox-active ester. (B) Representative substrate scope.

conditions, the researchers obtained 11 mg/L of propane per day.

2.1.5. Outlook. Despite only being reported six years ago, the FAP family of enzymes has been the topic of intense research efforts. While the mechanism of these proteins is now well understood, their applications in chemical synthesis remain under-explored. A looming question is whether C_vFAP can use the mechanism of oxidative decarboxylation for reactions beyond hydrodecarboxylations. Applying this step to new C–C, C–O, and C–N bond-forming reactions would significantly expand its use in chemical synthesis.

FAP enzymes hold immense promise as catalysts for biofuel production; however, several bottlenecks must be overcome. Perhaps the most significant is the low turnover numbers. While this level of activity is acceptable for fine chemicals, it is too low for bulk chemical production. The low activity is due, in part, to the photoinhibition of the enzyme via the mechanisms outlined above. Engineering a more photostable FAP variant could address this issue, although it might also result in a less active catalyst. An alternative is to run reactions *in vivo* to replace photoinhibited enzymes with active ones. However, photodegradation of the enzyme will result in lower yields, especially if the metabolism of the production organism is oriented toward protein production to compensate for photoinhibition rather than toward cellular fitness and substrate production. Finally, the hydrophobic nature of the products presents a challenge. While volatile hydrocarbons (C1–C4) can be easily recovered in the gas phase, removing long-chain hydrocarbons trapped in the cell membranes is more difficult. The development of platforms that enable the facile collection of the product is necessary for these reactions to be useful.

A general challenge in the field of photochemistry is how to scale up processes that are photon limited, such as photobiocatalytic reactions. Most studies focus on analytical scale

reactions rather than large-scale chemical manufacturing. In pharmaceutical manufacturing, flow reactors and innovative reactor design have begun to address these issues.^{65,66} The development of reactions for photobiocatalytic processes will be essential for implementing FAP proteins on an industrial scale.

2.2. Nicotinamide-Dependent Ketoreductase Photochemistry

Nicotinamide-dependent ketoreductases (KREDs) are widely used in chemical production for the enantioselective reduction of ketones to alcohols (Figure 14A).⁶⁷ In these enzymes, the NADH or NADPH cofactors act as hydride sources. Early studies by Ohnishi et al. demonstrated that the reducing power of these cofactors could be enhanced with light irradiation to enable the reduction of activated olefins.⁶⁸ In a subsequent study, Fukuzumi et al. demonstrated that *N*-benzyl nicotinamide could function as a potent single-electron reductant when irradiated with UV light to enable the hydrodehalogenation of alkyl halides.⁶⁹ This property was first leveraged in KREDs by the Hyster group, demonstrating that these enzymes could catalyze the stereoselective hydrodehalogenation of α -bromolactones under irradiation with blue light (Figure 14B).⁷⁰ Central to this process is forming an enzyme-templated charge-transfer (CT) complex between the bound nicotinamide cofactor and the bromolactone substrate that absorbs between 350 and 550 nm ($\lambda_{\text{max}} = 390$ nm). This complex only forms in the presence of protein, providing a mechanism for gating radical formation to the enzyme's active site. The proposed mechanism involves the excitation of this charge-transfer complex to generate a radical ion pair, followed by mesolytic cleavage of the C–Br bond to generate an α -acyl radical. At this point, isotopic labeling experiments indicate that the NADH or NADPH radical cation delivers a hydrogen atom selectively to one face of the prochiral α -acyl radical, providing the corresponding dehalogenated product. NAD⁺ or

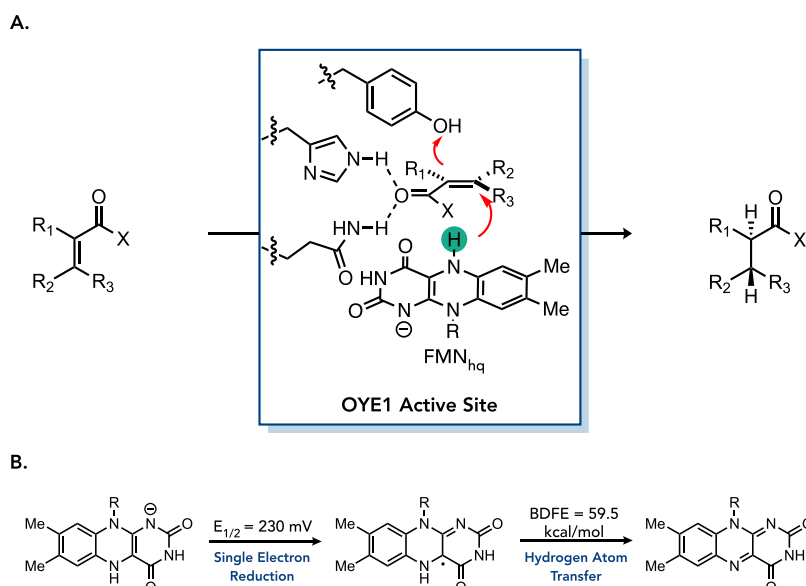


Figure 16. Mechanisms available to FMN in “ene”-reductases. (A) Mechanism of alkene reduction using flavin-dependent old yellow enzymes. (B) Flavin oxidation states available via radical mechanisms.

NADP⁺ is then reduced, either with isopropyl alcohol or by glucose dehydrogenase, to regenerate the active cofactor (Figure 14C).

Evaluation of various KREDs revealed optimal activity and selectivity in variants of the short-chain dehydrogenase from *Lactobacillus kefir* (*LkADH*). The most active variants were evolved KREDs from the Codexis KRED library and containing a mutation at position Y190 which breaks key hydrogen bonding contacts and expands the small binding pocket of the active site.⁷¹ In an independent protein engineering campaign, the Hyster group found three mutations (*LkADH*-E145F-F147L-Y190C) that enabled dehalogenation in 72% yield with 96:4 er. They hypothesized that active enzymes required large substrate binding pockets to accommodate the bulky substrate. Based on this hypothesis, the authors prepared a series of wild-type ADHs with large active sites and found that the one from *Ralstonia sp.* (*RasADH*) could catalyze the dehalogenation to provide the opposite enantiomer to the one formed by the *LkADH* variants. This scaffold tolerated *ortho*-substituents, γ -lactones, and less reducible benzyl substrates (Figure 14D). Interestingly, the enzymes used do not bind one enantiomer of starting material preferentially over the other, allowing for the conversion of racemic material to the enantioenriched product without kinetic resolution of the starting material.

Building on these enzyme-templated charge-transfer complexes, Zhao and co-workers found that KREDs can catalyze the intermolecular coupling of *N*-(acyloxy)phthalimides (NHPI esters) with Michael acceptors in a Giese reaction (Figure 15A).⁷² The NHPI ester can participate in a charge-transfer complex, expanding the radical precursor scope beyond previously explored lactones. The resulting radical adds to Michael acceptors before enantioselective hydrogen atom transfer, furnishing products with enantioenriched α -stereocenters. Directed evolution of an *LkADH* variant from Codexis produced a KRED capable of coupling the NHPI ester of phenylacetic acid with methyl methacrylate in 77% yield and 96:4 er. This variant can also reduce aliphatic NHPI esters or coupling into alternative Michael acceptors, including acryl-

amide and vinylpyridine (Figure 15B). In multiple cases, other KREDs tested achieved higher yields, higher enantioselectivity, or preference for the opposing enantiomer over that of the evolved variant. Molecular dynamics, quantum mechanics/molecular mechanics simulations, and experimental evidence suggest that radical formation occurs within the protein active site, with decarboxylation occurring before the Michael acceptor binds within the active site. Based on this mechanistic understanding, it is difficult to rationalize how C–C bond formation outcompetes reductive quenching of the nucleophilic radical by the nicotinamide radical cation

2.3. Flavin-Dependent “Ene”-Reductase Photochemistry

Flavin-dependent “ene”-reductases (EREDs) are a class of biocatalysts frequently used in organic synthesis.⁷³ The most common EREDs are old yellow enzymes (OYEs), which were initially isolated from brewer’s bottom yeast (*Saccharomyces pastorianus*) in 1932 and are thought to be expressed in response to oxidative stress.^{74,75} Subsequent studies revealed ERED homologues in all domains of life, with members found in natural product pathways and RNA modification.^{76,77} Traditionally, OYEs are used for the stereoselective reduction of activated alkenes and provide chiral products with high levels of stereoselectivity. This reduction occurs via a hydride transfer from flavin mononucleotide (FMN) hydroquinone (FMN_{hq}) to the electrophilic β -position of the activated alkene to afford FMN quinone and an enzyme-bound enolate, which is protonated by a conserved tyrosine. NAD(P)H can reduce FMN back to the FMN_{hq} in a ping-pong mechanism (Figure 16A).^{78,79} These enzymes reduce alkenes with *trans* selectivity, complementing traditional metal-catalyzed hydrogenations.⁸⁰

In the initial characterization (Figure 16B), Massey found that when photochemically reduced, OYE1 can kinetically and thermodynamically stabilize the anionic flavin semiquinone (FMN_{sq}^{•-}).⁸¹ While unrealized at the time, the ability of the protein to stabilize open-shell flavin oxidation states opens the door to radical reactivity in EREDs. In one scenario, FMN_{hq} could serve as a single-electron reductant (FMN_{hq}/FMN_{sq}^{•-} = –230 mV vs SCE) of an organic substrate.⁸² The resulting

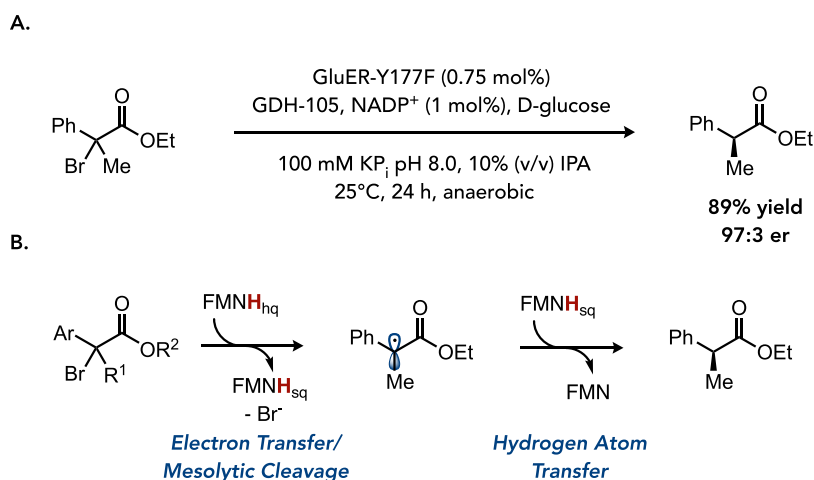


Figure 17. Dark radical chemistry using EREDs. (A) Dark hydrodehalogenation catalyzed by GluER-Y177F. (B) Proposed mechanism of dehalogenation.

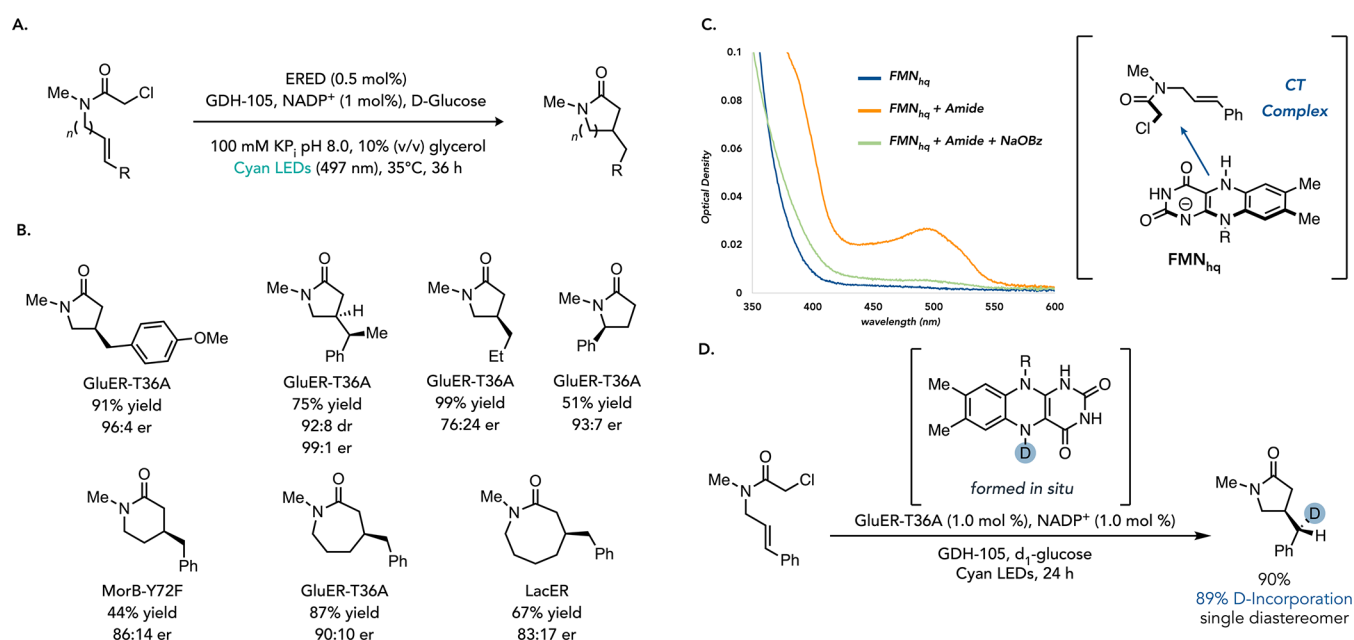


Figure 18. Photoenzymatic cyclization of amides. (A) General reaction scheme for the photoenzymatic radical cyclization with GluER-T36A. (B) Representative substrate scope with different EREDs. (C) UV-vis spectra of the enzyme-templated charge-transfer complex. (D) Isotope incorporation experiments support flavin as the source of a hydrogen atom.

substrate-centered radicals could be terminated via hydrogen atom transfer from the FMN_{sq} ($\text{BDE}_{\text{calc}} = 59 \text{ kcal/mol}$).⁸³

The Hyster group proposed and validated the viability of this general mechanism.⁸⁴ They found that an ERED from *Gluconabacter oxidans* (*GluER*) could reduce acyclic α -bromoesters without photoexcitation in 57% yield and 88:12 er with only 0.5 mol % of the enzyme and glucose dehydrogenase for cofactor turnover (Figure 17A). Mutation of the conserved tyrosine residue at position 177 to phenylalanine produced a variant with 89% yield and 97:3 er. Isotopic labeling of FMN_{hq} using the cofactor turnover mix and d_1 -glucose resulted in 81% deuterium incorporation at the α -position in the product, indicating that FMN_{sq} is serving as the source of a hydrogen atom (Figure 17B).

Having demonstrated that EREDs can catalyze a radical reaction, the Hyster group developed a radical cyclization of α -chloroamides to afford β -stereogenic lactams (Figure 18A), a

challenging reaction to control by other radical means.⁸⁴ However, FMN_{hq} is not sufficiently reducing to initiate the reaction. In Nature, DNA photolyase exploits excitation of the FAD_{hq} to access a more reducing excited state singlet state ($E(\text{FMN}_{\text{hq}}^*/\text{FMN}_{\text{sq}}) = -2.26 \text{ V vs SCE}$).¹⁹ Inspired by this reactivity, they hypothesized that a similar photoexcitation would be available to FMN_{hq} in EREDs.⁸⁵ An initial test showed *GluER* to be effective at this transformation when irradiated with violet light (390 nm), providing the desired lactam in 42% yield and 93:7 er as a 2:1 ratio of the desired cyclized to uncyclized dehalogenated product. Control experiments indicate that FMN alone cannot catalyze this reaction. Interpretations of these control experiments are complicated because of the poor solubility of the substrate in aqueous media and flavin oxidation states having different stability within the protein active site versus in solution. During optimization, they found that cyan light (497 nm) improved

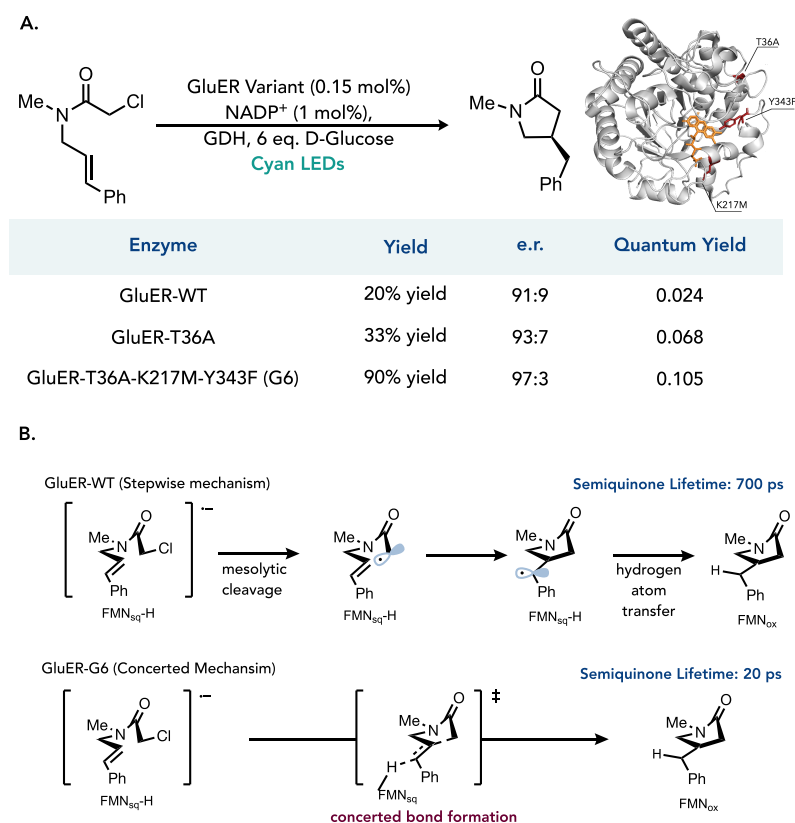


Figure 19. Enzyme engineering of EREDs for improved photon efficiency. (A) Engineering campaign for an improved *GluER* variant. (B) Transient absorption spectroscopy studies indicating a decreased radical lifetime in support of a concerted reaction mechanism.

yield (68%) with 94:6 er and no observed hydrodehalogenated product. The authors observe a new absorption feature ($\lambda_{\max} = 495$ nm) when the substrate was added to the reduced enzyme, indicating the intermediacy of a CT complex between FMN_{sq} and the substrate (Figure 18C). Importantly, this complex only forms in the presence of the protein, suggesting the protein scaffold is required for CT complex formation. Time-dependent density functional theory (TD-DFT) calculations on models where the substrate is docked into the protein active site predict that a CT complex should absorb at 510 nm, further supporting the experimental results. Isotopic labeling experiments suggest that radical termination occurs via hydrogen atom transfer from the flavin semiquinone, accounting for the high levels of enantioselectivity observed in the radical termination step (Figure 18D).

Mutation of the threonine residue at position 36 to alanine (T36A) improved yields and suppressed the formation of the acyclic hydrodehalogenated side product in 94% yield and 94:6 er (Figure 18B). This residue is located at the protein's surface, and the crystal structures of *GluER* and *GluER*-T36A are similar (backbone root mean squared deviation is 0.53 Å), so the structural basis for this improvement is unknown. *GluER*-T36A accommodates various substituents off of the alkene, including substituted aryl groups and alkyl groups. Other modes explored included *5-endo-trig* and *6-, 7-, and 8-exo-trig* cyclizations. All of these were possible in at least modest yield and selectivity, showcasing the utility of enzymatic methods when approaching these more challenging examples. Moreover, *GluER*-T36A can catalyze cyclizations with trisubstituted substrates with high enantio- and diastereoselectivity because the protein can precisely deliver a hydrogen atom to prochiral

radicals. Additionally, this transformation could be carried out using lyophilized cell-free lysate rather than purified enzyme, enabling gram-scale transformations for the model reaction.

One of the critical advantages of biocatalysts compared to other catalysts is the ability to tune the reactivity and selectivity of the catalyst using directed evolution.⁸⁶ The Hyster group applied directed evolution to the previously described photoenzymatic cyclization of α -chloroamides.⁸⁷ They developed a high-throughput optimization assay composed of 96-well LED arrays and cooling fans to ensure consistent irradiation and temperature across white microtiter plates with clear bottoms. A single round of error-prone mutagenesis strategy afforded *GluER*-T36A-K317M-Y343F (*GluER*-G6) as an improved biocatalyst, providing a 350% improvement in yield over wild-type *GluER* (Figure 19A). Detailed mechanistic studies suggest the improved yield for *GluER*-G6 is due to an almost-5-fold improvement in quantum yield compared to wild-type *GluER*. Moreover, *GluER*-G6 facilitates the reaction with a significantly decreased radical lifetime (20 ps) compared to the wild-type enzyme (700 ps) (Figure 19B). These lifetimes indicate rates of cyclization that are faster than those of radical cyclization in solution.⁸⁸

Additionally, this radical-ion pair appears to decay directly to FMN_{ox} with *GluER*-G6, whereas wild-type *GluER* forms a spectral signature consistent with FMN_{sq} . The authors propose that *GluER*-G6 optimally positions the alkene for cyclization, allowing it to participate in a hyperconjugative interaction with the C–Cl σ^* bond. Due to this interaction and the short lifetime of the FMN_{sq} , the authors proposed a concerted mechanism for the mesolytic cleavage, C–C bond formation, and HAT termination in *GluER*-G6, as opposed to a stepwise

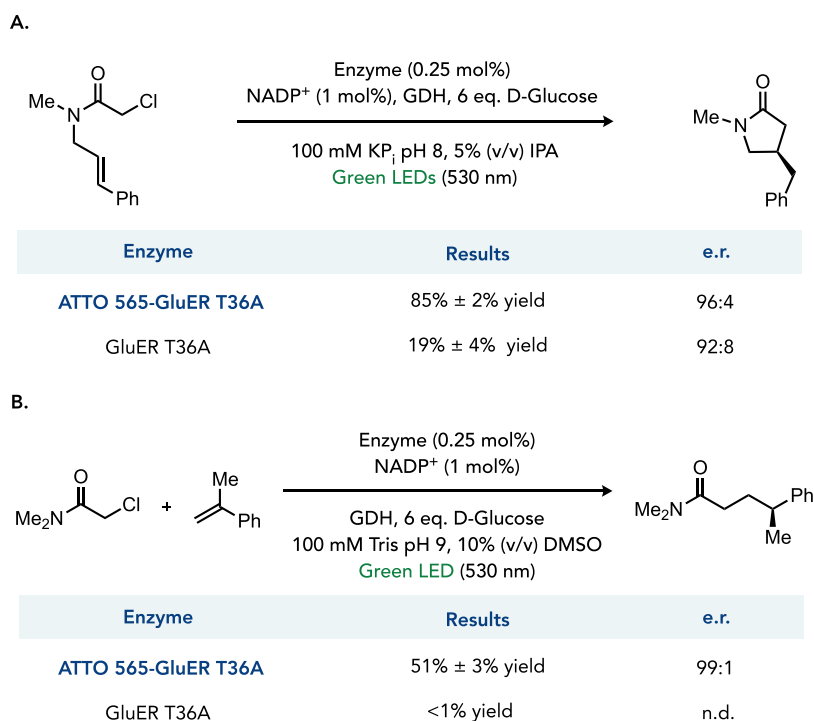


Figure 20. “Ene”-reductase conjugates for low-energy excitation. (A) Intramolecular reaction using the *GluER*-T36A dye conjugate. (B) Intermolecular reaction using the *GluER*-T36A dye conjugate.

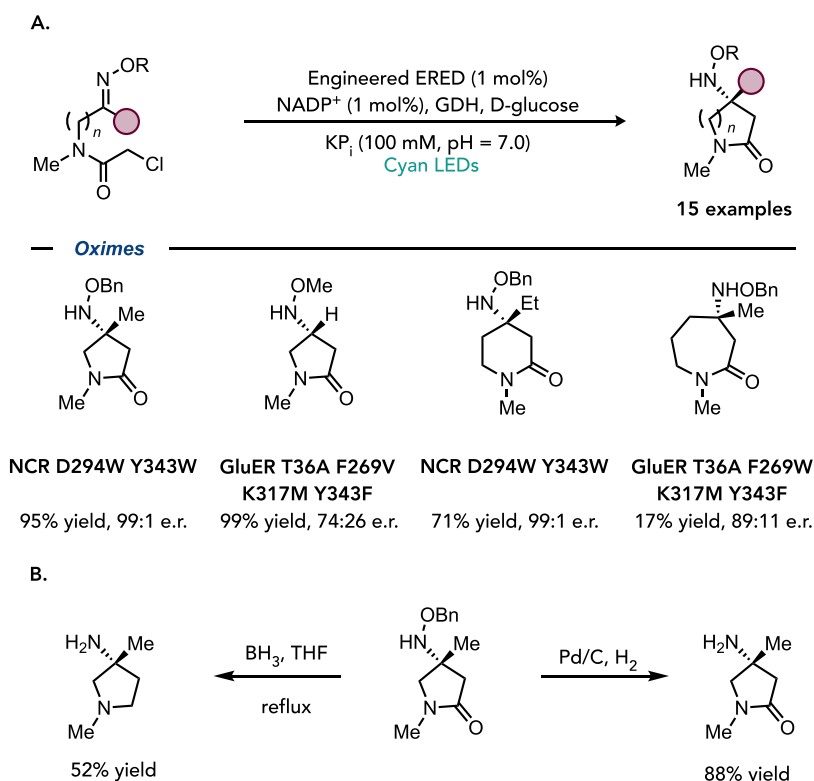


Figure 21. ERED radical cyclization involving oximes. (A) Scope of radical cyclization into oximes. (B) Derivatization of the hydroxylamine product.

mechanism in *GluER*-WT. This engineering method was expanded to synthesizing larger rings, enabling the identification of more effective catalysts for challenging radical cyclizations.

A striking feature of ERED's non-natural photoreactions is the relatively poor quantum yield compared to enzymes with native photoreactivity. This difference is largely due to EREDs not having evolved to use photon energy efficiently. To increase the photon efficiency of native photoenzymes, Nature

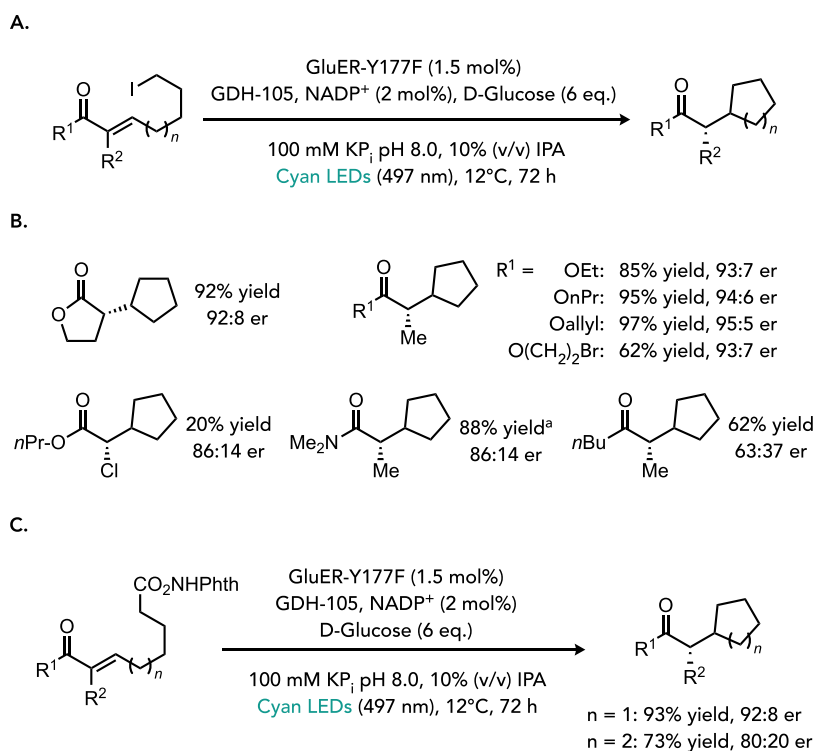


Figure 22. Formation of unactivated alkyl radicals. (A) General scheme for radical cyclizations involving alkyl iodides as precursors to nucleophilic radicals. (B) Representative substrate scope. (C) Radical cyclizations involving redox-active esters as a radical precursor.

often evolves independent proteins for light harvesting and catalysis. Together, the Hyster and Schlau-Cohen laboratories sought to improve the photon efficiency of EREDs by mimicking this strategy.⁸⁹ They conjugated highly absorbing dyes to the EREDs with the goal of having the dyes absorb the light and then transfer that energy to the enzyme-bound CT state to initiate radical chemistry.

They prepared a panel of conjugates with the different Atto dyes conjugated to the model enzyme *GluER-T36A*. Each dye had a different λ_{max} and fluorescence maximum. Controls with the same dyes conjugated to carbonic anhydrase showed a significant decrease in the fluorescence lifetime of the dye when it was conjugated to *GluER-T36A*. This indicated that *GluER-T36A* was quenching the dye's fluorescence and that energy transfer was occurring. Pleasingly, the fluorescence quenching corresponded to an increase in the photon efficiency of the enzyme for radical chemistry and a change in wavelength dependence. For the model lactam cyclization using an α -chloroamide, the yield with the Atto-565 *GluER-T36A* conjugate has a 4-fold improvement in yield (85%) when irradiated with dim green LEDs as compared to unconjugated *GluER-T36A* (19% yield) (Figure 20A). The enantioselectivity was improved using the Atto-565 *GluER-T36A* conjugate. This was an improvement in yield compared to cyan light at a similar intensity. Additionally, reactivity was enabled under these conditions for the intermolecular coupling with α -chloroamide and styrene (Figure 20B). Using the Atto-565 *GluER-T36A* conjugate resulted in a 51% yield of the coupled product while maintaining excellent enantioselectivity. Trace formation of the product was observed with just *GluER-T36A*.

Reductive cyclization of lactams using the biocatalytic CT complex mechanism produces very little hydrodehalogenated side product. This is postulated to be due to the hyper-

conjugative interaction of the alkene π -bond with the C–Cl σ^* necessary to form a strongly absorbing CT complex.^{85,87,90,91}

Based on this finding, the Hyster group then investigated whether other electron-rich SOMO-philes could provide the necessary $\sigma \rightarrow \pi^*$ interaction. It was found that oximes worked well to form the CT complex (Figure 21A) and act as a radical acceptor for the α -acyl radical to perform cyclizations.⁹² The product could then be derivatized to make valuable enantioenriched α -tertiary amines. Though wild-type EREDs failed to provide high yield and enantioselectivity, the authors used iterative site-saturation mutagenesis to generate three catalysts—*GluER-G6-F269V*, *GluER-G6-F269W*, and *NCR-D294W-Y343W*—that cyclized the model substrate with excellent yields and enantioselectivities with complementary reactivities on other substrates. Both 6- and 7-membered rings could be accessed using this method, and larger substituents on the oxime could be tolerated using a smaller oxime-protecting group. These products could be easily derivatized using reductants to form the α -tertiary amines or reduction of the lactam (Figure 21B).

Having demonstrated the ability of EREDs to template charge-transfer complexes that would not otherwise form in solution, the Hyster lab sought to exploit this feature to form CT complexes with functional groups that do not typically form such complexes in solution due to low electron affinity or poor electrostatic attraction to electron donors. Rather than generating electrophilic α -acyl radicals, it was proposed that alkyl iodides could be competent at forming these enzyme-templated charge-transfer complexes.⁹³ This would form an unstabilized nucleophilic alkyl radical capable of reacting with electrophilic alkenes, and enzymatic control over these additions could provide unprecedented levels of stereoselectivity at the resulting α -position.

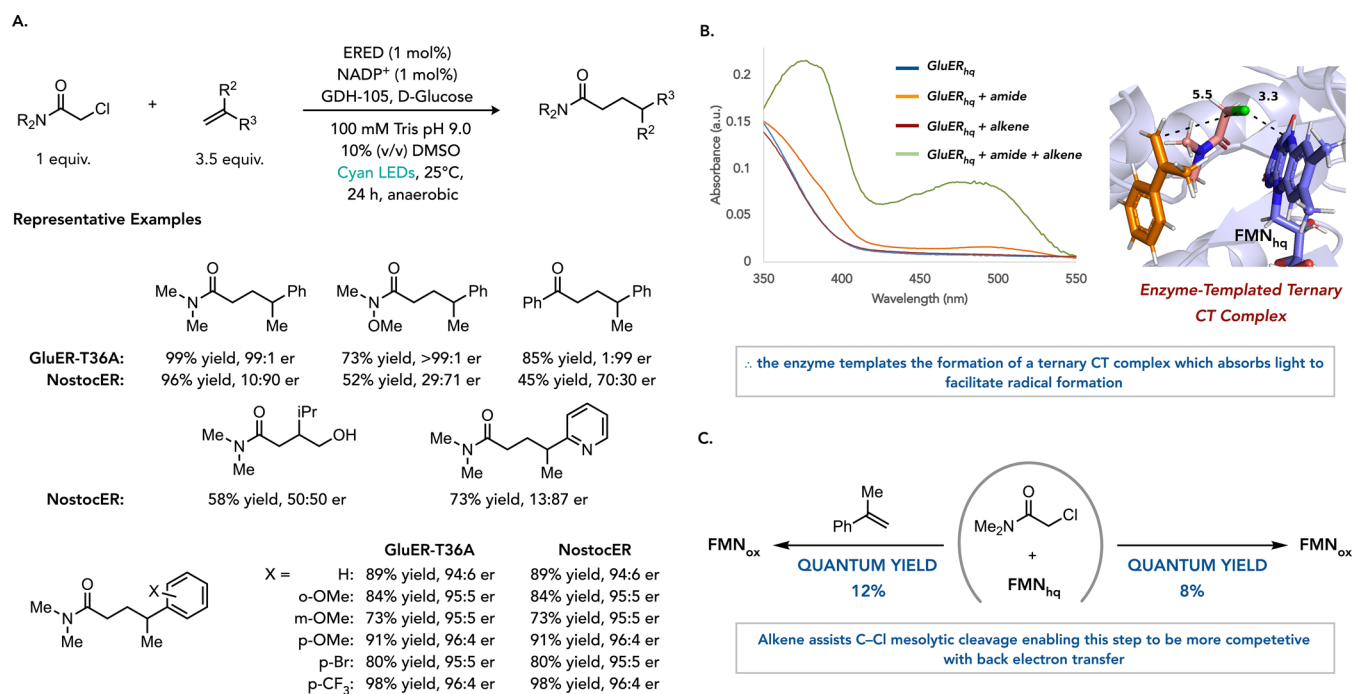


Figure 23. Intermolecular coupling of chloroamides with alkenes using EREDs. (A) General scheme for an intermolecular hydroalkylation of olefins catalyzed by GluER-T36A and NostocER. (B) UV–vis spectroscopy for an enzyme-templated ternary charge-transfer complex. (C) Quantum yield as determined by transient absorption spectroscopy.

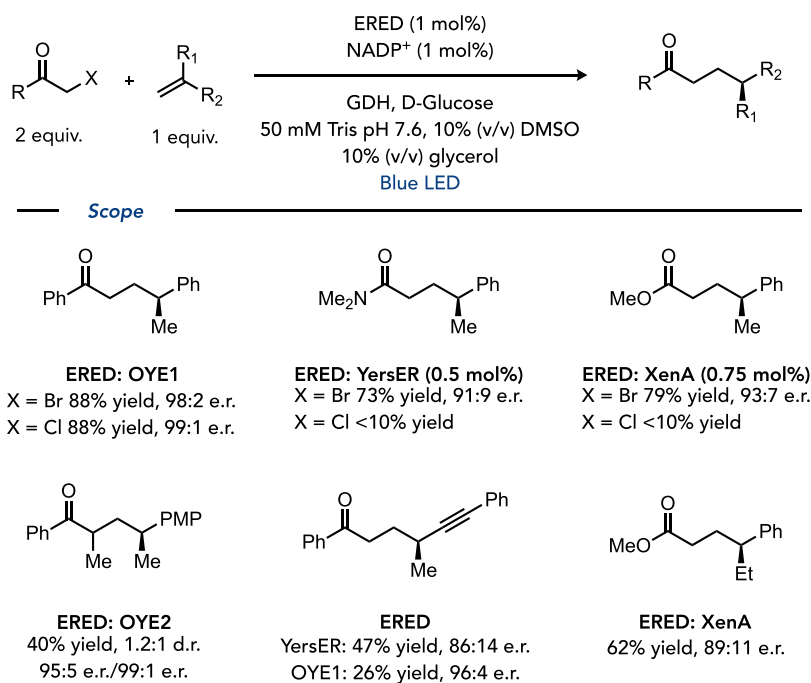


Figure 24. Intermolecular coupling using bromoketones.

Initial studies were conducted using a lactone-bearing substrate, revealing that the same GluER-Y177F mutant found previously provided higher yield and enantioselectivity. Cooling and degassing the reaction mixture increased the yield and selectivity, enabling the reactions to be conducted on a preparative scale. Reactions with acyclic acrylates were generally found to have high yields and enantioselectivities, and variation at the α -position is also tolerated (Figure 22B). This process was also viable for addition into α -unsaturated

ketones and acrylamides, though the latter required a different enzyme. 6-*exo*-trig cyclizations were shown to be feasible, though at higher enzyme loading. Finally, the authors demonstrated that NHPI esters could be used instead of alkyl iodides as nucleophilic radical precursors, expanding the types of substrates amenable to photoenzymatic catalysis (Figure 22C).

Having accomplished several intramolecular radical additions catalyzed by EREDs, the Hyster group investigated an

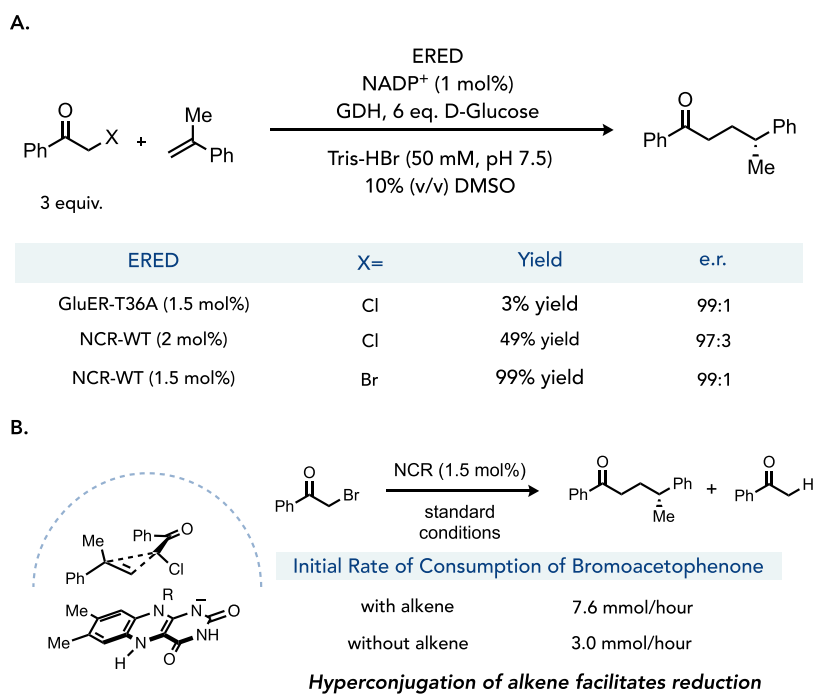


Figure 25. Dark hydroalkylation reactions with EREDs (A) Optimization of dark hydroalkylation by enzyme modification. (B) Alkene accelerated alkyl halide reduction.

intermolecular system to couple α -chloroacetamides with alkenes (Figure 23A).⁹⁰ For this type of coupling reaction to be effective, both substrates must be present within the protein active site before radical formation. The absence of the alkene coupling partner would result in the formation of the hydrodehalogenated product. In an initial survey, they found that α -methylstyrene could be coupled to α -chloroacetamide when irradiating *GluER-T36A* with cyan LEDs to afford the γ -stereogenic substrate (*R*-enantiomer) in good yield and excellent enantioselectivity. A homologous ERED from *Nostoc punctiforme* (*NostocER*) was used to access the *S*-enantiomer. The authors found that a higher-order CT complex was responsible for gating radical formation. When only the α -chloroacetamide is bound within the protein active site, a weakly absorbing CT complex is formed, which was found to have low molar absorptivity (Figure 23B). However, upon binding of the alkene, a more strongly absorbing CT complex is formed. This higher-order CT complex also displays higher quantum efficiency than the one formed without the alkene (Figure 23C). A gating mechanism is achieved, as both the alkene and α -chloroacetamide are required to form the CT complex responsible for radical formation. Various tertiary α -chloroacetamides are well-tolerated, and α -chloroacetophenone was also shown to be an effective substrate. Substitution on the styrene partner is tolerated on both the alkene's arene and the α -position (Figure 23A). Other alkene partners, including vinylpyridines, allylic amines, and allylic alcohols, are also tolerated, although the product is formed in modest yield.

Zhao and co-workers published a study detailing using old yellow enzyme 1 (OYE1) to catalyze the hydroalkylation of terminal olefins using α -bromo ketones as an organic halide using blue LEDs (Figure 24).⁹⁴ The opposite enantiomer of the product can be formed using either *XenA* or *XenB* in modest selectivity and low yield. This system is effective for styrenyl and enyne alkenes. Aromatic ketones are the highest yielding alkyl halides, although α -bromoester and α -bromo-

amides are also tolerated via this mechanism. UV–vis spectroscopy studies suggest that radical formation occurs via the excitation of a CT complex between the flavin cofactor and alkyl halide. Isotopic labeling experiments suggest that radical termination occurs via hydrogen atom transfer from flavin; however, the authors also postulate that a tyrosine within the protein active site (Tyr-196) can serve as a source of a hydrogen atom. Density functional theory (DFT) calculations supported the authors' proposed mechanism.

A key difference between the Zhao and Hyster systems is the wavelength of light used to initiate radical formation. Zhao reports a charge-transfer complex between the bromoacetophenone and FMN_{hq} with a maximum absorption at ~ 475 nm, while Hyster observes a complex between the chloroamide and FMN_{hq} with a maximum absorption at ~ 495 nm. As bromoacetophenone is more oxidizing than the chloroamide, one would expect it to have a red-shifted CT complex. Since substrate electronics do not strongly correlate with CT complex absorption, the Hyster group hypothesized that the protein significantly influences how strongly the cofactor and substrate interact. Based on this understanding, they reasoned that certain proteins would cause the substrates to interact more strongly with the cofactor, resulting in more ground state charge transfer, enabling certain reactions to proceed in the dark rather than relying on photoexcitation. When looking at the coupling of α -chloroacetophenone with α -methylstyrene, they found that *GluER-T36A* could catalyze the coupling in the dark in 3% yield with 97:3 er (Figure 25A). However, when using NCR (nicotinamide-dependent cyclohexenone reductase (NCR) from *Zymomonas mobilis*), the reaction occurred in 49% yield with the same enantioselectivity.⁹⁵ Changing to α -bromoacetophenone led to product formation in 99% yield with 99:1 er. The rate of α -bromoacetophenone consumption is enhanced in the presence of alkene, suggesting that the alkene influences substrate reduction. The Hyster group hypothesized that a hyperconjugative interaction

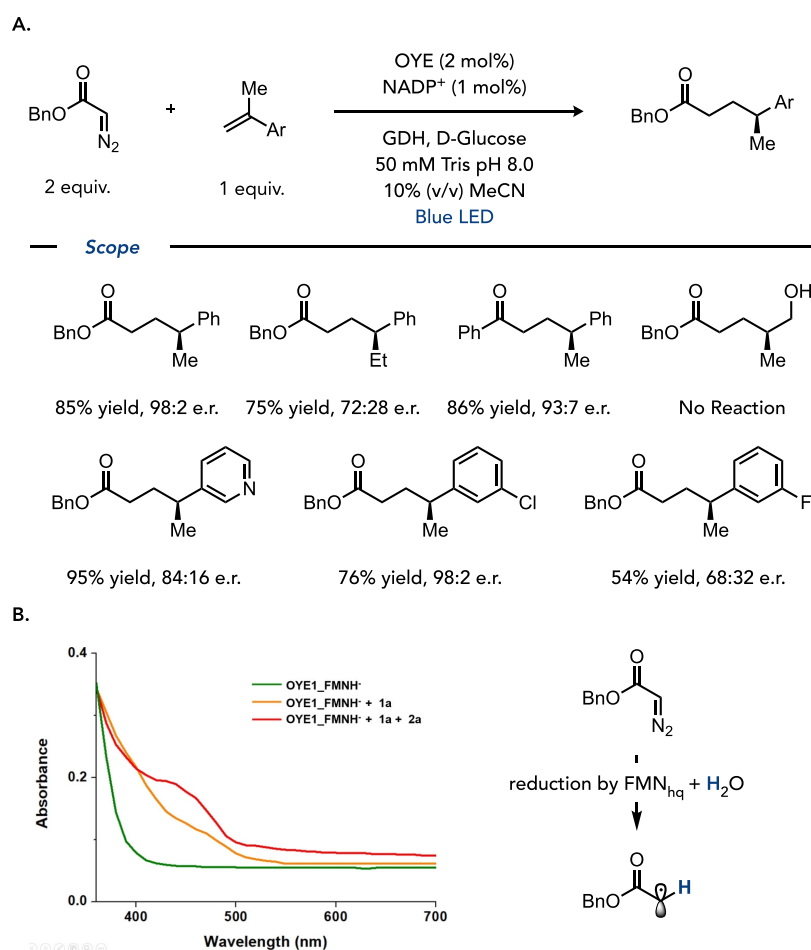


Figure 26. Diazoesters and electrophiles for photoenzymatic coupling with alkenes. (A) General scheme for an intermolecular hydroalkylation of olefins using diazoesters. (B) UV-vis spectroscopy for an enzyme-templated ternary charge-transfer complex and mechanism of proton-coupled diazo reduction. Adapted with permission from *Angew. Chem. Int. Ed.* **2023**, *62*, e202214135. Copyright 2023 John Wiley and Sons.

between the alkene and the σ^* orbital of the C–Br bond is responsible for the enhanced consumption rate (Figure 25B). This interaction functions as a gating mechanism to ensure radical formation only occurs when the alkene is present, an essential feature for intermolecular couplings. These studies suggest that the wavelength of light used to promote this family of reactivity is highly dependent on how well the protein facilitates ground state charge transfer in the CT complex. Blue light can initiate reactions in poorly coupled systems, while highly coupled systems can initiate using cyan or potentially longer wavelengths of light.

In a subsequent study, Jia and Xu explored diazoesters as electrophiles for photoenzymatic hydroalkylations with EREDs (Figure 26A).⁹⁶ Using OYE1, benzyl 2-diazoacetate could be coupled with α -methylstyrene when irradiated with visible light to afford the coupled product in 85% yield with 98:2 er. In contrast to the α -haloesters, which are prone to hydrolysis, the diazoesters afford coupled products across a wide variety of styrenyl substrates. Non-styrenyl substrates were unreactive. UV-vis experiments indicate the intermediacy of an enzyme-templated charge-transfer complex formed between the diazoester, alkene, and reduced enzyme, mirroring the observation by Hyster and co-workers with α -chloroamides (Figure 26A). Isotope incorporation experiments indicate that the diazoester is photoreduced in a proton-coupled electron-transfer event to afford an α -acyl radical that can react with the

alkene to form a benzylic radical which is quenched via hydrogen atom transfer from flavin.

The Hyster lab sought a new radical termination pathway that differed from the reductive radical quench that had been typically studied for photoenzymatic reactions. A β -scission or radical/polar crossover from a β -silyl radical was thought to be an effective new strategy for radical termination that would lead to an alkene-containing product capable of further manipulation. This hypothesis was tested using an α -chloroamide substrate bearing a pendant allyl silane. Using a mutated ERED, *GluER-G6*, and conditions like those used in previous α -chloroamide cyclizations,⁸⁵ the desired product was observed in 92% yield with >99:1 er. <5% yield of the reductive TMS-containing product was observed (Figure 26A). Control experiments show that an NADPH cofactor turnover system (GDH, glucose) is required for high yield: a unique feature for a redox-neutral transformation.

Further experiments show that the initial electron transfer does not occur from a ground state flavin species. Transient absorption spectroscopy (TAS) was used to further elucidate the mechanism. Pump-probe experiments showed multiple species being formed and consumed throughout the catalytic turnover. The data is consistent with an initial mesolytic cleavage, like the previously studied reductive mechanism, followed by an event attributed to the β -scission of the TMS group. The final event corresponds to the decay of the FMN

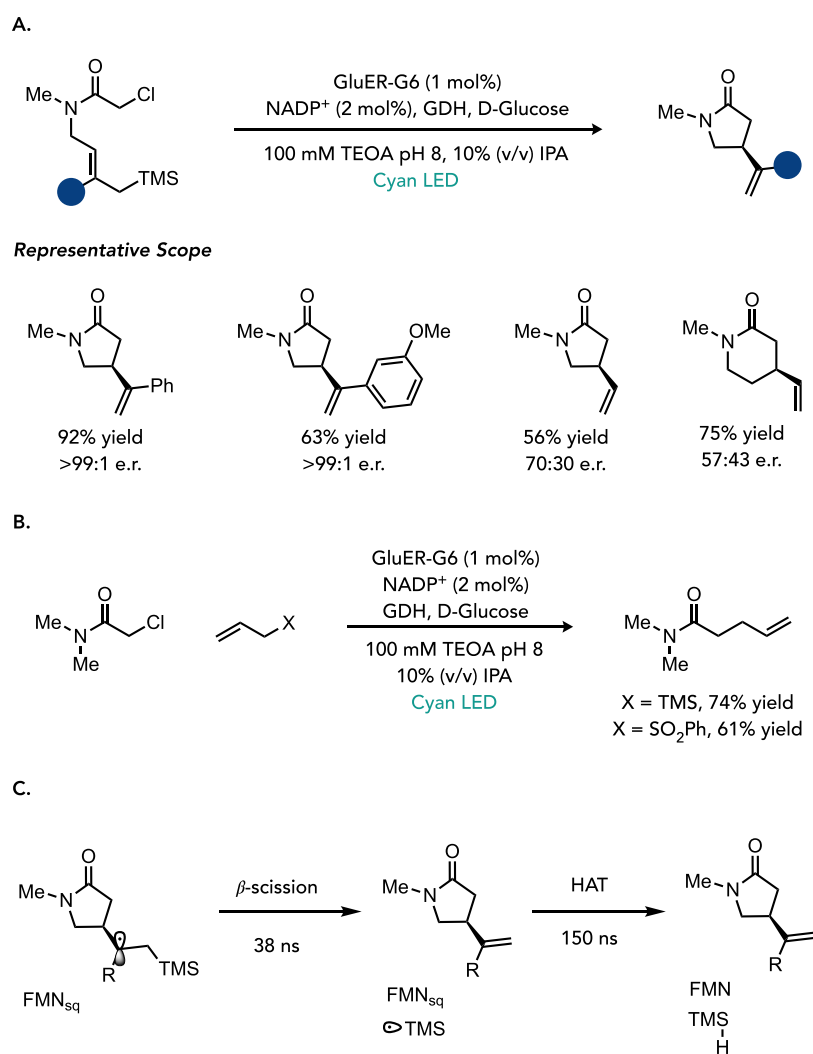


Figure 27. Radical termination via β -scission of silyl groups. (A) General scheme and scope for a radical allylation involving allyl silanes. (B) Examples of an intermolecular coupling. (C) Radical lifetimes as supported by transient absorption spectroscopy.

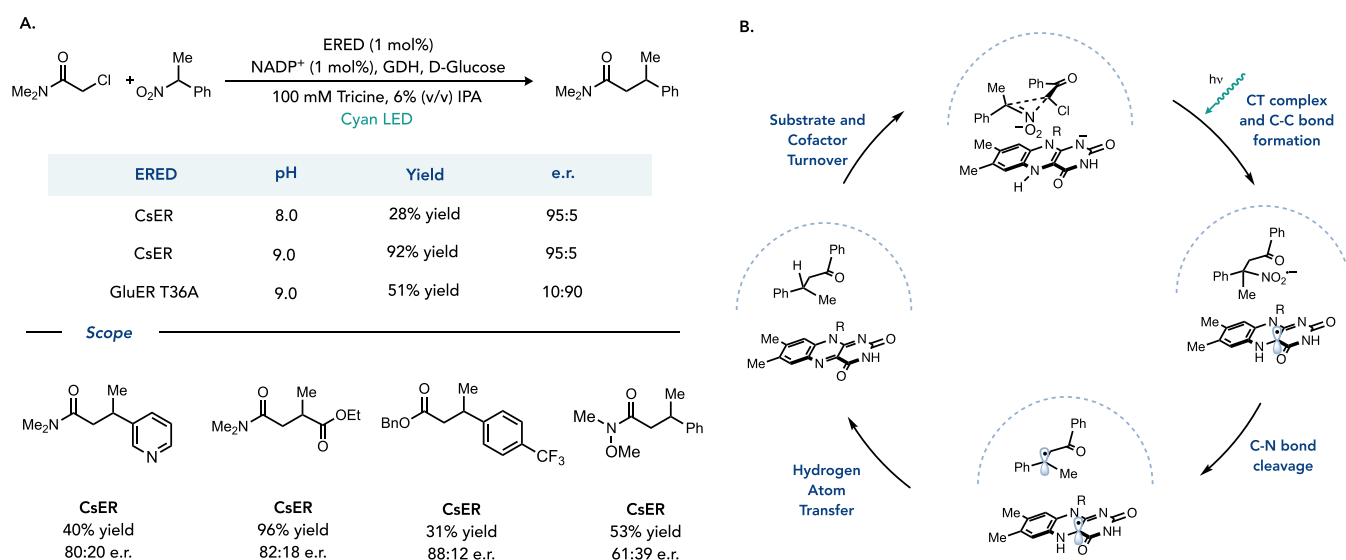


Figure 28. Enzymatic Csp^3 - Csp^3 cross electrophile coupling. (A) General scheme for ERED-catalyzed cross-electrophile coupling and representative substrate scope. (B) Proposed reaction mechanism.

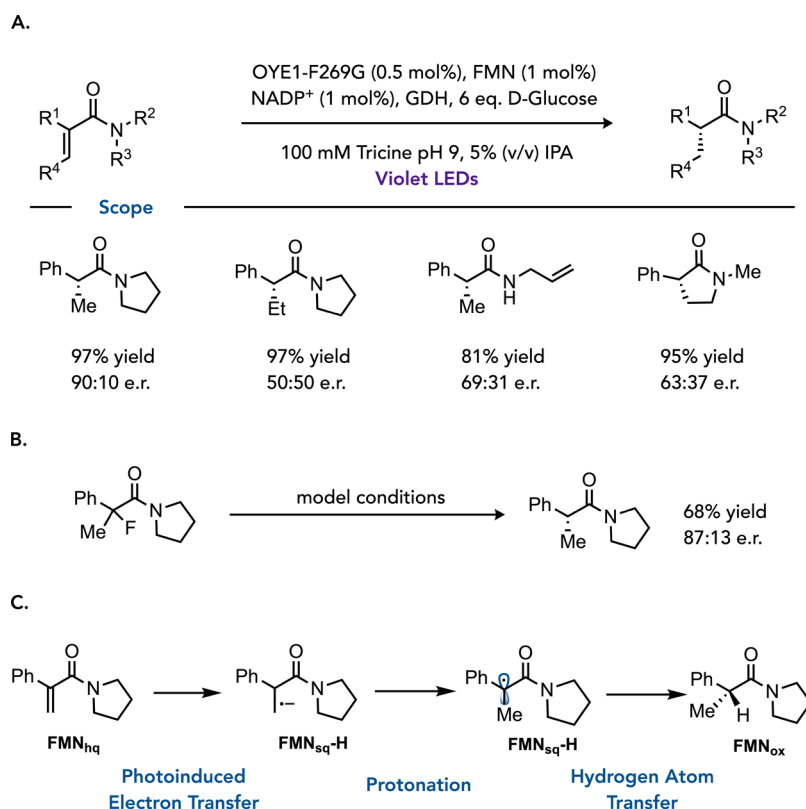


Figure 29. Direct excitation of flavin. (A) General reaction scheme for photoinduced alkene reduction. (B) Defluorination of α -fluoroamides using this approach. (C) Mechanism of reduction involved direct excitation of FMN_{hq} .

semiquinone to the oxidized quinone, indicating that the released silyl radical abstracts a hydrogen atom from FMN_{sq} (Figure 27C).

The enzyme accommodates substrates with arenes bearing *ortho*, *meta*, and *para* positions and alkyl substituents giving good yields and enantioselectivity. Unsubstituted allyl silanes also gave good yields but modest enantioselectivities. *5-exo-trig*, *6-exo-trig*, and *7-exo-trig* cyclizations were all well-accommodated with this approach. Intermolecular couplings were also afforded to form amides with terminal alkenes. The β -scission strategy was also extended to other cleavable groups, such as sulfones and silyl enol ethers (Figure 27B).⁹⁷

Cross-electrophile couplings are difficult to achieve using traditional metal catalysis due to the metal's inability to distinguish between coupling partners.⁹⁸ They are also difficult to render asymmetric.⁹⁹ The Hyster lab sought to develop a biocatalytic, asymmetric cross-electrophile coupling using nitronates as coupling partners in a quaternary CT complex mechanism (Figure 28A).¹⁰⁰ Although nitronates are easier to reduce, the α -chloroamide should be preferentially reduced due to its unique ability to form CT complexes with FMN_{hq} . Pleasingly, an ERED from Prozomix, CsER, catalyzed the desired transformation with moderate yield and excellent enantioselectivity. Increasing the pH to 9 further increased the yield to 92%, which the authors hypothesize is because the more-basic pH increased the concentration of active nitronate species. *GluER* T36A could catalyze the same transformation to give the opposite enantiomer with slightly decreased yields (51% yield, 10:90 er). The reaction tolerates electron-rich and -poor arenes but was limited to smaller α -substituents on the nitronate.

UV-vis studies indicated the proposed CT complex between FMN_{hq} , the nitronate, and the α -chloroamide was formed (Figure 27B). A nitronate was used instead of the model nitronate due to ground state reduction of the nitronate by flavin observed via UV-vis studies. Interestingly, no reduction products of the nitronate were observed when the nitronate was mixed with CsER, turnover mix, and visible light irradiation. When photoredox methods were used, only reduction products of the nitronate were observed, with no coupled product formed. This suggests that enzymatic reduction is reversible, and the enzyme cannot further reduce the nitronate. A resubjection experiment was performed to prove the mesolytic C–N bond cleavage was responsible for the denitration to form the coupled product. When nitromethylbenzene was used as a coupling partner, the denitrated and nitro-containing products were formed. The nitro-containing product was resubjected to the reaction conditions; however, no conversion was observed. This indicates the nitro-containing product is not an intermediate in this reaction and mesolytic cleavage is responsible for the denitration.

The previous examples of non-natural photoreactivity in EREDs are substrate-specific since they go through a photoexcitation of a CT complex formed between the FMN_{hq} and a substrate in the active site.^{85,91,93,90} While this enables electron transfer to be initiated with blue or cyan light, it limits the types of substrates that can be reduced. In response to this limitation, the Hyster lab sought to develop a substrate-agnostic reaction utilizing direct excitation of flavin in EREDs to initiate electron transfers.¹⁰¹ It was envisioned that the stereoselective reduction of acrylamides could be achieved using a direct excitation mechanism. Because they resemble the native substrate of EREDs, it was expected that the radical

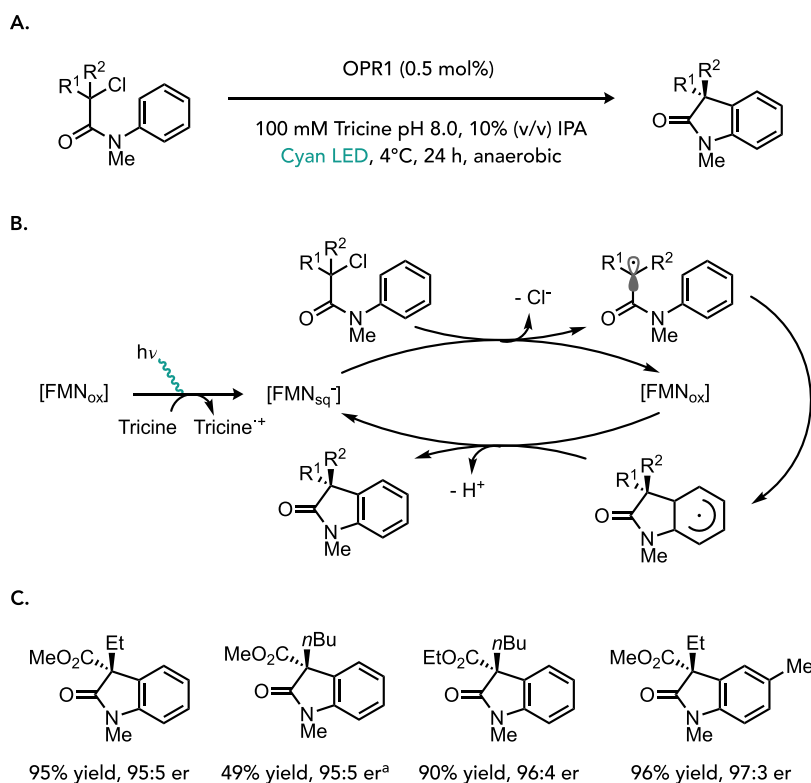


Figure 30. Radical initiation from flavin semiquinone. (A) General scheme for OPR1-catalyzed oxindole synthesis. (B) Proposed reaction mechanism involving initiation from FMN_{sq} . (C) Representative substrate scope.

formation could be constrained to the active site. These substrates cannot be reduced via the native mechanism. Excitingly, irradiation of model substrate across a panel of EREDs with violet LEDs furnished products with good yields and differing enantiomeric ratios, with OYE1 giving the best er (Figure 29A). The yield with OYE1 was further improved by adding exogenous FMN to ensure the protein was saturated with the cofactor. A single round of site-saturation mutagenesis yielded the improved variant OYE1-F269G, which catalyzed the reduction with quantitative yield and 90:10 er. The direct excitation mechanism could also be extended to reductively cleave C–F bonds (Figure 29B).

The reaction is initiated via excitation of FMN_{hq} by violet LEDs to generate a potent single-electron reductant that reduces the acrylamide alkene, producing the radical anion and neutral FMN_{sq} (Figure 29C). Protonation of the radical anion furnishes a stabilized α -acyl radical, which can be terminated via HAT from the semiquinone to set the α -stereocenter. Deuterium incorporation experiments support the protonation step of the mechanism, where the β -position is 90% deuterated when the reaction is run in a deuterated buffer. However, there is an appreciable amount of deuteration of the α -position with deuterated buffer and a lack of deuteration when the reaction is run using d_6 -glucose. This indicates significant deuterium washout due to the acidification of the N5–H bond in the semiquinone state.

In both cases, the flavin cofactor is responsible for two single-electron reductions, starting from the fully reduced FMN_{hq} state, moving through the semiquinone FMN_{sq} and ultimately terminating the radical species through hydrogen atom transfer to generate the fully oxidized FMN_{ox} state. At this point, the cofactor is reduced back to FMN_{hq} by NADPH to complete the catalytic cycle. In a departure from this

pattern, the Hyster group envisioned a redox-neutral mode of reactivity in which flavin is competent as both a reductant and an oxidant. This was accomplished via asymmetrically generating 3,3-disubstituted oxindoles (Figure 30A).¹⁰²

To achieve this redox-neutral reactivity without reductive side-product formation, the authors developed a system to take advantage of the deprotonated anionic semiquinone FMN_{sq}^- as the initiating reductant producing FMN_{ox} to act as the terminating oxidant (Figure 30B). This system relies on the photoreduction under cyan light of FMN_{ox} to FMN_{sq}^- by tricine present in the buffer solution. At this point, FMN_{sq}^- can reduce the chloroamide substrate, generating an α -acyl radical and FMN_{ox} . Since FMN_{ox} cannot further reduce this substrate, cyclization into the pendant aromatic ring occurs to generate the oxidizable vinylogous α -amido radical. This cyclization occurs with excellent facial selectivity, resulting in high enantioselectivity. Oxidation by FMN_{ox} triggers elimination to restore aromaticity, yielding the desired oxindole product and regenerating FMN_{sq}^- .

Initial studies indicated good yield and selectivity from the enzyme 12-oxophytodienoate reductase (OPR1), and this enzyme was used to demonstrate scope (Figure 30C) following reaction optimization. Variation of the α -substituent is well-tolerated, particularly among longer linear groups. Different ester substituents were accepted and afforded products with high yield and selectivity. Though *ortho* substituents were unreactive on the aryl ring, electron-donating *para* substituents were well-tolerated, and electron-withdrawing ones were functional under high-temperature conditions. Electron-donating *meta* substituents were also reactive but produced a mixture of regioisomers. Lastly, product formation was still observed when the substrate-activating ester group was removed, though

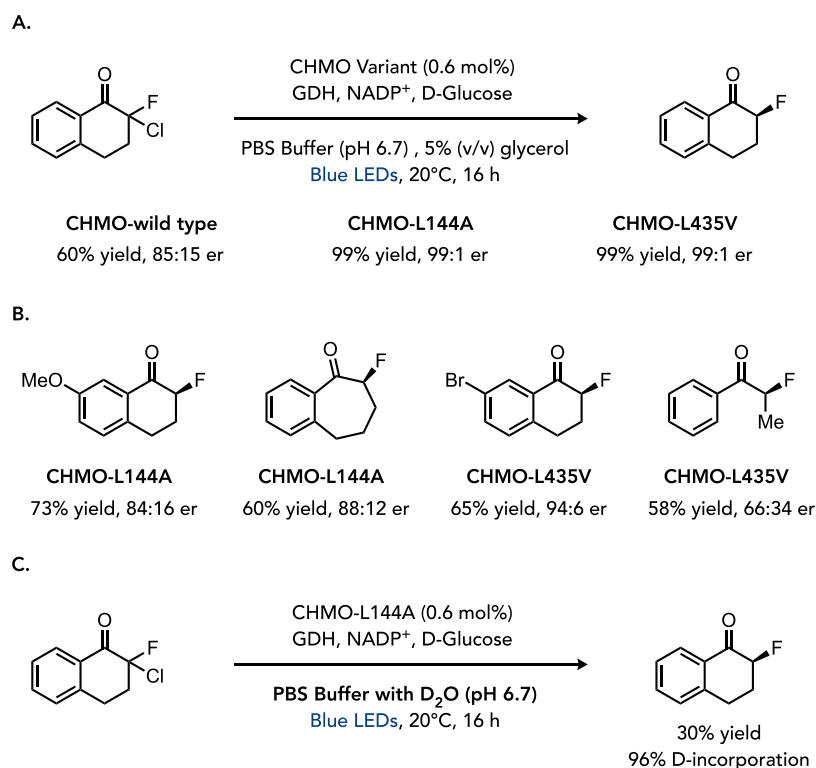


Figure 31. Radical hydrodehalogenation using cyclohexane monooxygenase. (A) General scheme for BVMO-catalyzed hydrodehalogenation. (B) Representative substrate scope. (C) Mechanistic experiment to support radical termination via an electron-transfer/proton-transfer process.

Monomer	GOx (0.75 μ M)			
10% w/v	glucose (3 mM) 200 mM Tris, pH 5.5 405 nm LED, 6 h			
Polymer	Conv (%)	M_{th} (kg/mol)	M_{GPC} (kg/mol)	\bar{D}
poly-DMA ₂₀₀	>99	20.4	22.8	1.04
poly-AML ₁₈₈	94	27.2	23.4	1.13
poly-PEGA ₂₀₀	>99	96.6	82.1	1.16
poly-PEGMA ₂₀₀	>99	100.6	100.1	1.14

DMA AML PEGA PEGMA

Figure 32. Polymer synthesis of photoexcited glucose oxidase.

the mechanism by which this reaction initiates is not yet understood.

2.4. Flavin-Dependent Baeyer–Villiger Monooxygenase Photochemistry

Building on the observations with EREDs, Xu and Wu demonstrated that Baeyer–Villiger monooxygenases could serve as photoenzymes for radical hydrodehalogenation reactions (Figure 31A).¹⁰³ Using the cyclohexanone monooxygenase from *Acinetobacter* sp. (CHMO_{aciento}), the authors could hydrodehalogenate α -fluoro- α -chloro ketones to prepare the corresponding α -fluoro ketone in modest yield and enantioselectivity, targeting residues within the protein active site for a limited mutagenesis campaign, where large hydro-

phobic residues (leucine and phenylalanine) were mutated to hydrophobic residues of different sizes (alanine, valine, leucine, and phenylalanine). Using single mutations (CHMO-L144A or CHMO-L435V) afforded hydrochlorination of a tetralone in 99% yield with 99:1 er. The reaction was effective across various substituted tetralones, affording products with good yield and selectivity (Figure 30B). The reaction was also effective for acyclic ketones; however, the enantioselectivities were more modest. The authors propose that electron transfer occurs via photoexcitation of an enzyme-templated charge-transfer complex, mimicking electron-transfer mechanisms in EREDs. Additionally, the authors found that radical termination occurs via reducing the radical to the corresponding

Monomer 10% w/v	GOx (1.5 mM)				
	glucose (30 mM) 20 mM PBS, pH 7 405 nm LED				
Polymer	time (h)	Conv (%)	M_{th} (kg/mol)	M_{GPC} (kg/mol)	\mathcal{D}
PNVP ₄₆₅₀	24	93	517.0	489.2	1.32
PNVP ₄₆₅₀ -b-PNVP ₄₆₀₀	24	92	1028.2	1058.7	1.30
PDMA ₅₀₀₀	12	>99	495.9	528.9	1.33
PDMA ₅₀₀₀ -b-PNVP ₄₇₀₀	24	94	1018.3	998.2	1.35

Figure 33. Photoenzymatic polymerizations.

enolate, followed by stereoselective protonation, confirmed with isotopic labeling experiments (Figure 30C). This mechanism is distinct from what is often observed with EREDs.

2.5. Flavin-Dependent Photoenzymes for Radical Polymerization

The use of photoenzymatic catalysis has also been expanded beyond the synthesis of small molecules and into the realm of polymers. In 2019, the An group demonstrated that when irradiated, FAD-dependent glucose oxidase (GOx) can become an effective catalyst for a controlled radical polymerization process (Figure 32).¹⁰⁴ Inspired by the action of DNA photolyase, they show that irradiation of GOx with 405 nm light produces a photoexcited FAD cofactor that can initiate radical polymerization through sequential photoinduced electron-transfer (PET) events. Using *N,N*-dimethyl acrylamide (DMA) as a model monomer, quantitative conversion was observed in 6 h, producing PDMA with close to theoretical molecular weight (22.8 kg/mol vs 20.4 kg/mol predicted) and low dispersity ($\mathcal{D} = 1.04$), regardless of the presence of a chain-transfer agent. The reaction's monomer scope was investigated and found to be general and broad (Figure 31). High conversions were observed for most monomers within 6 h, with low dispersity and predictable molecular weights. Block copolymers and nanoparticles could also be synthesized under the optimized conditions. Most notably, poly(ethylene glycol) methyl ether methacrylate (PEGMA) was found to form an ultrahigh molecular weight (UHMW) polymer, PPEGMA, with molecular weight 973.5 kg/mol vs 990.6 kg/mol predicted, $\mathcal{D} = 1.39$. UHMW PPEGMA is unprecedented via controlled radical polymerization due to PPEGMA's high steric demand and low propagation rate coefficient. UHMW PPEGMA was generated in >99% conversion within 4 h, highlighting the power of this photoenzymatic method. It should be noted that these polymerizations are likely occurring outside the protein active site.

Several mechanistic studies were also undertaken. Control experiments showed that GOx, glucose, and light were necessary for polymerization. Replacing GOx with free riboflavin gave no conversion of DMA, indicating that fully reduced FADH, formed in the active site of GOx, is the photoactive species responsible for electron transfer. Electron spin resonance (ESR) indicates that polymerization occurs via a radical mechanism, while light on/off experiments indicate that photoexcitation is necessary for polymerization. The polymerization was observed to follow pseudo-first-order kinetics after an initial induction period of 40 min to 2 h.

The cause of the induction period is not well understood and is still under investigation. Further, this polymerization was found to be active even in the presence of oxygen, as the innate deoxygenation capability of GOx was not destroyed during irradiation.

In 2020, this photoenzymatic system was extended to synthesize ultrahigh molecular weight (UHMW) polymers using unconjugated monomers.¹⁰⁵ These monomers are typically difficult to develop into UHMW polymers due to the high incidence of chain termination and chain transfer during the process. As such, they are uncharacteristically difficult to control. Although reversible addition fragmentation chain-transfer polymerization (RAFT) polymerization techniques have been successfully developed to polymerize unconjugated monomers, the resulting products are usually of low molecular weight with high dispersity and low conversions. The photoenzymatic GOx conditions were adapted to the polymerization of *N*-vinylpyrrolidone (NVP) to assess the capability of GOx to catalyze the polymerization of unconjugated monomers. The product was obtained with good molecular weight (18.8 kg/mol vs 20.7 kg/mol predicted) and low dispersity ($\mathcal{D} = 1.19$) after 24 h in the presence of a xanthate chain-transfer agent (Figure 33). Control experiments showed that GOx, glucose, and light were all required for conversion, but the presence of the chain-transfer agent was not necessary.

High degrees of polymerization (DPs) ranging from 5000 and 10,000 were targeted to obtain an ultrahigh molecular weight PNVP. Ultrahigh molecular weight polymers were obtained with close to predicted molecular weights but high dispersity ($\mathcal{D} = 1.42$). The authors then assessed the impact of temperature on the dispersity of the formed UHMW PNVP. Lower temperatures led to lower dispersities at both DPs of 5000 and 10,000, with 10 °C being the optimal condition for the best balance of molecular weight and dispersity. It was hypothesized that the lower temperature likely mitigates deleterious side reactions like chain transfer and chain termination. After condition optimization, the system was extended to various unconjugated monomers and chain-transfer agents to enable a one-pot system for synthesizing block- and star-copolymers up to 1100 kg/mol (Figure 33).

2.5.1. Outlook for Flavin-Dependent Photoenzymes.

The versatility of the flavin cofactor opens the door to many modes of radical initiation and termination. While the current reports rely on reductive radical formation, oxidative methods should be accessible to flavoproteins, enabling new types of radical precursors. Radical termination occurs primarily via reductive mechanisms. The versatility of FMN_{sq} opens the

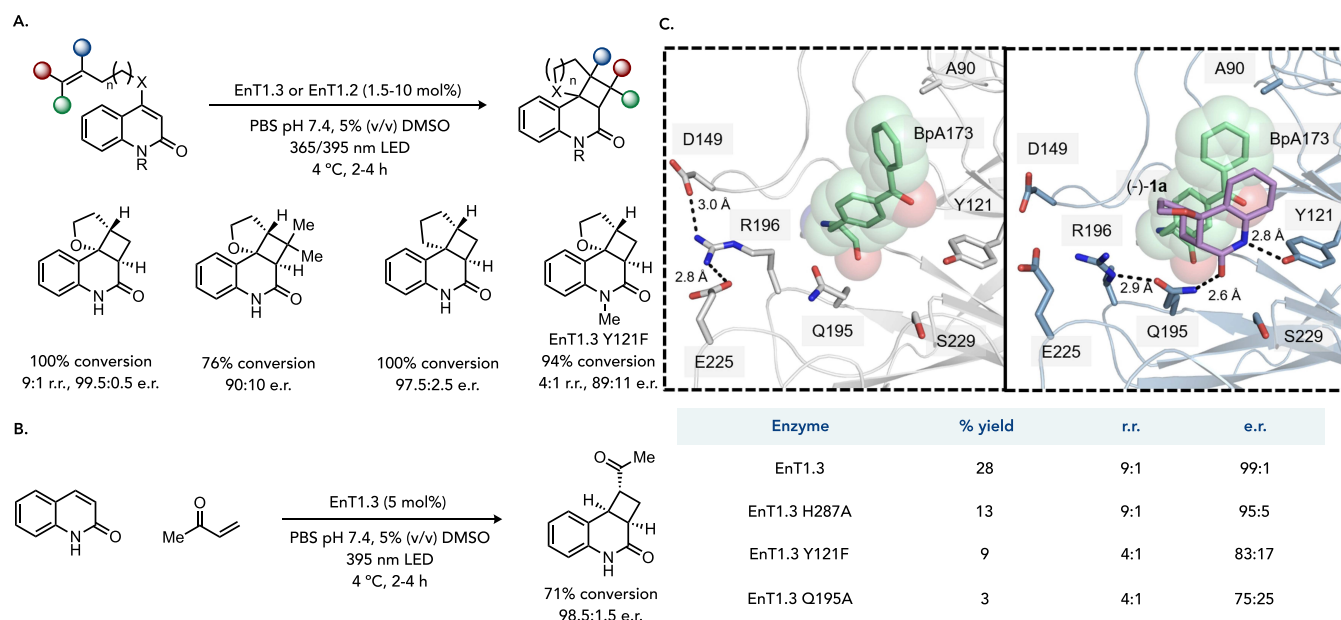


Figure 34. Computationally designed Diels–Alderase repurposed for $[2 + 2]$ cycloaddition. (A) General reaction scheme and representative substrate scope. (B) Example of an intermolecular $[2 + 2]$ reaction. (C) Crystal structures of the protein with the substrate in the active site and key hydrogen bonding interactions highlighted. (D) Knockout studies where key residues are mutated to break a hydrogen bonding contact. Adapted with permission from *Nature* **2022**, *611*, 709–714. Copyright 2022 Springer Nature.

door to oxidative mechanisms of radical termination. The discovery of new mechanisms for radical initiation and termination will significantly expand the synthetic utility of these reactions.

Beyond new reactions, this area of research will benefit from more mechanistic studies and a deeper understanding of their photophysics. For instance, the structural features that influence the absorption wavelength and intensity are poorly understood. Studies that provide more insight into these complexes could open the door to using new types of radical precursors or different wavelengths of light. In contrast to the FAP proteins, the EREDs and BVMOs display excellent photostability. However, total turnover numbers and turnover frequencies are poor. These metrics need to be improved for these reactions to be useful in chemical manufacturing.

2.6. Photoenzymes Using Non-natural Cofactors and Amino Acids

In contrast to the breadth of work on expanding the natural reactivity of enzyme cofactors with light irradiation, there has been relatively little progress on photoinitiated transformations via a covalently linked chromophore. Introducing non-natural cofactors opens the door to accessing reactivities inaccessible to chromophores in Nature. Green and co-workers recently reported a designed enzyme for enantioselective $[2 + 2]$ cycloadditions enabled by a noncanonical 4-benzoyl-phenylalanine (BpA) residue.¹⁰⁶ The authors selected a computationally designed Diels–Alderase (DA_20_00) as the starting scaffold because of the mechanistic similarities between thermal $[4 + 2]$ cycloadditions and photochemical $[2 + 2]$ reactions.¹⁰⁷ The authors introduced the BpA residue at position 173 in the active site of a computationally designed Diels–Alderase to generate the enzyme EnT1.0. Irradiation with 365 and 395 nm LEDs promoted triplet-energy-transfer (EnT) photocatalysis between the BpA residue and substrate, enabling the $[2 + 2]$ cycloaddition in modest yield, regioselectivity, and enantioselectivity.

Three rounds of directed evolution were conducted targeting residues that surround the enzyme active site. Ultimately a variant (EnT1.3) was accessed that catalyzed the desired $[2 + 2]$ reaction in 100% conversion with a 9:1 regioisomeric ratio and 99.5:0.5 er (Figure 34A). A crystal structure of the evolved biocatalyst with the quinolone product bound reveals substrate π -stacking interactions between the BpA173 and H287 side chains crucial for effective triplet energy transfer. The crystal structure also revealed hydrogen bonding interactions between the quinolone product and residues Y121 and Q195, postulated to be important for substrate orientation and activity. Indeed, the Y121F or Q195A mutation reduces yield and enantioselectivity (Figure 34C). In contrast to versions of this reaction catalyzed by small molecule catalysts, this reaction is not sensitive to O_2 , suggesting that the protein environment protects the benzophenone amino acid from O_2 and limits the formation of singlet oxygen. The authors demonstrated the scope of this transformation across various substituted alkenes and even found a variant that can catalyze an intermolecular reaction (Figure 34B).

Sun et al. concurrently published a similar enzyme-templated intramolecular enantioselective $[2 + 2]$ cycloaddition enabled by energy transfer from a noncanonical BpA residue.¹⁰⁸ The authors adapted a dimeric multidrug resistance regulator LmrR, previously known for its use in artificial metalloenzymes, as this protein has a large hydrophobic pocket at the subunit interface.¹⁰⁹ After incorporating the BpA residue as an F93BpA mutation, two additional rounds of site-saturation mutagenesis identified the beneficial mutants W96L and M8L to generate the photobiocatalyst TPe3.0. TPe3.0 can enable a $[2 + 2]$ cyclization of an alkene into a tethered indole in 85% yield with a 95:5 enantiomeric ratio. The free benzophenone can only catalyze this transformation in 10% yield under these reaction conditions. It is important to note that the interpretation of this type of control is complicated by the decreased solubilities of the photo-

catalyst and substrate under aqueous conditions. Running these controls in organic solvent can provide a better indication as to the inherent reactivity of the cofactor. The authors further improved upon this biocatalyst in a new variant designated TPe4.0_FBpA by layering in the A11N mutation to generate a new hydrogen bonding contact with the Boc-carbonyl on the indole core and modifying the BpA cofactor to 3'-fluoro-4-benzoylphenylalanine (FBpA), thus generating a new H–F hydrogen bonding contact. The evolved variants could catalyze [2 + 2] cycloadditions on various substituted indoles (Figure 35).

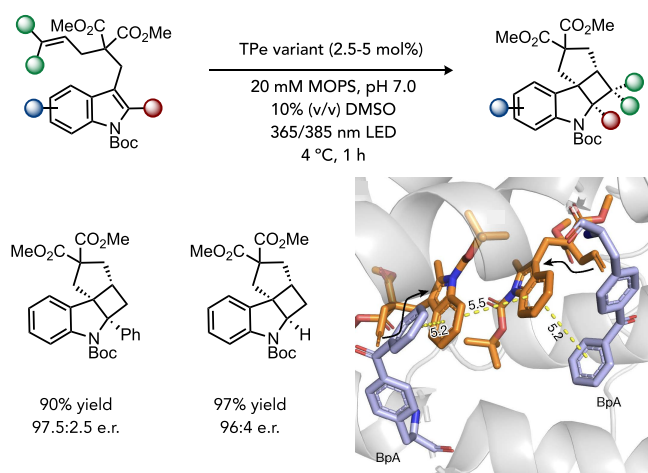


Figure 35. BpA substituted LmrR derived triplet photosensitizer biocatalyst for [2 + 2] cycloadditions. Adapted with permission from *Nature* **2022**, *611*, 715–720. Copyright 2022 Springer Nature.

In related studies, Wang and co-workers bioconjugated metal complexes to the surface of fluorescent proteins to drive CO₂ reduction to CO and phenyl synthesis from aryl halides (Figure 36A).¹¹⁰ In their initial study, the researchers targeted superfolder yellow fluorescent protein (sfYFP) as a chromophore for driving electron transfer to a transition metal complex appended to the surface of the protein. As sfYFP has a long excited state lifetime, the researchers replaced the chromophore residue tyrosine at position 66 with (BpA). When this mutation was coupled with mutations at positions 203 (Y203D) and 148 (H148E), they accessed a variant (PSP) where the benzophenone moiety can be photoreduced to the corresponding radical anion using ascorbate as a biologically relevant electron donor. Next, a nickel–terpyridine complex was covalently linked to the protein's surface through cysteine bioconjugation with an iodoamide appended to the terpyridine ligand. The distance between the metal complex and the chromophore proved important for achieving the most active metal complex. This best distance was 1.19 nm, which involved bioconjugation of the metal complex at position 95. Longer or shorter distances resulted in decreased catalyst activity. This biohybrid artificial metalloenzyme provides 75 catalyst turnovers for converting CO₂ to CO. These turnover numbers could be increased to 87 TON by introducing tyrosines close to the metal complex to facilitate the proton-coupled electron-transfer events. Ultimately, this catalyst achieves a quantum efficiency of 2.6%, surpassing what was achieved with CdS nanorods with the same nickel–terpyridine catalyst (Figure 36B).

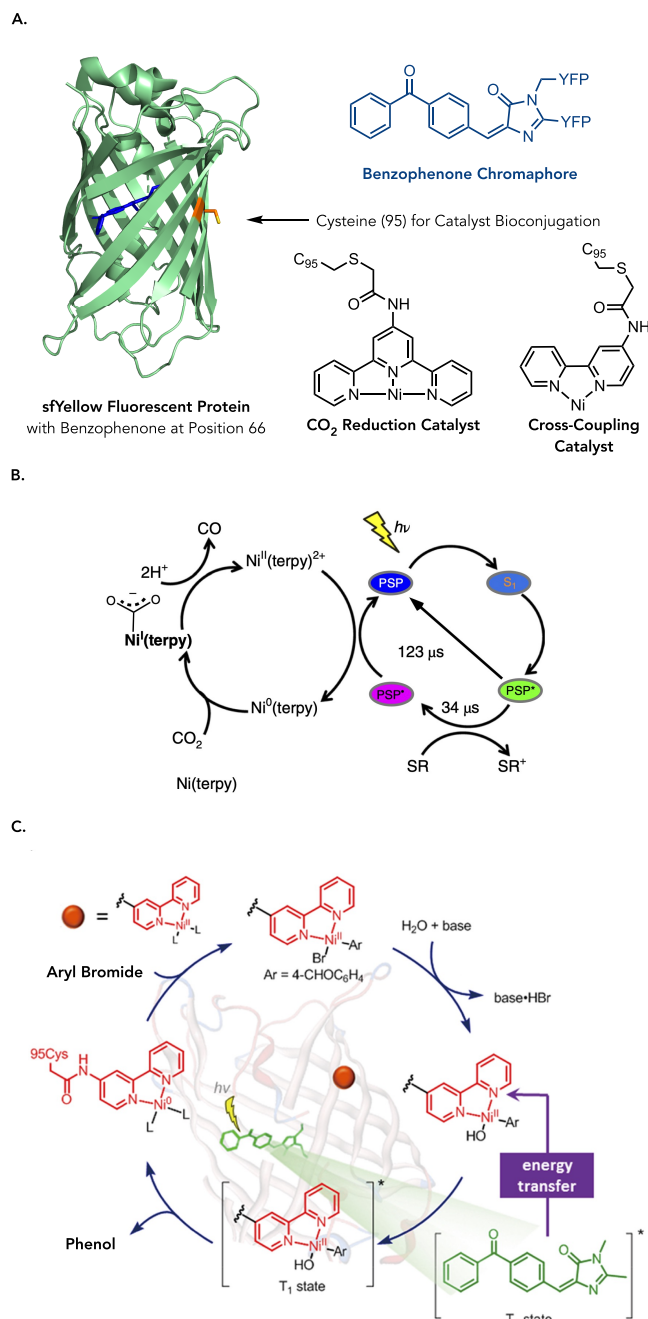


Figure 36. Genetically encoded photosensitizers for artificial metalloenzymes. (A) Design of an artificial metalloenzyme using a genetically encoded chromophore. (B) General mechanism for CO₂ reduction using a Ni(terpy) complex linked to a genetically encoded photoreductant. Adapted with permission from *Nat. Chem.* **2018**, *10*, 1201–1206. Copyright 2018 Springer Nature. (C) Mechanism of phenol synthesis using an artificial metalloenzyme with a genetically encoded photosensitizer. Adapted with permission from *J. Am. Chem. Soc.* **2021**, *143*, 617–622. Copyright 2021 American Chemical Society.

In a follow-up study, Wang used the same chromophore for a nickel-catalyzed conversion of aryl halides to phenols.¹¹¹ In the initial report of this reactivity, MacMillan used a nickel–bipyridine catalyst with an iridium photocatalyst.¹¹² Using the same PSP protein previously reported but instead bioconjugated with a bipyridine ligand at position 95 resulted in a catalyst that could catalyze the conversion of *p*-bromobenzyl-

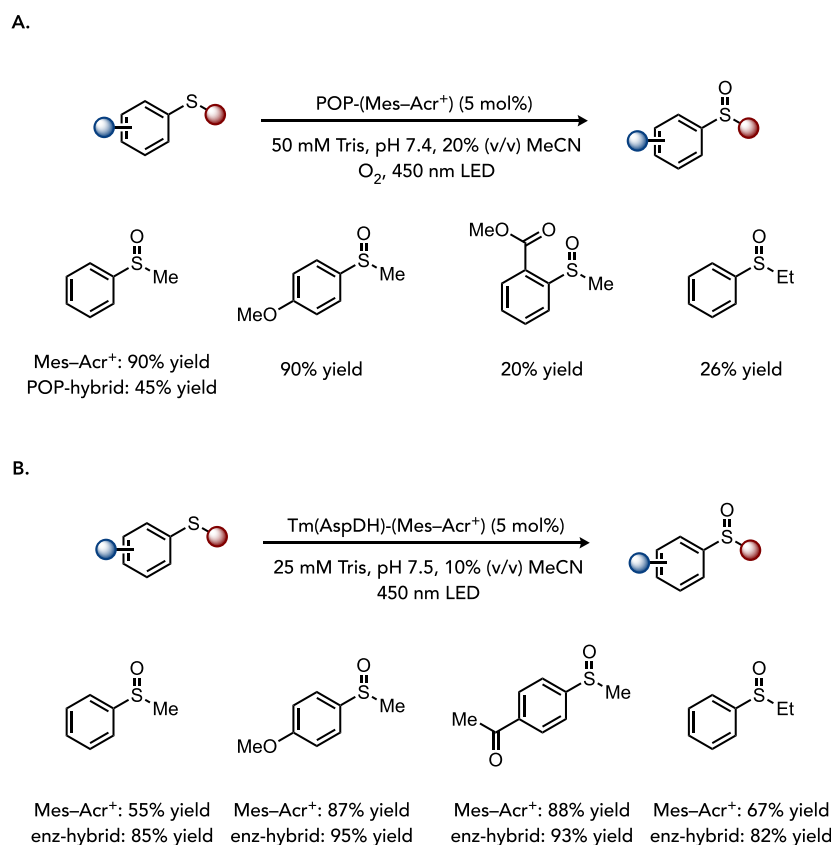


Figure 37. Bioconjugation approach to photoenzyme preparation. (A) Artificial photoenzyme prepared by bioconjugation of an acridinium photocatalyst into prolyl oligopeptidase for thioether oxidation. (B) Artificial photoenzyme prepared by bioconjugation of an acridinium photocatalyst into thermostable aspartate dehydrogenase for thioether oxidation.

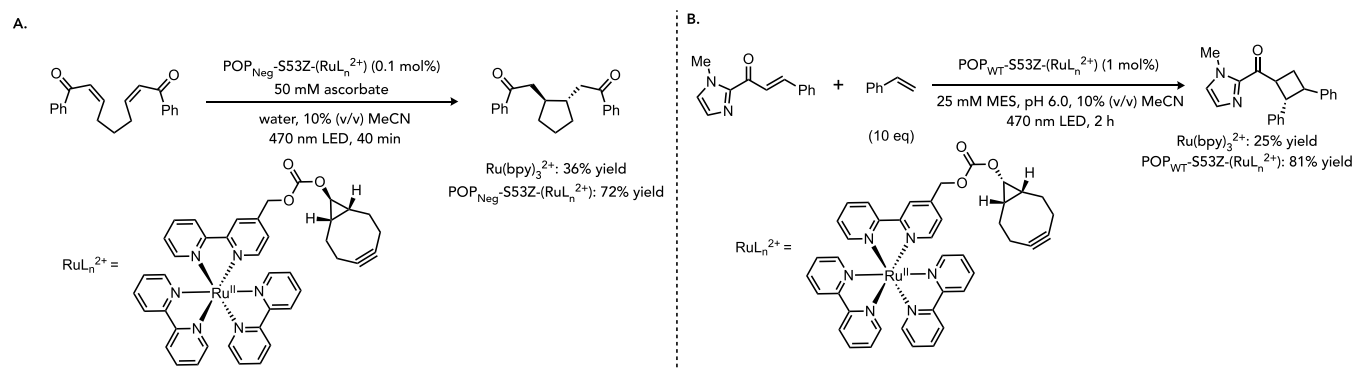


Figure 38. Click bioconjugation for photoenzyme synthesis. (A) Artificial photoenzyme prepared by bioconjugation a Ru(bpy)₃ photocatalyst into prolyl oligopeptidase for an intramolecular 2 + 2 reaction. (B) The intermolecular variant.

aldehyde to *p*-hydroxybenzaldehyde in 98% yield. This artificial metalloenzyme was effective for various aryl halides, including aryl chlorides, bromides, and iodides. Moreover, this catalyst could be used for C–N bond formation to afford anilines in promising yields. **Transient absorption spectroscopy** experiments suggest that the reaction occurs via triplet sensitization of the nickel(II) complex by the benzophenone moiety in the protein to facilitate reductive elimination. While this mechanism is distinct from the redox one originally proposed by MacMillan, where the photocatalyst oxidizes the nickel complex to Ni(III) to facilitate reductive elimination, this mechanistic pathway cannot be conclusively ruled out by their experiments.¹¹² Energy transfer to facilitate reductive elimination has been observed for related metallophotoredox

reactions, supporting the viability of the proposed mechanistic pathway (Figure 36C).¹¹³

In a complementary approach incorporating chromophores in enzyme active sites, Lewis and co-workers covalently linked Mes-Acr⁺ photocatalysts into a prolyl oligopeptidase from *Pyrococcus furiosus* (POP).¹¹⁴ The authors selected this protein based on its large β -barrel enclosed active site. The active serine was mutated to *p*-azido-*L*-phenylalanine (Z) to facilitate a strain-promoted azide–alkyne cycloaddition (SPAAC) with a cyclooctyne functionalized photocatalyst. The photocatalyst–protein hybrid was competent at thioanisole sulfoxidation in up to 90% yield, although the product is formed as a racemate (Figure 37A).

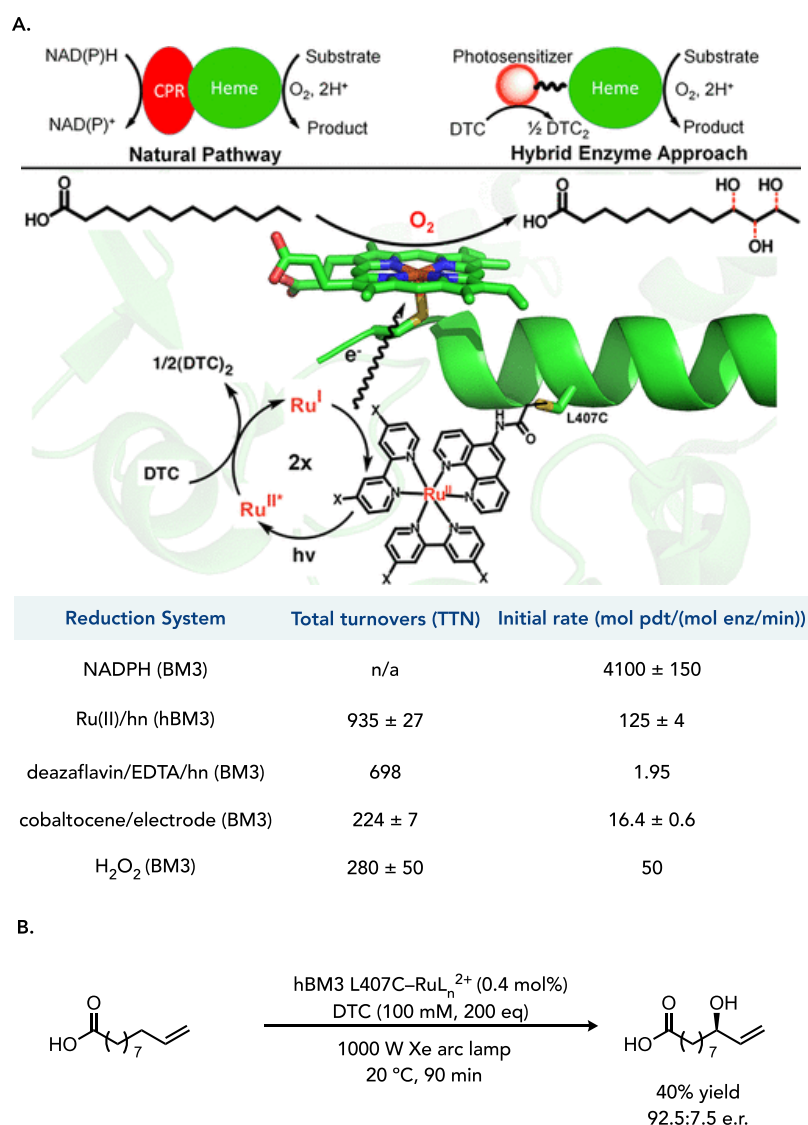


Figure 39. Synergistic catalysis in P450s. (A) Design strategy for driving P450 reactions using reducing equivalents supplied by a photocatalyst. (B) A fatty acid hydroxylation using this approach. Adapted with permission from *Journal of the American Chemical Society* 2013, 135, 14484. Copyright 2013 American Chemical Society.

Brustad and colleagues further demonstrated that Mes-Acr⁺ photocatalysts with a pendant alkyl iodide could be conjugated to cysteine single-site mutants in the active site of a thermostable aspartate dehydrogenase (*Tm*(AspDH)).¹¹⁵ These protein–photocatalyst hybrids were competent at catalyzing the oxidation of aryl thioethers in up to 95% yield (Figure 37B). Most notably, the *Tm*(AspDH)–photocatalyst hybrids catalyzed up to three times as many turnovers as the Mes-Acr⁺ photocatalyst alone.

In a subsequent advance on the SPAAC conjugation of photocatalysts to the POP protein scaffold, Lewis and co-workers explored the factors influencing the binding and photophysics of the polypyridyl ruthenium complexes bioconjugated to the previously characterized POP-azide mutants.¹¹⁶ Using luminescence lifetime titrations, the authors found Ru(bpy)₃²⁺ noncovalently binds to POP with a k_D of 28 ± 9 μM, enabling the study of noncovalent protein and photocatalyst interactions. By mutating the active site aromatic (W142 and Y326) and basic residues that have repulsive interactions with the cationic ruthenium complex (R55, R198,

K255, and R338) to alanine, termed POP_{Neut}, the protein affinity for the photocatalyst increased with $k_D = 1.7 ± 0.7 μM$. There were further effects on the binding affinity by mutating active site residues G99, W142, and Y326 to aspartic acid (POP_{Neg}), with the k_D having an upper bound of 1.1 ± 1.7 μM. The authors used these improved binding variants with the POP-azide mutants to test a variety of known Ru(bpy)₃²⁺-catalyzed photoredox reactions, including a reductive cyclization of dienones via an electron-transfer process (Figure 38A) and a [2 + 2] cycloaddition via an energy transfer (Figure 38B). The POP–photocatalyst hybrid outperformed free Ru(bpy)₃²⁺ under the stated reaction conditions in both cases.

2.6.1. Outlook for Photoenzymes with Non-natural Cofactors. The prospect of introducing non-natural chromophores into protein active sites to reveal new functions is a promising approach that holds the promise of significantly expanding the types of transformations available to enzymes. Even with the current photoenzymes, there is an opportunity for other reactions, such as radical initiation via hydrogen atom transfer, that have yet to be demonstrated. A key challenge in

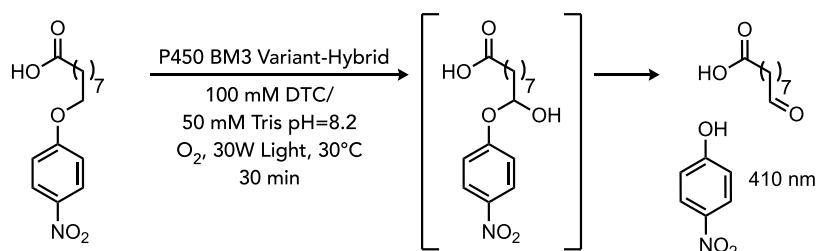


Figure 40. Colorimetric assay for P450–photocatalyst hybrids.

this work will be developing systems with well-defined active sites that can achieve high levels of enantioselectivity with highly reactivity intermediates. As with all photoenzymes, increased turnover numbers and frequencies will be necessary to utilize these reactions on an industrial scale.

3. SYNERGISTIC PHOTOENZYMATIC CATALYSIS

Synergistic photoenzymatic catalysis describes enzymatic transformations where the mechanism for converting starting material to product involves electron or energy transfer from an exogenous photocatalyst to a substrate or cofactor within the protein active site. This family of reactivity is distinct from photobiocatalytic cascades for cofactor turnover because the electron-transfer event involving the photocatalyst is essential for the biocatalytic mechanism for converting starting material to product.

3.1. Synergistic Reactions Involving Native Reactivity

3.1.1. Cytochromes P450. Cytochrome P450s are powerful catalysts for the asymmetric and regioselective hydroxylation of unactivated C–H bonds using molecular oxygen and a reductant. These proteins require a heme domain for oxygen activation and hydroxylation and a reductase domain to deliver electrons from NADPH to the heme domain for catalysis (via flavin mediators). The most widely used cytochrome P450 for biocatalytic transformations is P450_{BM3}, a catalyst with the reductase domain covalently linked to the heme domain.¹¹⁷ Fundamental studies by Gray and others demonstrated how electrons travel through proteins. In these studies, small molecule photocatalysts were often used to initiate electron-transfer events.^{118,119} Building on these studies, Cheruzel and co-workers demonstrated that the heme domain of P450_{BM3} bioconjugated with polypyridyl ruthenium photocatalysts could facilitate the C–H hydroxylation without requiring the traditional NADPH reductant.¹²⁰ Ru(bpy)₂(phenA)Cl₂ was linked to the heme domain via cysteine bioconjugation to P450_{BM3}-L407C, a variant containing cysteine that can react with the mutant via the iodoacetamide functional handle on the phenA ligand. Perhaps unsurprisingly, the location of photocatalyst bioconjugation plays an important role in the efficiency of the strategy, with other positions providing lower yields and total turnover numbers.^{121,122} To improve the driving force of electron transfer, the 2,2'-bipyridine (bpy) ligands were substituted to 4,4'-dimethoxy-2,2'-bipyridine ligand, resulting in an 80 mV decrease in reduction potential. The authors proposed the following mechanism for this non-natural system (Figure 39A). Photoexcitation of the ruthenium photocatalyst furnishes an excited state that is reductively quenched by sodium diethyldithiocarbamate (DTC) to provide a long-lived Ru(I) state, which supplies the electrons required for hydroxylation.

While total turnover numbers (TTNs) could not be compared to the native holoenzyme, initial product formation rates are roughly an order of magnitude lower. However, this synergistic approach performs favorably compared to other reduction strategies, such as electrochemical reduction or photochemical reactions with deazaflavin (Figure 39A). The P450_{BM3} enzymes were also demonstrated to regioselectively hydroxylate the allylic position of 10-undecenoic acid in 40% yield and 92.5:7.5 er (Figure 39B).¹²³ In subsequent studies, Cheruzel applied this system to the benzylic hydroxylation of trifluoromethylated substrates.¹²⁴ The authors used a photo-redox reaction developed by Stephenson et al. to trifluoromethylate aromatic rings with alkyl substituents to form trifluoromethylated products with various regioselectivities.¹²⁵ Next, they used the P450_{BM3} photocatalyst hybrid to hydroxylate the benzylic position. Interestingly, in cases where the trifluoromethylation protocol produced a mixture of *para*, *meta*, and *ortho* isomers, the subsequent hydroxylation would occur preferentially on one product, indicating that the steric and electronic properties of the substrate strongly influence its reactivity in the hydroxylation reaction. Moreover, the authors found that mutations within the protein active site could influence the selectivity of the hydroxylation step.

Using the P450_{BM3}-Ru(II) photosensitizer hybrid, Lam et al. explored the hydroxylation of fatty acids containing *p*-nitrophenyl ether moieties (Figure 40).¹²⁶ Schmid and co-workers previously demonstrated that P450_{BM3} could hydroxylate fatty acids with terminal *p*-nitrophenylethers. When the enzyme hydroxylates the ether methylene to form a hemiacetal, these unstable intermediates collapse to form an aldehyde and *p*-nitrophenol, which strongly absorbs at 400 nm.¹²⁷ Lam et al. used this basic strategy with ten different *p*-nitrophenoxy derivatives of fatty acids of differing chain lengths using their P450_{BM3}-Ru(II) photosensitizer hybrids. They found that the longest fatty acid derivative provided the highest total turnover numbers (120 TTN) and that the overall reactivity trends mirrored what was reported for the *holo*P450_{BM3}. This method was effective for conducting enzyme kinetics and determining relative reactivity with different substrates, making it a potentially valuable method for enzyme engineering campaigns.¹²⁸

In a follow-up study using the *p*-nitrophenol assay, the Cheruzel group studied the impact of photocatalyst electronics on these biohybrids' function.¹²⁹ From the general formula [Ru(4,4-X₂bpy)₂bpy]²⁺, Shalan et al. made the substitutions X = Cl, tBu, Me, OPh, OMe, and NMe₂ and characterized their activity using ¹H NMR, mass spectrometry, cyclic voltammetry, UV–vis, and luminescence spectroscopy. They found that the tBu substituted photocatalyst provided a hybrid with the highest catalytic activity.¹²⁹ When relative activities were plotted against Hammett parameters, a nonlinear relationship was observed that is the best fit to two independent linear plots

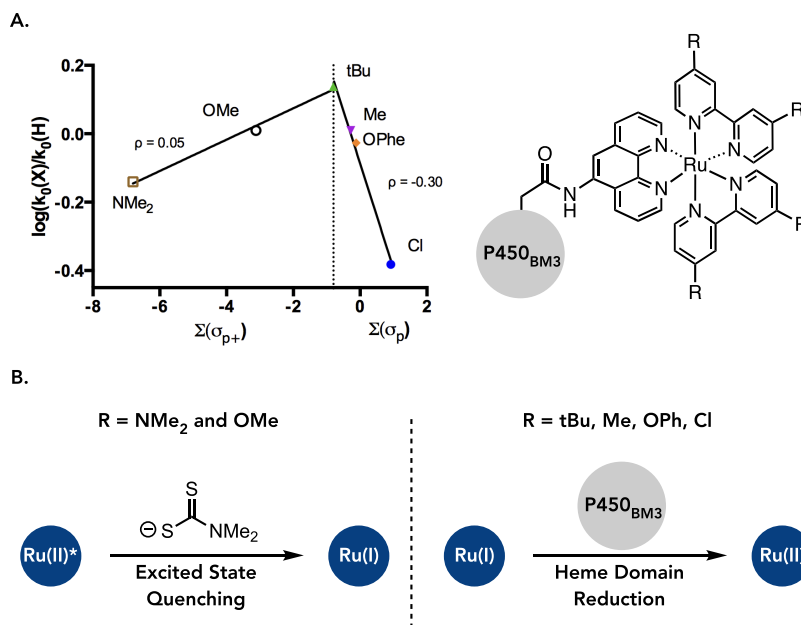


Figure 41. Impact of photocatalyst electronics on the rate of C–H hydroxylation. (A) Hammett correlation between photocatalyst electronics and product formation. (B) Rationale for the change in mechanism based on photocatalyst substituent. Adapted with permission from *Inorganic Chemistry* 2017, 56, 6558. Copyright 2017 American Chemical Society.

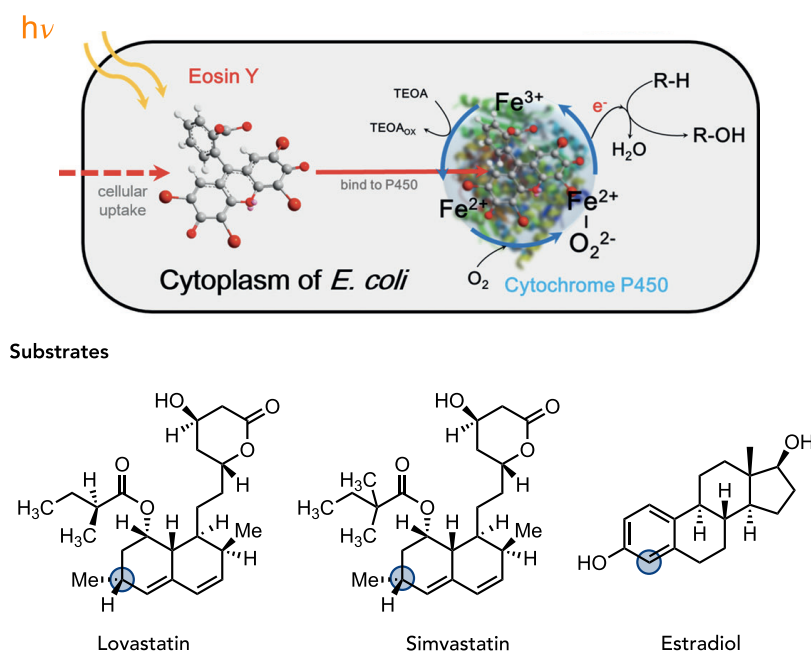


Figure 42. Eosin Y photoreduction of P450 heme domains. Adapted with permission from *Angew. Chem. Int. Ed.* 2015, 54, 969. Copyright 2015 John Wiley & Sons.

indicating a change in the rate-limiting step of the reaction (Figure 41A). The authors postulated that the rate-limiting step is the **electron-transfer step** between the Ru photosensitizer and the enzyme's heme center. This is supported by the negative slope between the X = Cl, OPh, Me, and tBu substituents on the Hammett plot. However, for X = OMe and NMe₂ substituents, the positive slope indicates that the rate-limiting step is **quenching of the Ru(II) excited state** by DTC (Figure 39B). These studies indicate that the electronic properties of the photocatalysts can play an important role in synergistic hybrid enzymes.

A subsequent study by Park and co-workers demonstrated that covalently linking a photocatalyst to the P450 heme domain is unnecessary for cofactor reduction.¹³² Eosin Y, a commonly used photocatalyst,¹³⁰ can bind to proteins.¹³¹ When *E. coli* cells containing the heme domain of various cytochrome P450s are supplied with Eosin Y and an electron donor (TEOA), the P450 can hydroxylate substrates (Figure 42).¹³² Confocal microscopy indicates that the photocatalyst is bound to the heme domain, while spectrofluorometric and CO binding analyses indicate that Eosin Y is necessary and sufficient to reduce the heme domain. Finally, the authors used this reduction system with a small collection of heme domains

from different P450s and explored the oxidation of various small molecule substrates (Figure 42). This study demonstrates that photocatalysts with a native affinity for proteins can reduce cofactors within the protein environment. Presumably, this strategy can be broadly applied to other proteins.

3.1.2. Rieske-type Non-heme Iron Enzymes. Mirroring the strategy employed with P450s, researchers have used photocatalysts to reduce non-heme iron centers in Rieske-type enzymes. Stc2 is an enzyme that oxidatively demethylates *N,N*-dimethylproline using NADPH and reductase proteins to prepare *N*-methylproline.¹³³ Intending to replace the reductase proteins with a photocatalyst, Elliott, Chen, and Liu tested various photocatalysts with sacrificial electron donors to arrive at the combination of Eosin Y as the photocatalyst with sulfite as an electron donor, resulting in between 20 and 30 turnovers of the enzyme. The authors hypothesized that competing O₂ reduction by the photocatalyst was responsible for the modest turnover numbers. To overcome this limitation, they developed a flow chemistry approach where the enzyme is reduced by the photocatalyst and then introduced to a mixture of sodium chlorite with chlorite dismutase, which produces O₂ to be consumed by Stc2. The resulting oxidized mixture was reintroduced to the photochemical reactor to initiate another round of enzyme reduction. Using this approach, 65–70 catalyst turnovers were achieved (Figure 43). This photochemical reduction and flow method was applied to turnover other Rieske enzymes and a flavin-dependent deiodinase.

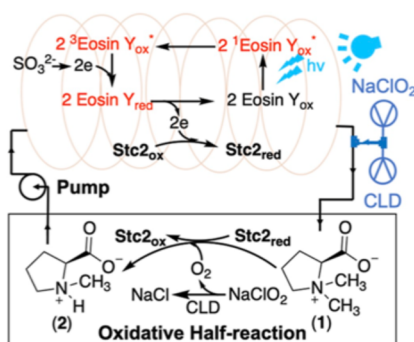


Figure 43. Photocatalyst turnover of Rieske-type non-heme iron enzymes. Adapted with permission from *ACS Catal.* 2022, 12, 14559–14570. Copyright 2022 American Chemical Society.

3.2. Synergistic Reactions Involving Non-natural Reactivity

3.2.1. Nicotinamide-Dependent Enzymes. Exogenous photocatalysts can also enable non-native reaction mechanisms. The photocatalyst in this scenario is responsible for the electron-transfer events, while the protein provides a chiral scaffold for the desired reactivity. In this case, the central challenge lies in identifying mechanisms that ensure that radical formation only occurs within the protein's active site. Reports in this area have primarily relied on the well-known phenomenon that binding to proteins alters the redox properties of substrates and cofactors.

The Hyster group demonstrated the viability of this synergistic strategy in a radical deacetoxylation of α -acetoxyketones using nicotinamide-dependent double-bond reductases and exogenous photoredox catalysts (Figure 44A). This enzyme cannot catalyze deacetoxylation reactions. However, upon adding a photocatalyst, this enzyme gains

this catalytic ability. The best results were achieved using Rose Bengal as a photocatalyst, where the desired product was formed in 87% yield with 93:7 er.¹³⁴ In solution, the xanthene dye Rose Bengal ($E_{1/2}^{\text{red}}[\text{RB}/\text{RB}^{\bullet-}] = -0.99 \text{ V vs SCE}$)¹³⁵ is incapable of reducing the model ketone ($E_{1/2}^{\text{red}} = -1.30 \text{ V vs SCE}$). However, enzymatic binding of the ketone substrate attenuates its redox potential, making it accessible to $\text{RB}^{\bullet-}$ reduction only within the enzyme active site. Based on the native reaction mechanism, the authors propose that a tyrosine hydrogen bonds to the carbonyl of the substrate. This bonding provides 170 mV of electronic activation, enabling reduction within the protein active site. Upon reduction of the starting material, the resulting ketyl radical undergoes a spin-center shift to eliminate acetate and form an enzyme-bound α -acyl radical that is subsequently terminated by enantioselective HAT from enzyme-bound NADPH. Isotopic labeling experiments support the hypothesis that nicotinamide functions as the source of the hydrogen atom (Figure 44B). This reaction is amenable to various functionalities, including alkyl groups and arene substituents. This general strategy can also dehalogenate α -bromoamides using ketoreductases with good yields and excellent enantioselectivity. These substrates do not form CT complexes with NADPH, preventing direct excitation mechanisms. In all these reactions, the stereocenter is set via stereoselective hydrogen atom transfer, a challenging step to render asymmetric using traditional small molecule reagents and catalysts.

3.2.2. Flavin-Dependent Enzymes. Redox activation by the enzyme was expanded to EREDs with $\text{Ru}(\text{bpy})_3\text{Cl}_2$ as an exogenous photocatalyst. The Hyster group demonstrated that these interactions could activate ketones for single-electron reduction. Using a Ru(II) photoredox catalyst with an ERED from *P. putida* (MorB), they could perform enantioselective reductions of acetophenone derivatives to the corresponding secondary alcohol with 99% yield and 80:20 er (Figure 45A).¹³⁶ The authors propose that the flavin cofactor is reduced to its hydroquinone oxidation state (FMN_{hq}) using the cofactor turnover system. Acetophenone can bind within the protein's active site, activating it for single-electron reduction by the photocatalyst ($E_{1/2} = -2.1 \text{ V in MeCN}$) (Figure 45C). The authors propose that photoreduction of the $\text{Ru}(\text{bpy})_3^{2+}$ affords a longer-lived Ru(I) oxidation state, which reduces the ketone to the ketyl radical within the protein active site. Mutation of the canonical binding residues to alanine (N189A and H186A) diminished the yield and enantioselectivity, indicating the importance of these binding residues for both the reaction yield and selectivity. A broad range of substrates are tolerated, including *para*, *meta*, and *ortho* substituted arenes, naphthyl rings, and other bulky moieties. Substrates with more electron-withdrawing substituents proved more reactive due to their increased reduction potential. Finally, using an α,β -unsaturated ketone, they could control the natural 1,4 reduction and non-natural 1,2 reduction in 89% yield and 83:17 er to afford a net global reduction.

Poelarends demonstrated that similar reactivity could be achieved using nitroreductases, a flavin-dependent oxidoreductase (Figure 45B and C).¹³⁷ They found that the nitroreductase from *B. amyloliquefaciens* could catalyze the reduction of acetophenone and cinnamyl methyl ketone in excellent yield and enantioselectivity. In contrast to the work by Hyster, carbonyl reduction outcompetes alkene reduction for cinnamyl ketones. Additionally, the nitroreductase system can utilize a broader range of photocatalysts than the

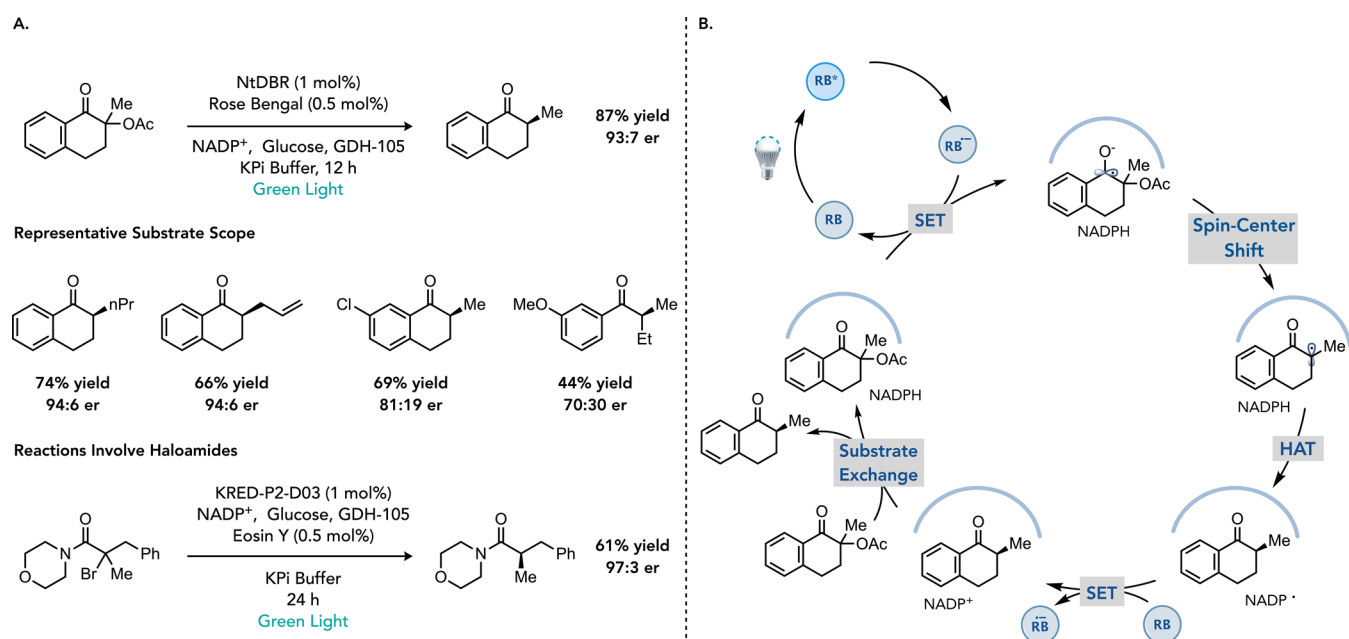


Figure 44. Radical deacetoxylation using synergistic photoenzymatic catalysis. (A) General scheme for synergistic deacetoxylation of ketones using photoredox catalysts and a nicotinamide-dependent double bond reductase. (B) Proposed reaction mechanism.

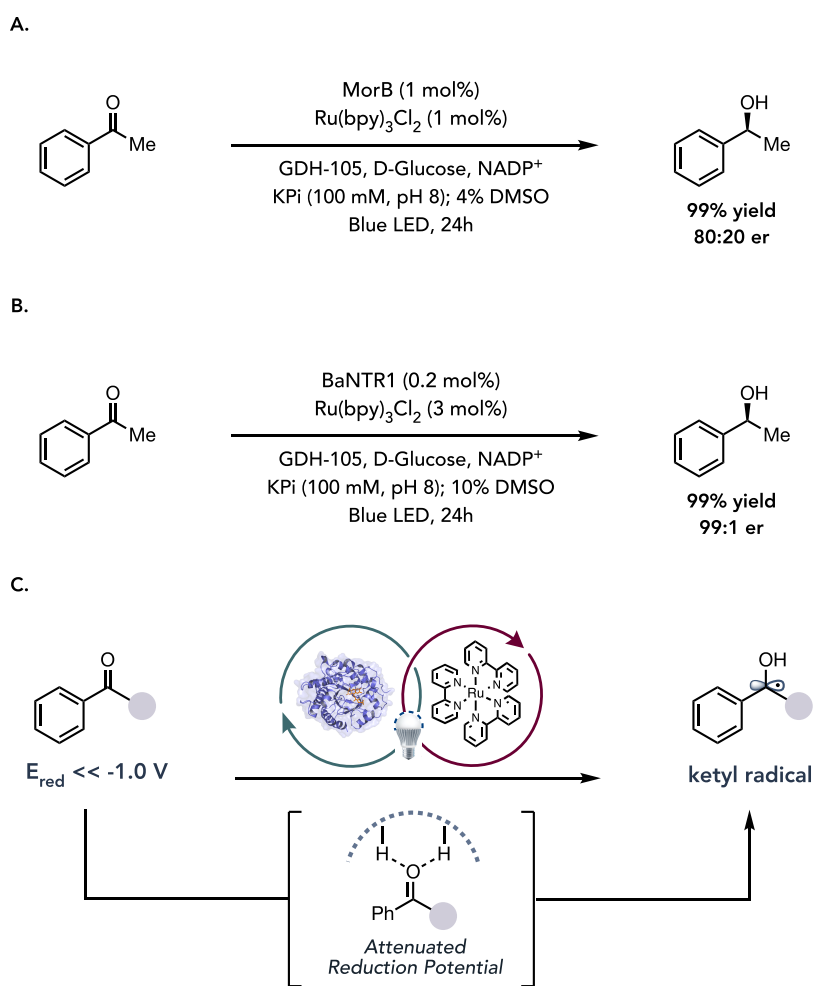


Figure 45. ERED-catalyzed ketone reduction using photoenzymatic catalysis. (A) Synergistic photoenzymatic reduction of ketones using EREDs and $\text{Ru}(\text{bpy})_3$. (B) Reduction of ketones using a nitroreductase with $\text{Ru}(\text{bpy})_3$. (C) General scheme describing enzymatic redox activation.

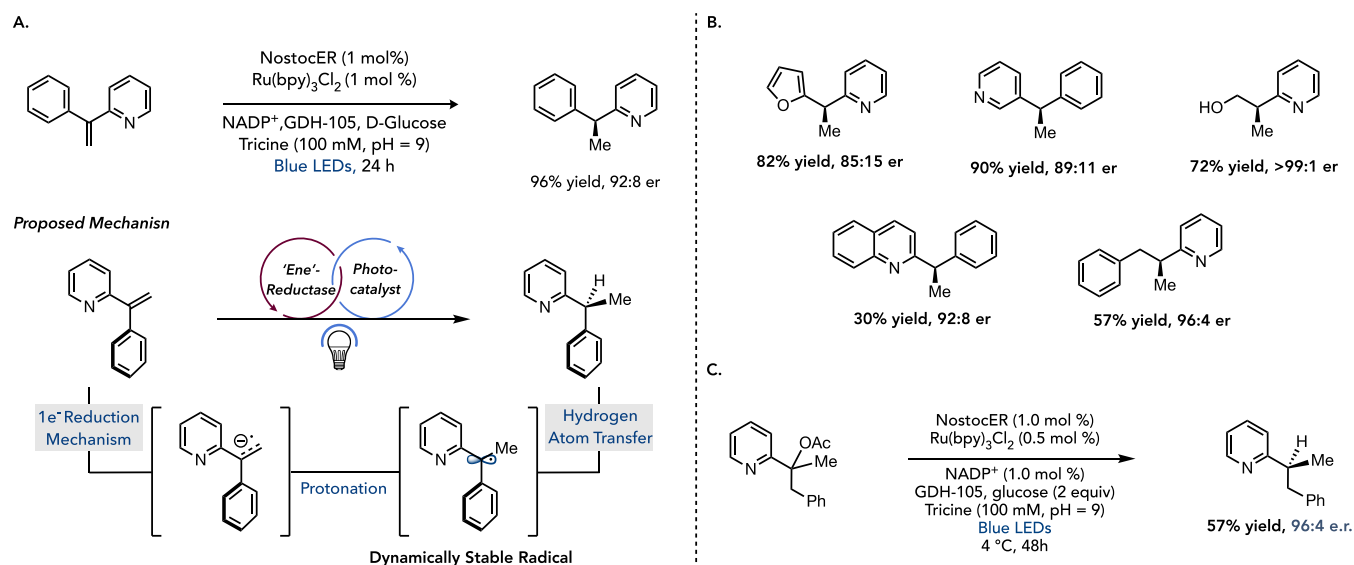


Figure 46. Vinylpyridine reduction by EREDs. (A) General reaction scheme and mechanism of vinylpyridine reduction. (B) Representative substrate scope. (C) Radical deacetoxylation.

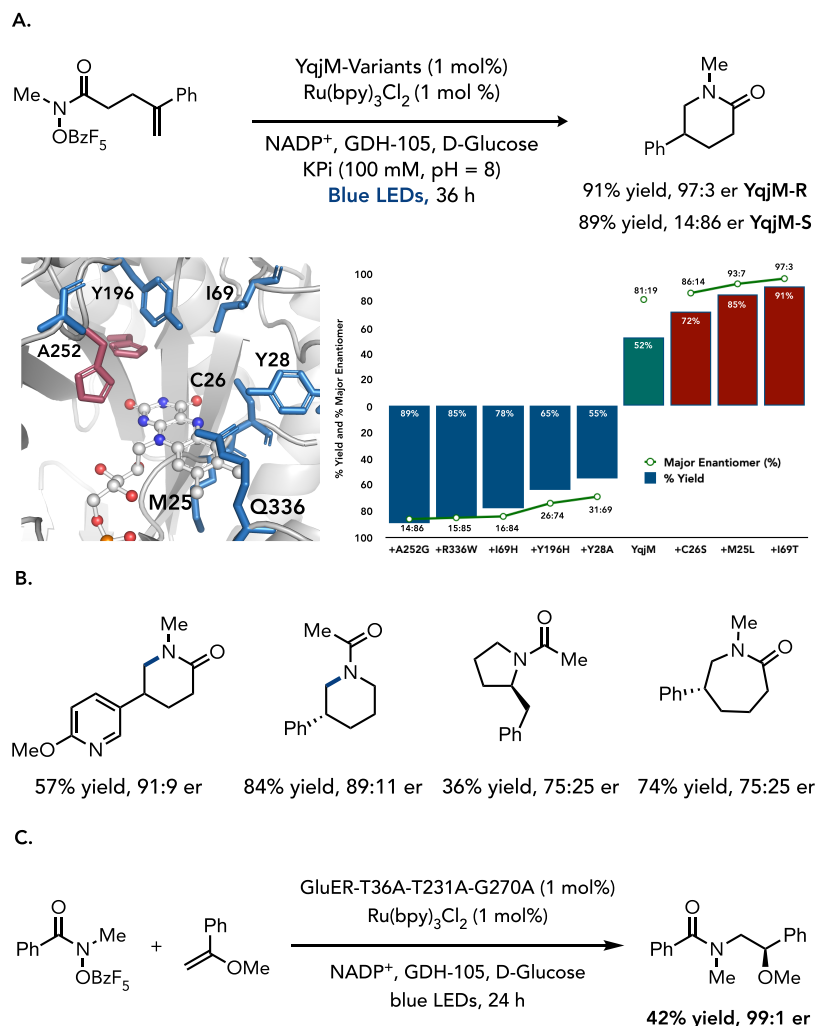


Figure 47. Asymmetric photoenzymatic hydroamination reactions. (A) Synergistic photoenzymatic hydroamination reaction with protein engineering campaign. (B) Representative substrate scope. (C) Intermolecular variation of this reaction.

analogous ERED approach, indicating that the level of electronic activation is potentially higher in the prior case.

Building on this strategy, the Hyster group demonstrated that photoredox catalysts could enable EREDs to reduce

vinylpyridines. While electrophilic, these substrates cannot be reduced by EREDs using their native reaction mechanism. Adding $\text{Ru}(\text{bpy})_3\text{Cl}_2$ to a reaction mixture containing the ERED from *N. punctiforme* (*NostocER*) reduced phenyl vinylpyridine with 96% yield and 92:8 er (Figure 46A).¹³⁸ Mechanistic studies suggest that Ru(I) reduces the alkene to the corresponding radical anion, which is rapidly protonated under the reaction conditions to afford a benzylic radical. Calculations indicate that this radical is dynamically stable and has properties that resemble those of persistent radicals. Based on published studies, it is difficult to determine whether the protein facilitates substrate reduction. Radical termination within the protein active site results in product formation in high yield and excellent enantioselectivity. This non-natural olefin hydrogenation is amenable to various functionalities, including electron-donating and electron-withdrawing arene substitution, as well as 3-furanyl, 3-thiophenyl, and alkyl substituents instead of the phenyl moiety (Figure 46B). Further, 3-vinyl and 4-vinylpyridine substrates, while difficult to hydrogenate using traditional methods, can be reduced with 90% and 99% yield, respectively, while maintaining high enantioselectivities (89:11 and 84:16 er). Interestingly, deacetoxylation of α -acetoxy pyridine substrates provides the product with the same yield and enantioselectivity, suggesting that the alkene reduction and deacetoxylation involve a shared reactive intermediate (Figure 46C).

Photocatalysts can be used to generate nitrogen-centered radicals within protein active sites. As these species are highly reactive, they readily engage in electron and hydrogen atom-transfer events, making them incompatible with reactive cofactor oxidation states. For instance, Hyster and co-workers found that nitrogen-centered radicals could be formed from hydroxamic esters when FMN_{hq} in EREDs is directly excited with a 390 nm LED. However, this radical is reductively quenched by FMN_{sq} , making this activation mode incompatible with these intermediates.¹³⁹ To overcome this challenge, $\text{Ru}(\text{bpy})_3\text{Cl}_2$ was added to initiate the reaction so that the nitrogen-centered radical would be formed adjacent to the less reactive FMN_{hq} . This approach enabled a 6-*endo-trig* hydroamination using the hydroxamic ester within the active site of YqjM (an ERED from *Bacillus subtilis*) in 52% yield and 81:19 er (Figure 47A). Protein engineering over three rounds of site-saturation mutagenesis afforded a biocatalyst that provides the *R*-enantiomer in 91% yield and 97:3 er. During the engineering campaign, it was found that the mutation of the tyrosine at position 28 (Y28A) flipped the enantiomeric preference of the reaction. Subsequent evolution afforded a variant that provided the product with 89% yield with 86:14 er (Figure 44B). These variants were effective across various substrates, facilitating 5-*exo*, 7-*endo*, and 8-*endo-trig* cyclization (Figure 47B). An evolved variant of *GluER* could also catalyze an intermolecular hydroamination in excellent enantioselectivity but modest yield (Figure 47C).

In these reactions, the photocatalyst is rapidly reduced to afford $\text{Ru}(\text{bpy})_3^{+}$, which reduces the hydroxamic ester substrate. Reduction of the substrate within the protein active site generates the NCR intermediate with the loss of benzoate. The highly reactive radical species performs a 6-*endo-trig* cyclization into the pendant alkene, and a HAT selectively terminates the resulting benzylic radical from the FMN_{hq} . The flavin radical (FMN_{sq}) is subsequently oxidized by excited state Ru(II) to yield FMN_{ox} —which is then turned over by the cofactor regeneration system. While the initial enzyme requires

highly activating perfluorobenzoyl leaving groups, the evolved variants, presumably due to increased activation by the enzyme, can use less activated benzoyl leaving groups.

4. TANDEM PHOTOCATALYST/ENZYME REACTIONS

Tandem photocatalyst/enzyme reactions are biocatalytic transformations where an enzyme and photocatalyst are present in a reaction, but the photocatalyst is not involved in the electron-transfer events required to convert the starting material to product. In this scenario, the photocatalyst is operating entirely independently of the enzyme. The most common variant of this cascade strategy is cofactor reduction by the photocatalyst or *in situ* peroxide generation. More recently, research has been focused on organic transformations that can be run in the presence of enzymes for dynamic kinetic resolutions. This section is organized based on the role of the photocatalyst in the reaction.

4.1. Light-Driven Cofactor Regeneration

4.1.1. "Ene"-Reductases. Cofactor turnover in "ene"-reductases involves the reduction of FMN to FMN_{hq} using NAD(P)H via a hydride-transfer mechanism. Consequently, EREDs' reactions typically involve a cofactor turnover system to regenerate NAD(P)H utilizing simple alcohols or glucose as terminal reductants. The Hollmann group recognized that the photochemical reduction of EREDs by an exogenous photocatalyst would enable a broader array of reagents to serve as reductants.

In their initial study, Hollmann explored the reduction of ketoisophorone to levodione by YqjM, an ERED from *Bacillus subtilis*,¹⁴⁰ using a photocatalyst for cofactor reduction (Figure 48).¹⁴¹ They tested a combination of flavin-derived photo-

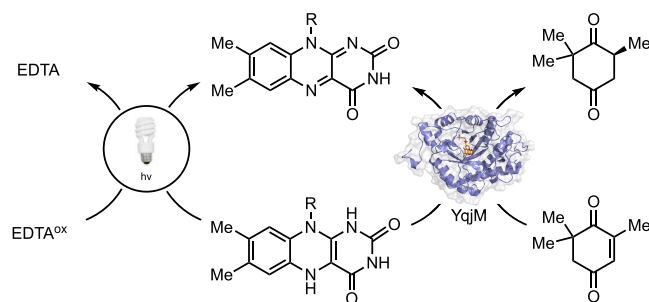


Figure 48. Photocatalytic reduction with riboflavin in EREDs.

catalysts with small molecule reagents as sacrificial electron donors under visible light irradiation.¹⁴² Ultimately, they found that the combination of free flavin as a photocatalyst and ethylenediaminetetraacetic acid (EDTA) as an electron donor afforded optimal yield and enantioselectivity. One of the primary challenges in optimizing the photocatalyst was avoiding the nonenzymatic reduction of the substrate. Deazaflavin, for instance, formed the reduced product as a racemic mixture. Hollmann also found that anaerobic conditions were crucial for achieving high conversions, presumably due to the high reactivity of reduced flavins with molecular oxygen yielding hydrogen peroxide or sensitization of O_2 .^{142,143} The photochemical turnover system was particularly attractive when running reactions in cell lysate, as it avoids forming NADH equivalents that cellular alcohol dehydrogenases could use to consume starting material or product. Finally, the authors observe a 65% increase in the

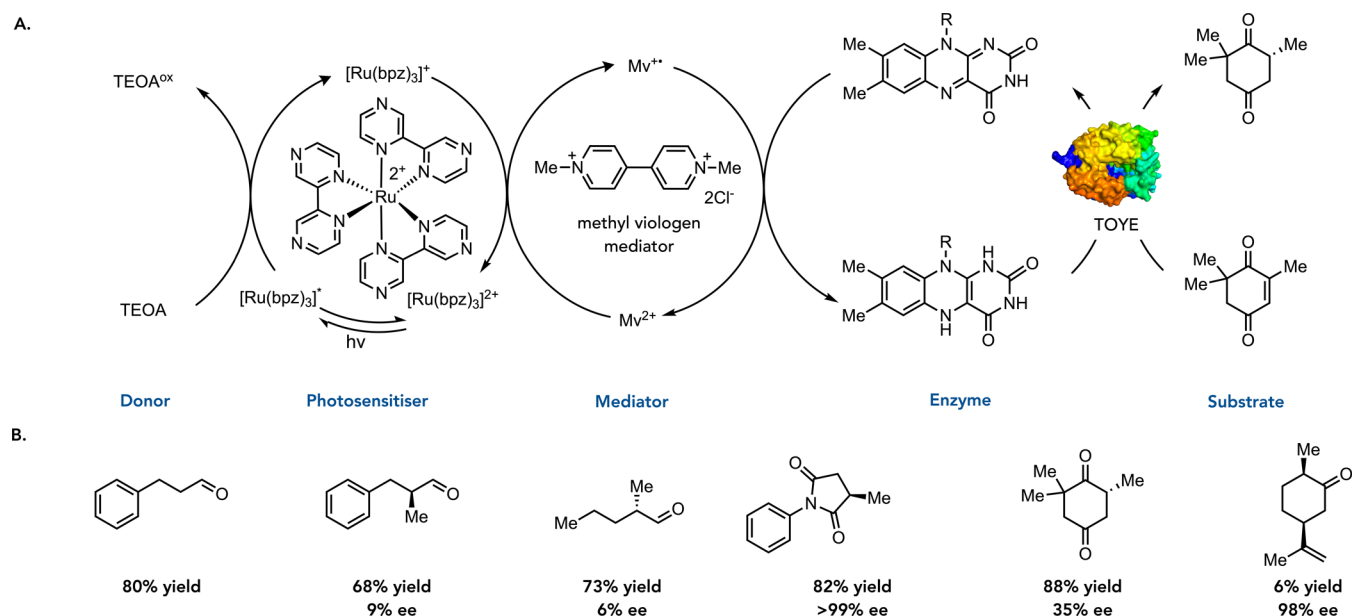


Figure 49. Triethanolamine for cofactor turnover. (A) Catalytic cycle for cofactor turnover. (B) Representative substrate scope.

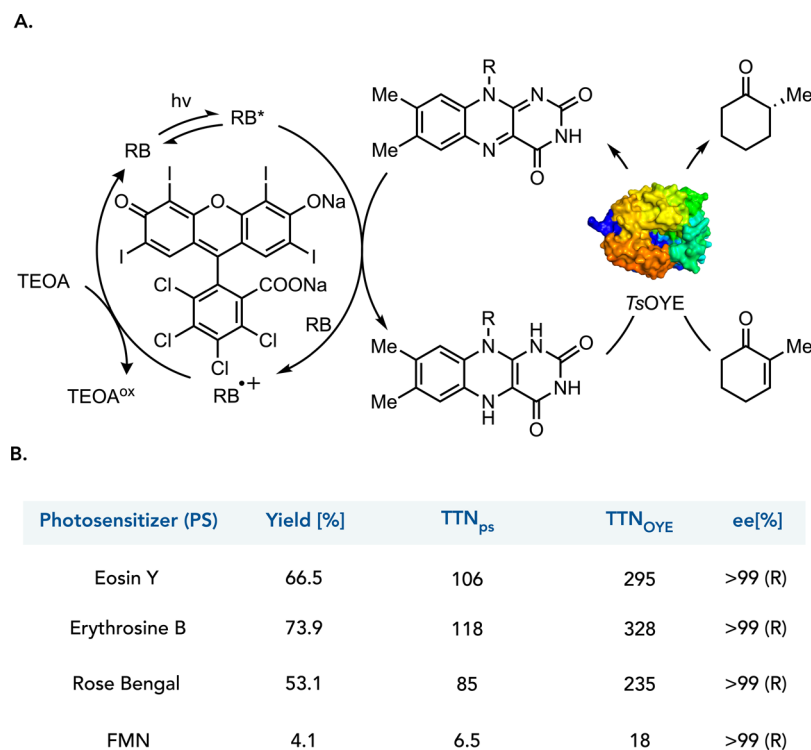


Figure 50. Rose Bengal for cofactor turnover. (A) Organic photoredox catalysts for old yellow enzyme turnover. (B) Results with different photoredox catalysts.

enzyme's specific activity when adding a photocatalyst, suggesting that the photocatalytic turnover can be competitive with traditional methods.

Building on the initial study by Hollmann, Scrutton et al. demonstrated that metal photocatalysts can reduce TsOYE and pentaerythritol tetranitrate reductase (PETNR) (Figure 49A).¹⁴⁴ Ruthenium(II) photocatalysts are some of the most extensively studied molecules for electron transfer.¹⁴⁵ The authors recognized that using stable metal photocatalysts might provide superior reaction kinetics to what was observed when flavin was used as a photocatalyst. When [Ru-

(bpz)₂(dClbpy)]Cl₂ was mixed with PETNR in triethanolamine (TEOA) buffer and irradiated with visible light, only minor spectral changes were observed, suggesting inefficient electron transfer between the photocatalyst and enzyme. The authors added methyl viologen (*N,N*-dimethyl-4,4'-bipyridinium dichloride) as an electron mediator and observed reduction of the protein in 50 min. When this system was irradiated with light in the presence of substrate, they observed reductive enzymatic activity. The authors proposed a mechanism where the photocatalyst oxidizes TEOA and donates the electron to methyl viologen. Two equivalents of

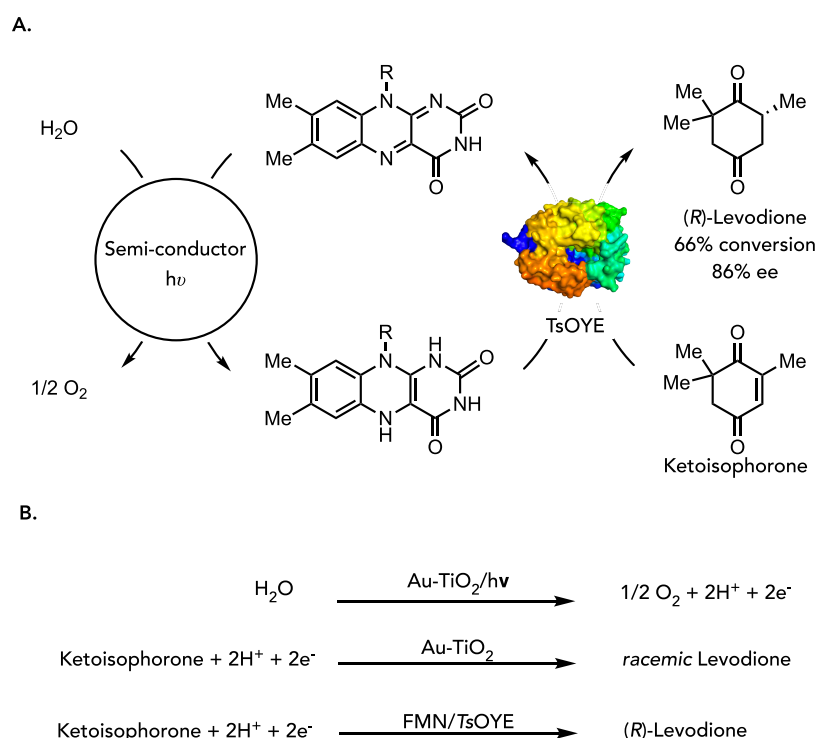


Figure S1. Photobiocatalytic reduction of alkenes using a semiconductor for flavin reduction. (A) General schematic for turnover over an old yellow enzyme via water oxidation. (B) Mechanistic steps of water oxidation and electron transfer to the enzyme.

methyl viologen is required to reduce FMN to FMN_{hq}, which the enzyme uses to stereoselectively reduce the substrate (Figure 49A).

During reaction optimization, the authors found that increasing the concentration of TEOA resulted in higher yields. They hypothesize that the rate-determining step of this cascade is the generation of the reduced photocatalyst. The ideal pH was between 8 and 10 to avoid protonation of the bpz ligands. When exploring the substrate scope, they found that ketoisophorone was susceptible to a background reduction by methyl viologen resulting in decreased enantioselectivity. The system was effective for the reduction of several substrates (Figure 49B). *N*-Phenyl-2-methylmaleimide could be reduced with high levels of enantioselectivity but with a more modest yield due to the formation of an unidentified side product which is not produced by the enzyme.

In a follow-up study, Hollmann and Park examined the photoreduction of TsOYE using xanthene dyes for the stereoselective reduction of 2-methylcyclohexane (Figure 50A).¹⁴⁶ The authors selected Rose Bengal as a model photocatalyst and found in spectroscopic studies that it could reduce the cofactor in TsOYE to FMN_{hq} when irradiated with visible light using triethanolamine (TEOA) as a buffer and sacrificial electron donor. A shift in the absorption of Rose Bengal in the presence of the protein indicates the photocatalyst binding to the protein's surface. This binding interaction presumably lowers the kinetic barrier to electron transfer from the photocatalyst to the flavin cofactor. When using 0.225 mol % TsOYE and 0.625 mol % Rose Bengal under visible light irradiation, the reaction afforded the reduced product in 53% yield with >99:1 *r* favoring the (*R*)-2-methylcyclohexanone. This represents 85 turnovers of the photocatalyst and 235 turnovers of TsOYE. They found improved reaction efficiencies when using Eosin Y or Erythrosine B as

photocatalysts (Figure 50B). Overall, this study demonstrates that organic photocatalysts that bind to the protein surface can effectively reduce flavin within a protein active site, enabling biocatalytic reactions that otherwise required additional enzymes for cofactor turnover.

In photosynthesis, visible light drives water oxidation to produce molecular oxygen and NADPH. Corma et al. demonstrated that simple semiconductors, such as titanium dioxide (TiO₂), can facilitate water oxidation to produce reducing equivalents relayed to proteins using a redox mediator (Figure 51A).¹⁴⁷ In their initial study, the authors explored the asymmetric reduction of ketoisophorone to (*R*)-levodione using a thermally stable old yellow enzyme (OYE) from *Thermus scotoductus* SA-01 (TsOYE).¹⁴⁸ They found using gold nanoparticles deposited on TiO₂ (Au-TiO₂) and flavin mononucleotide (FMN) as a redox mediator led to an efficient reduction of TsOYE from FMN to FMN_{hq}.¹⁴⁹ When irradiating the catalytic system containing Au-TiO₂, FMN, and TsOYE with UV light at 50 °C, 66% conversion of ketoisophorone into (*R*)-levodione was observed in 6 h in 86% ee. The authors observed an erosion of enantioselectivity over time. A background reduction of the substrate by Au-TiO₂ is responsible for decreased enantioselectivity. Kinetic analysis suggests that enzymatic reduction of the substrate outcompetes reduction by the photocatalyst. However, at extended reaction times, the protein can be denatured, making reduction by the photocatalyst competitive (Figure 51B).

4.1.2. Baeyer–Villiger Monoxygenases. Baeyer–Villiger monoxygenases (BVMOs) have emerged as a powerful enzyme class for stereo- and regioselective catalysis, showing wide substrate promiscuity under mild conditions.¹⁵⁰ The flavin- (FMN or FAD) dependent enzymes incorporate O₂ to form a peroxy adduct with the cofactor as a reactive intermediate—capable of transforming various carbonyls into

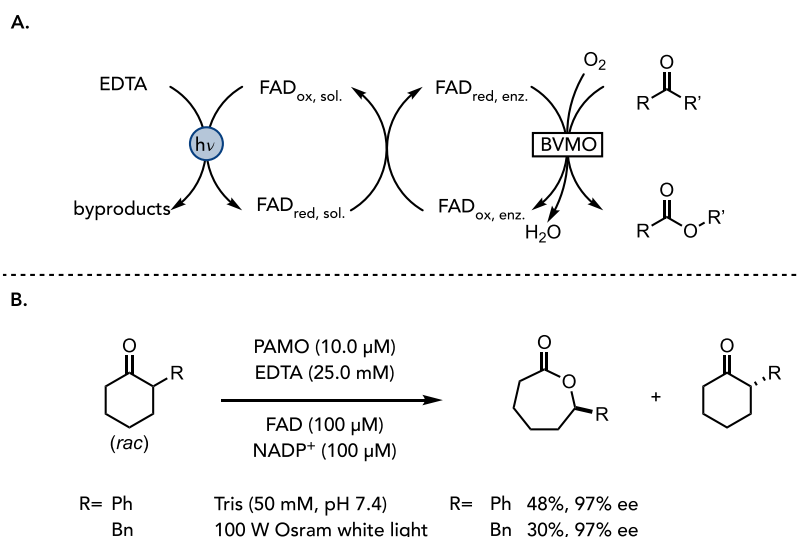


Figure 52. BVMO cofactor turnover using FAD as a photocatalyst. (A) Schematic for BVMO turnover using a photocatalyst. (B) Kinetic resolution of a substituted cyclohexanone.

the corresponding esters. However, NADPH is required for catalytic turnover, which is expensive and would ideally be replaced by a cheaper alternative.^{151,152} Reetz and co-workers proposed to use a turnover system originating from a photocatalytic method, using a sacrificial amine as a substitute (Figure 52A).¹⁵¹ The addition of EDTA without any NADP⁺ did not yield any product, which was attributed to the two-cofactor dependence of the enzyme, requiring the cofactor for activity of the enzyme. However, adding catalytic amounts of NADP⁺ led to the transformation of carbonyl to product, catalyzing the reaction in a very similar fashion to the canonical NADP⁺-based regeneration system (Figure 52B). Control experiments confirmed that light and EDTA were necessary for product formation. Furthermore, sunlight readily catalyzed the reaction, showing 20% conversion after 2 h.

4.1.3. FAD-Dependent Halogenases. Using a similar turnover strategy to the one employed with the Baeyer–Villiger monoxygenase, FAD-dependent halogenases can be reduced using light and an exogenous electron donor. Kottke and co-workers demonstrated that tryptophan 5-halogenase (PyrH) can convert tryptophan into 5-chlorotryptophan using NaCl as the chloride source and EDTA as the reductant (Figure 53).¹⁵³ The authors found the higher concentrations of

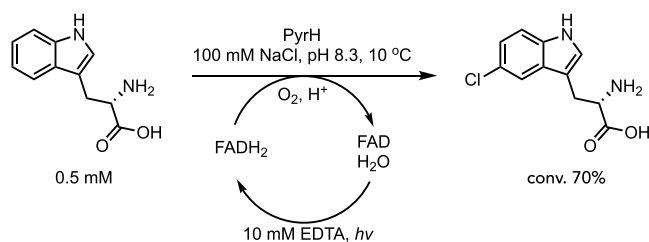


Figure 53. Photochemical reduction of FAD-dependent halogenases

5-chlorotryptophan were produced when photoreduction occurs within the protein active site rather than when exogenous photocatalysts were added. The authors hypothesize that eliminating free FAD reduces the undesired generation of H₂O₂. Additionally, these results suggest that

FAD is photoactive within the active site of PyrH, opening the door for non-natural photoenzymatic activity.

4.1.4. Ketoreductases. KREDs are oxidoreductase enzymes important in producing chiral alcohols or amino acids.^{154–157} As these enzymes use one equivalent of cofactor (NADP⁺ or NAD⁺) for each catalyst turnover, efficient systems for cofactor regeneration are essential when using these enzymes on large scales. While cofactor turnover enzymes are most often used for this application, recent efforts have been focused on developing photochemical methods for regenerating nicotinamide cofactors.^{158,159}

The utilization of photons from solar light is an attractive approach for the synthesis of optically active compounds.¹⁶⁰ Yadav and co-workers designed a method for reducing NADP⁺ under visible light employing a graphene-based photocatalyst and a rhodium hydride-transfer catalyst.¹⁶⁰ The photocatalyst consists of chemically converted graphene, which covalently bonds to triazine-linked 4,4'-difluoro-4-bora-3a,4a-diaza-s-indacene moieties (GBP-BODIPY). This photocatalyst can oxidize TEOA to generate the reduced form of the photocatalyst. This species can donate electrons to [Cp*Rh-(bpy)(H₂O)]²⁺ in two sequential electron-transfer events and, upon protonation, form [Cp*Rh(bpy)(H)]⁺. Reduction of NADP⁺ by the rhodium catalyst forms NADPH and [Cp*Rh(bpy)(H₂O)]²⁺.¹⁶¹ The alcohol dehydrogenase can then use NADPH to reduce the ketone (Figure 54A).

Initially, the NADP⁺/NADPH regeneration was studied without any light source, and no NADPH regeneration was observed. Upon irradiation with visible light irradiation ($\lambda > 420$ nm, cutoff-filter), a conversion of $\sim 55\%$ NADPH was obtained after 2 h. For comparative purposes, previously reported photocatalysts such as homogeneous BODIPY, (aminophenyl)triphenylporphyrin, or chemically converted graphene linked to (aminophenyl)triphenylporphyrin only afforded 11%, 9%, and 21% yields for NADPH regeneration, respectively.¹⁶² The photoregeneration system of the nicotinamide cofactor was then coupled with an enzymatic reaction using alcohol dehydrogenase (ADH) from *Lactobacillus kefir* for the reduction of various ketones to their corresponding chiral alcohols. A range of substrates that comprise aromatic, aliphatic cyclic, acyclic, and heteroaromatic functionalities were

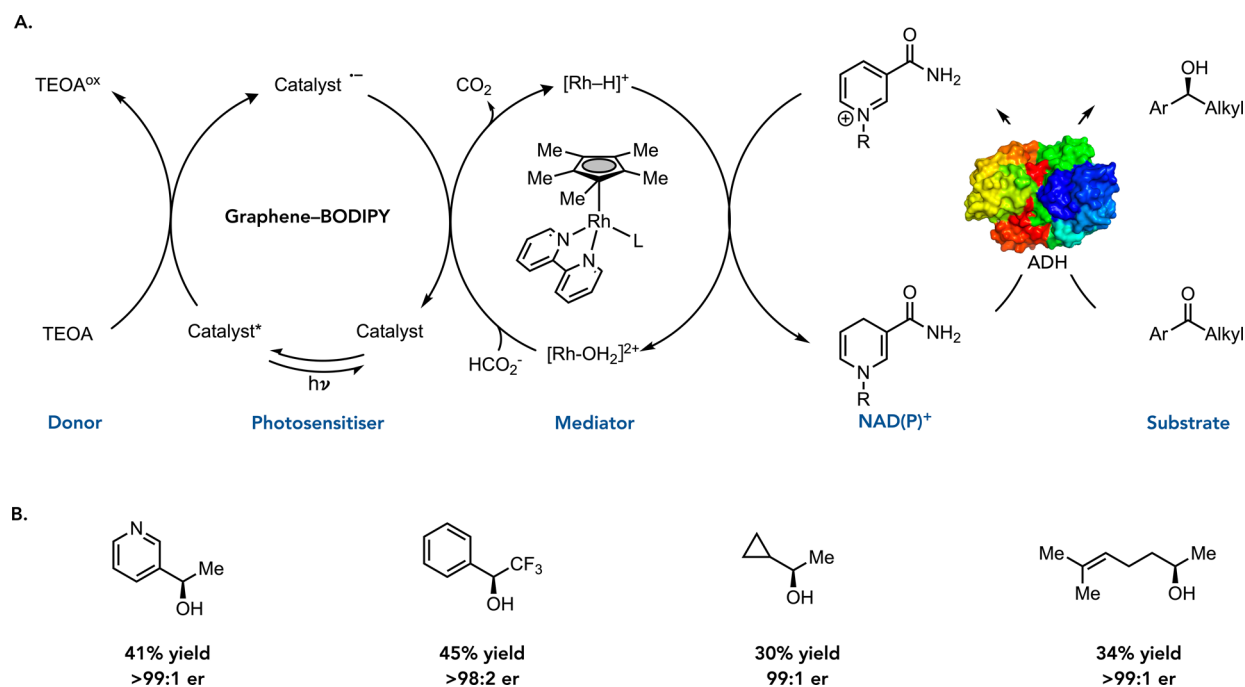


Figure 54. Alcohol dehydrogenase turnover using a photocatalyst/metal hydrogenation cascade. (A) Schematic for NAD(P)⁺ turnover using a photocatalyst and hydride-transfer catalyst. (B) Representative substrate scope.

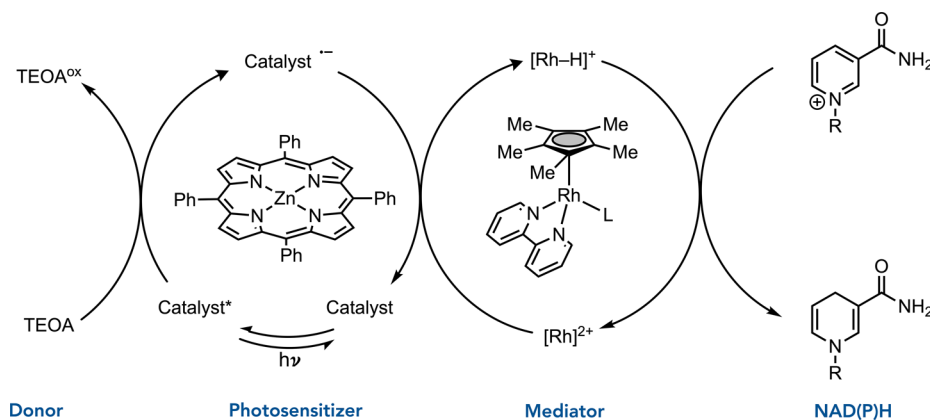


Figure 55. Porphyrin turnover of NADPH.

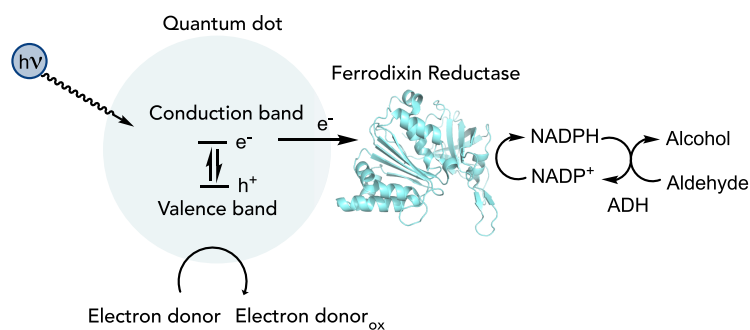
tested, giving access to a broad range of chiral alcohols in good yields (67–74%) and good enantioselectivities (97–99%) (Figure 54B).

Organic dyes like porphyrins are relatively cheap photocatalysts and could be used *instead of* graphene for cofactor turnover.¹⁶³ The porphyrin excited state is a potent oxidant that accepts electrons from many sacrificial donors. The radical anions can reduce various catalysts to facilitate NAD(P)⁺ reduction (Figure 55).¹⁶⁴ However, as some porphyrins are unstable,¹⁶⁵ it would be attractive to immobilize them onto solid supports.¹⁶⁶

Liu et al. demonstrated that tetrakis(4-carboxyphenyl)porphyrin (TCPP) could facilitate NADH turnover with visible light in the presence of [Cp*Rh(bpy)(H₂O)]²⁺.¹⁶⁷ The authors initially compare TCPP, zinc porphyrins (ZnTCPP), and Eosin Y (EY) for NAD⁺/NADH regeneration using a 300 W xenon lamp with a cutoff filter ($\lambda > 400$ nm) as the light source. The highest NADH obtained using the TCPP system showed a 2.37 and 1.47 fold increase in yield using the ZnTCPP and EY systems, respectively. The authors proceeded

to optimize the electron donor, pH value, and phosphate buffer concentration. Triethanolamine (5 mM) was the most efficient electron donor in phosphate buffer (pH = 7.0, 50 mM). Under these conditions, 81.5% of NADH was achieved after 60 min. Immobilization strategies of the TCPP onto various surfaces, such as TiO₂ and SiO₂, were evaluated. The highest activity was observed with silica microspheres containing thiol groups and coated with polydopamine and polyethylenimine, yielding 9.64% NADH after 90 min in the cofactor regeneration system.

The authors found homogenous TCPP to be more active than the heterogenous form. The authors rationalize this observation as being due to the adsorption of TCPP on the support, impeding the desired electron transfer. Nevertheless, the NADH yield using the heterogeneous TCPP was improved to 22.5% with the addition of the rhodium mediator, which was attributed to the two isomeric forms, 1,4-NADH and 1,6-NADH, being present, but only 1,4-NADH is active for the enzymatic synthesis. The cofactor regeneration system can frequently lead to loss of stereospecificity of the overall transformation.¹⁶⁸



Substrate	Product	Conv(%)
Isobutyraldehyde	Isobutanol	8.9
Butyraldehyde	Butanol	8.7
2-methylbutyraldehyde	2-methylbutanol	8.3
isovaleraldehyde	3-methylbutanol	6.9

Figure 56. Using quantum dots for ferredoxin reductase turnover.

Rather than relying on two catalysts to relay electrons to NAD(P)^+ , other groups have explored direct electron transfer from photocatalysts. Materials such as semiconductor quantum dots,¹⁶⁹ metallic nanoparticles,¹⁷⁰ and carbon nitride¹⁷¹ have been tested for this purpose; however, these systems have low selectivity for formation of the correct regioisomer of NAD(P)^+ H and typically require high overpotentials to overcome the kinetic barriers to reduction of NAD(P)^+ by a single-electron mechanism. An alternative strategy is to use a biohybrid system for cofactor photoregeneration, where a photocatalyst is linked to an enzyme capable of cofactor regeneration.¹⁷² These strategies overcome the kinetic barrier by reducing the flavin cofactor using sequential single-electron reduction to access FAD_{hq} which can reduce NAD(P)^+ using a hydride transfer mechanism. These enzymes deliver hydride with high levels of regioselectivity.

This strategy was outlined by Brown et al. where they combined the ferredoxin NADP^+ reductase (FNR) from *Chlamydomonas reinhardtii*,¹⁷³ a FAD-dependent enzyme,¹⁷⁴ and a CdSe quantum dot (QD) capable of photocatalytic regeneration of NADPH under illumination. When the quantum dot is photoexcited, an electron is transferred to ferredoxin reductase. Ascorbic acid, a sacrificial electron donor, quenches the resulting hole on the quantum dot. Two sequential photocycles reduce FAD to FAD_{hq} , which can reduce NADP^+ to NADPH (Figure 56).

The ability of QD–FNR complexes to reduce NADP^+ was studied via irradiation with 405 nm light. The authors observed that the NADPH concentration increased linearly with illumination time for up to 2 h, when all the available NADP^+ was reduced. The designed photoregeneration system was then coupled with the enzyme *Thermoanaerobium brockii* alcohol dehydrogenase (*TbADH*)¹⁷⁵ to reduce a small set of aldehydes to alcohols in low conversions (Figure 56). The authors concluded that the factor influencing the stagnation in the rate was QDs' precipitation during illumination due to oxidation and loss of ligands.¹⁷⁶ Furthermore, the precipitation of the CdSe QDs may release Cd^{2+} ions that will chelate with the amino acids at both the FNR and quinone binding sites.¹⁷⁷

These effects limit the active lifetime of the QD–FNR complexes under illumination to ~ 3 h.

4.1.5. Cytochromes P450. Photocatalytic cofactor turnover has also been used to drive P450 oxidation reactions. Park and co-workers reported that Eosin Y and $[\text{Cp}^*\text{Rh}(\text{bpy})\text{H}_2\text{O}]$ could reduce NADPH (Figure 57).¹⁷⁸ In this system, TEOA is

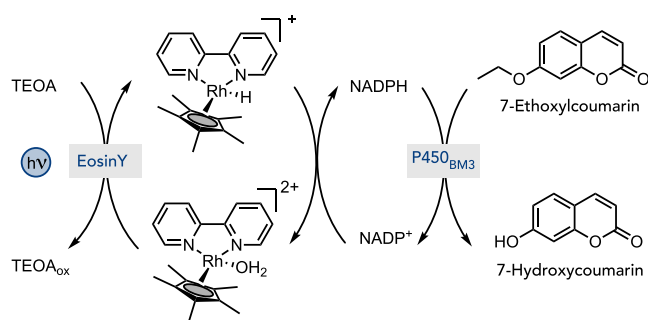


Figure 57. NADPH turnover with P450s using a photocatalyst and $\text{Cp}^*\text{Rh}(\text{bpy})$.

oxidized by photoexcited Eosin Y to produce the corresponding EY radical anion. This species can reduce $[\text{Cp}^*\text{Rh}(\text{bpy})\text{H}_2\text{O}]^{2+}$ to produce $[\text{Cp}^*\text{Rh}(\text{bpy})\text{H}]^+$, which reduces NADP^+ to NADPH. In a model reaction, the authors explored the oxidation of 7-ethoxycoumarin using P450_{BM3} -Y51F-F87A to produce 7-hydroxycoumarin. The effect of each component on the enzyme was studied, and Eosin Y was found not to oxidatively degrade the protein. Interestingly, a high concentration of TEOA and $[\text{Cp}^*\text{Rh}(\text{bpy})\text{H}_2\text{O}]$ leads to inactivation of the enzyme. Based on previous studies by the authors, they proposed that high concentrations of Eosin Y result in the uncoupling of the electron-transfer events in P450, leading to oxidative degradation of the protein scaffold.

The fatty acid P450 decarboxylase OleT_{JE} catalyzes the decarboxylation of fatty acids to the corresponding terminal alkenes using H_2O_2 . However, the enzyme could not tolerate high concentrations of H_2O_2 , thus leading to limited activity. The efficiency of OleT_{JE} catalysis was improved through a coupled photochemical pathway in the presence of FMN and

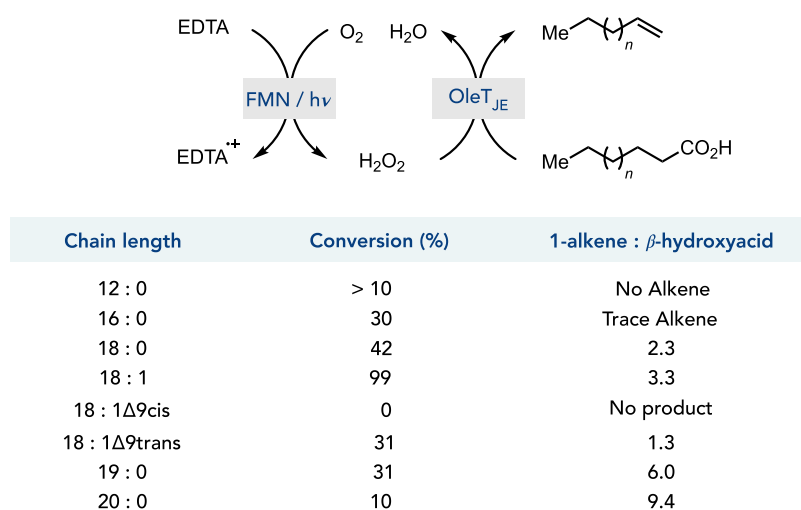


Figure 58. Photocatalytic peroxide formation catalyzed by OleT_{JE}.

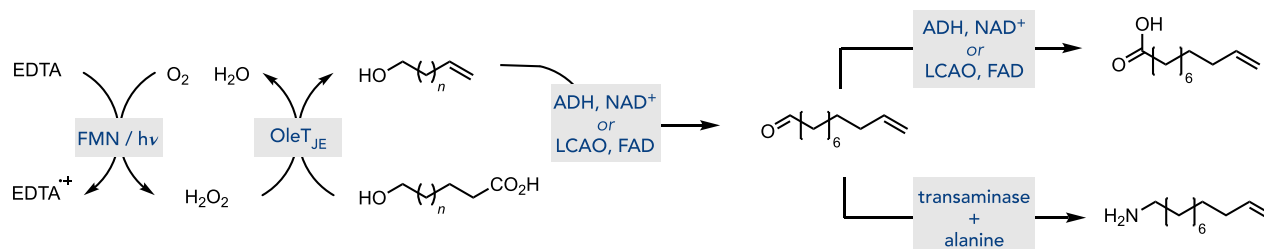


Figure 59. Decarboxylation of ω-functionalized fatty acids by OleT in an enzyme cascade.

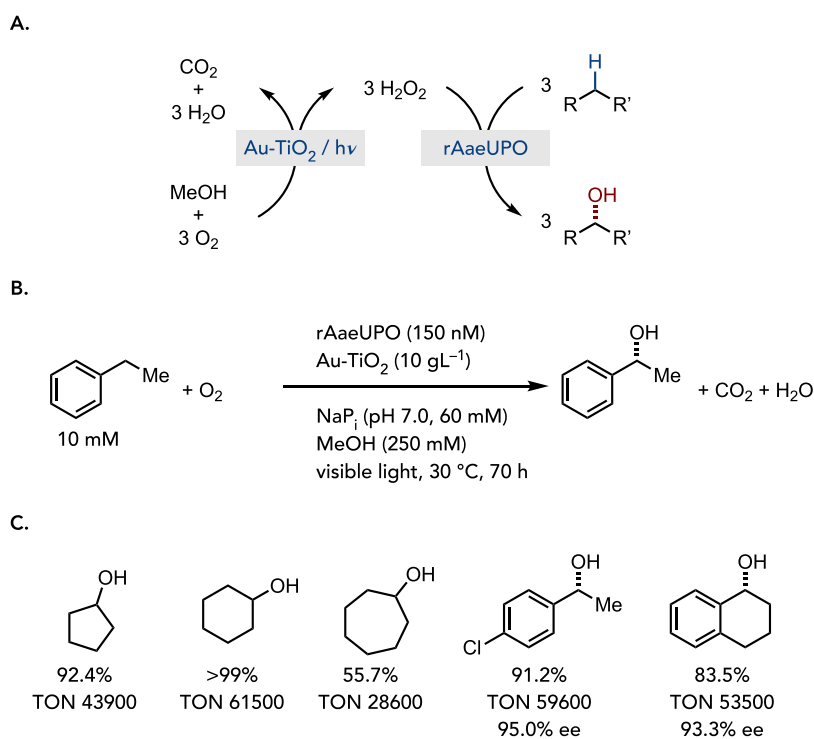


Figure 60. TiO₂-driven peroxide formation from methanol. (A) General schematic for peroxygenase turnover using a photocatalyst to convert O₂ to peroxide. (B) Reaction scheme. (C) Representative substrate scope.

O₂ to generate H₂O₂ *in situ* (Figure 58A). Here FMN functions as a photocatalyst.¹⁷⁹ The β-hydroxy acid is a byproduct of the decarboxylation reaction, and the authors revealed that the ratio of decarboxylation and hydroxylation is

dependent on the chain length of the substrates, as shown in Figure 58. With growing chain length, the ratio is increased. The natural fatty acid from hydrolyzed hardened palm oil was subjected to this condition, although only preliminary results

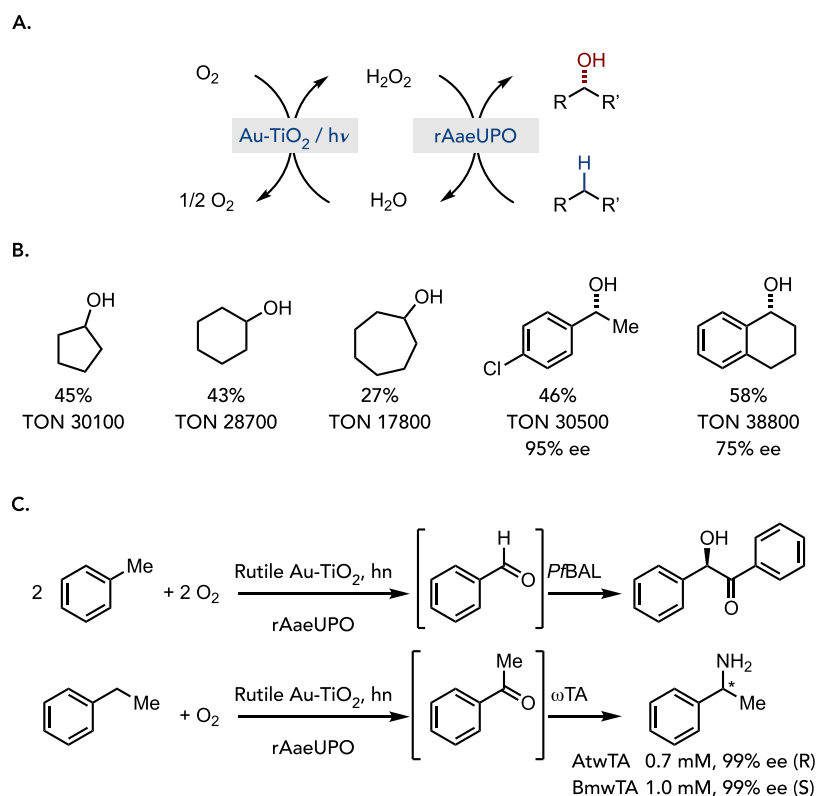


Figure 61. TiO_2 -driven peroxide formation from water. (A) General reach scheme. (B) Representative substrate scope. (C) Enzyme cascades involving peroxygenases.

were obtained. This platform provides a potential method to convert fatty acids into valuable terminal alkenes.

Based on the above platform ($\text{OleT}_{\text{JE}}/\text{FMN}/\text{O}_2/h\nu$), the same group starting from ω -hydroxyl fatty acids synthesized ω -alkenol, followed by several enzymatic or chemical cascades to transform the hydroxyl group or double bond (Figure 59).¹⁸⁰ The first step, photoassisted enzymatic decarboxylation, resulted in the ω -alkenol formation. Considering the hydroxylation side product in the OleT_{JE} -catalyzed reactions, the authors studied the influence of the buffer system, cosolvent, and pH on the selectivity. Except for the effect of substrate chain length, as mentioned above, the Britton–Robinson buffer at pH 7 and 10% (v/v) DMSO favored decarboxylation over hydroxylation. Subsequently, oxidation of the resultant alcohol leads to the formation of aldehyde or acid. Transaminase can convert the aldehyde into an amine product. Besides, the ruthenium-catalyzed olefin metathesis provides the internal alkene product (Figure 59).

4.1.6. Peroxygenases. Peroxygenases offer an efficient way to oxidize carbon–hydrogen bonds to the corresponding alcohols.¹⁸¹ These heme-dependent enzymes are substrate-promiscuous and consume H_2O_2 to form the catalytically active oxyferryl heme species, offering a distinctly different mode of reactivity from that of the well-studied P450 enzymes, which consume O_2 . However, a large issue is enzyme deactivation with a half-life of 38 min in the presence of 50 μM H_2O_2 at room temperature, resulting in low efficiency and turnover with increasing concentrations of the peroxide reagent.¹⁸² By generating H_2O_2 *in situ* and thus avoiding the accumulation of excess reagents, Hollmann and co-workers developed a methodology powered by methanol.¹⁸³ Nevertheless, peroxygenases suffer from poor scalability due, in part,

to the excessive amounts of glucose used to generate H_2O_2 using glucose oxidase. Moreover, the gluconic acid product poses an issue to the pH stability of the mixtures and, thus, scalability. To overcome these issues, the team developed a mild photocatalytic regeneration system for the cofactor (Figure 60A). Applying a heterogeneous gold catalyst on a TiO_2 platform was central to their methodology, promoting the formation of H_2O_2 from methanol via photoexcitation of the cluster. The distinct polymorphic structures of TiO_2 were leveraged for their studies, whereas a rutile catalyst developed for hydrogen evolution was investigated (Figure 60B).¹⁸⁴ The rutile catalyst was used in 10 g L^{-1} , with more catalyst leading to decreased product formation, which was attributed to the increasing cloudiness of the mixture. Investigations into the methanol concentrations showed that the maximum peroxide generation was reached at 250 mM. They hypothesized that the rate of the enzyme transforming substrate and the rate of peroxide formation leveled, leading to the rate limitation by the enzyme. In addition, the use of methanol proved to increase the stability of the mixture, which is attributed to the inhibition of hydroxyl radical formation. Enzyme loadings exceeding 150 nM concentrations showed no increase in the overall reaction rate. The team investigated a set of cycloalkane and benzylic alkane substrates showing excellent yields, TONs, and enantioselectivities (Figure 60C).

To minimize the waste and complexity of the reaction, the water-based solvent could ideally serve as a cosubstrate to form the peroxide *in situ* by an oxidation process. With the previous development of water oxidation catalysts, Hollmann and team proposed the development of a peroxygenase reaction fueled by water (Figure 61A).^{185–187} Initial investigations on

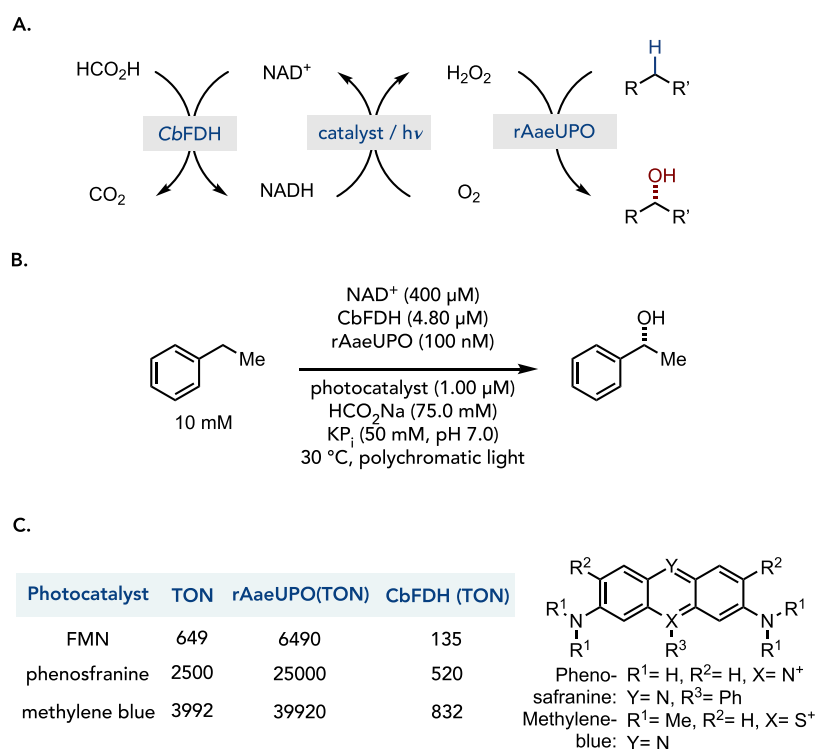


Figure 62. Photocatalytic peroxide generation using formate dehydrogenase and a photocatalyst. (A) General schematic for peroxygenase turnover. (B) Model reaction. (C) Survey of different photocatalysts.

arbitrarily chosen conditions revealed that the approach was feasible, forming a benzylic alcohol in the process.

Investigations with H₂¹⁸O under the exclusion of air were conducted to identify whether the proposed mechanism was reasonable. The product predominantly showed incorporation of ¹⁸O, whereas controls under ambient air showed only minor incorporations supporting the hypothesis of O₂ and, subsequently, H₂O₂ formation from water. One of the main challenges was the accumulation of short-lived hydroxyl radicals in solution, which were identified by EPR studies. These radicals were formed on the surface of the TiO₂ catalyst, leading to enzyme decomposition. To overcome this issue, immobilization and spatial separation of the enzyme were evaluated. Using rutile rather than anatase polymorphs of TiO₂ or immobilization via imine condensation, the enzyme activity was maintained for 120 h, corresponding to a 20-fold increase in robustness. Due to the minimization of the observed background reaction without enzyme, using a rutile gold photocatalyst was chosen as the ideal method. Surprisingly, rutile-Au-TiO₂ improved overall stability despite generating more hydroxyl radicals than the corresponding anatase polymorph. The team hypothesized that the adsorption of the enzyme is much lower and that the lifetime of the radicals is too short for them to react.

The scope of substrates (Figure 61B) included aliphatic cyclic substrates, benzylic compounds, and aliphatic chains, enabling the transformations with high TONs and high enantioselectivities. Furthermore, the overoxidation products observed by the method were used in one-pot downstream processes (Figure 61C), performing enzymatic benzoin reactions and stereodivergent transaminations in excellent yields and enantioselectivities.

The relatively limited range of applicable wavelengths for heterogeneous Au-TiO₂ catalysts and flavin-based catalysts to

harvest light led to the development of applying photosensitizers for generating peroxide *in situ*. Hollmann and team evaluated a proposed cascade relying on formate as the source of NAD⁺ cofactor regeneration (Figure 62A) which was previously described without a photocatalytic turnover.^{188–191} CbFDH generates NADH, which is consumed by the photocatalyst to transform oxygen into H₂O₂ to be used by the peroxygenase.

They investigated their proposal with the model substrate 1-phenylethane (Figure 62B). After evaluating 23 commercial photocatalysts, six acridine catalysts showed catalytic activity. Out of these, phenosafranine (*I*_{max} = 522 nm), methylene blue (*I*_{max} = 664 nm), and FMN (*I*_{max} = 450 nm) were selected, as they are soluble in water and cover a broad range of the visible light spectrum. The observed reaction rates with the respective photocatalysts all correspond to the photocatalytic generation of hydrogen peroxide. Investigations of the concentration of the photocatalysts revealed that all but methylene blue, which had a linear dependency, displayed saturation-type behavior. Furthermore, the light intensity linearly correlated with the percentage of product formed. Interestingly, changing the concentrations of the NAD⁺ and CbFDH altered the rate, whereas changing the concentration of the rAaeUPO did not indicate any clear influence. Hence, the photochemical oxidation of NADH was concluded to be the rate-determining step.

FMN turned out to deactivate the CbFDH, putatively, due to the modification of surface-bound residues of the enzyme, resulting in lower TONs (Figure 62C). On the other hand, phenosafranine and methylene blue did not exhibit such a deactivation pathway, with the latter showing the highest TON for all three catalysts involved.

4.2. Synthetic Photochemical/Enzyme Cascades

In the previous section, the photocatalysts were functioning on a cofactor, catalyst, or substrate to generate an intermediate required for the enzymatic reaction. This section will focus on photocatalytic reactions that modify the substrate with which the enzyme reacts. This family of reactivity falls into two basic categories: (i) reactions where the enzymatic and photochemical reactions occur simultaneously (one-pot/one-step reactions) and (ii) reactions where the enzymatic and photochemical reactions occur in separate steps (one-pot/two-step reactions).

4.2.1. One-Pot/One-Step Cascades. Photoredox catalysts generate radical intermediates under mild conditions and are compatible with thermally sensitive proteins. Moreover, in contrast to thermal radical initiators that can only generate a single radical chain, photoredox catalysts can initiate multiple radical chains and rescue intermediates that fall into unproductive pathways. These features make photoredox catalysts well-suited for facilitating racemizations in dynamic kinetic resolutions. In pioneering studies, Bertrand and Gil found that lipases can participate in dynamic kinetic resolutions of amines when using thiyl radicals as reagents for substrate racemization.^{192–195} In many of their studies, thiyl radical formation was initiated using AIBN. As AIBN decomposes over time, multiple recharges of AIBN were required to achieve high yield and selectivity.

Zhou and co-workers explored the same type of dynamic kinetic resolution using $\text{Ir}(\text{ppy})_2(\text{dtbbpy})\text{PF}_6$ as a photocatalyst for radical initiation and mercaptooctanol as a hydrogen atom-transfer catalyst for racemization of the amine substrate (Figure 63A).¹⁹⁶ Mechanistically, racemization occurred via oxidation and deprotonation of mercaptooctanol to afford a thiyl radical that selectively abstracts the α -amino hydrogen atom of the substrate to afford the α -amino radical.

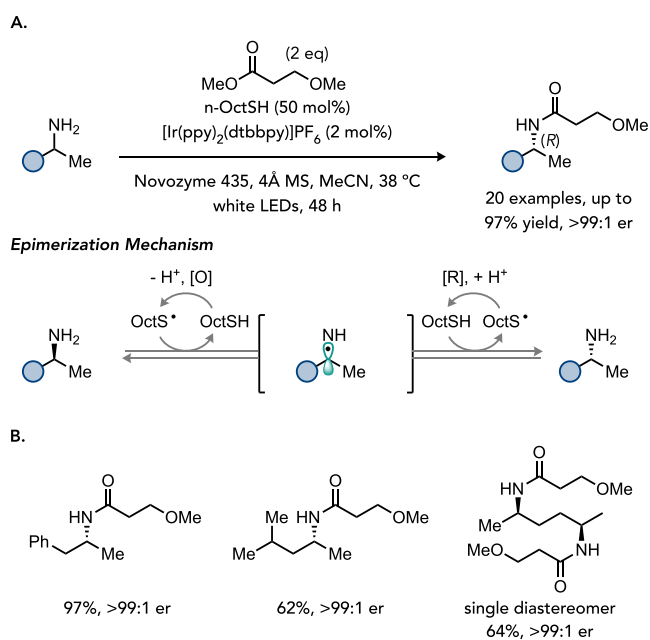


Figure 63. Dynamic kinetic resolution using photoredox catalyzed racemization. (A) General reaction schematic with mechanism for starting material racemization. (B) Representative substrate scope. Adapted with permission from *ACS Catalysis* 2022, 12, 8911. Copyright 2022 American Chemical Society.

The α -amino radical then abstracts a hydrogen atom from another equivalent of the thiol to form the racemized product and re-form a thiyl radical (Figure 63A). When this racemization is run in the presence of the immobilized lipase B from *Candida antarctica* (Cal-B) and an ester as an acyl source, a dynamic kinetic resolution can be carried out in high yields and excellent enantioselectivities (Figure 63B).

Wenger and Ward demonstrated that photoredox catalysis could be merged with monoamine oxidase (MAO) to prepare chiral amines from imines (Figure 64A).¹⁹⁷ In this reaction, a

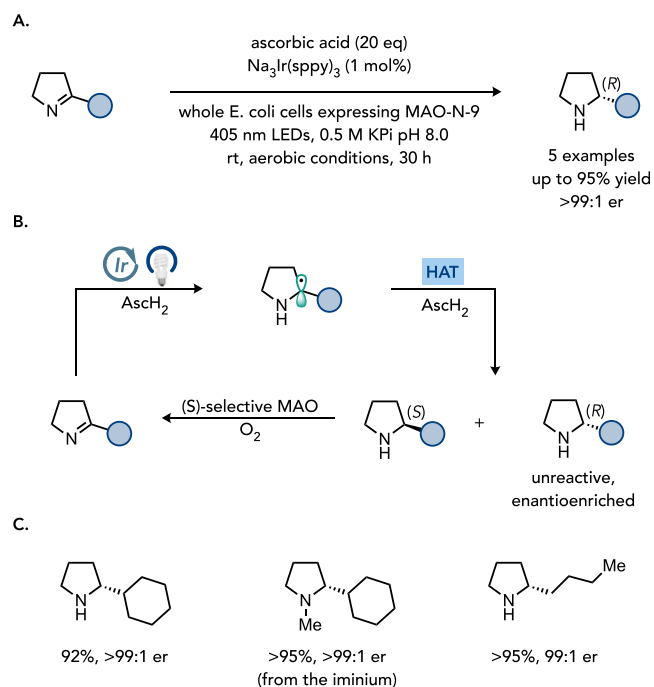


Figure 64. Photobiocatalytic amine deracemization using monoamine oxidases. (A) General scheme for the dynamic kinetic resolution. (B) Reaction mechanism. (C) Representative substrate scope. Adapted with permission from *ACS Catalysis* 2022, 12, 8911. Copyright 2022 American Chemical Society.

cyclic imine is reduced by a water-soluble sulfonated iridium photocatalyst to afford an α -amino radical, which is quenched via hydrogen atom transfer by ascorbic acid to afford a racemic amine. Selective oxidation of the *S*-enantiomer of the amine by the MAO regenerates the imine, leaving behind the unreactive *R*-enantiomer (Figure 64B). Multiple iterations of this cycle led to the accumulation of amine products with high enantioselectivity. These reactions must be run in whole *E. coli* cells to achieve high activity and selectivity, suggesting the photocatalyst has a detrimental effect on the reaction.

Gilmour and co-workers have explored the contra-thermodynamic isomerization of alkenes catalyzed by photocatalysts.¹⁹⁸ Mechanistically, these reactions occur via energy transfer from the photocatalyst to the alkene to form a diradical that readily undergoes isomerization. Hartwig and co-workers recognized that this isomerization mechanism could be used with “ene”-reductases in a dynamic kinetic reduction (Figure 65A).¹⁹⁹ The “ene”-reductase (ERED) from *Yersinia bercovieri* (YersER) can reduce the *E*-isomer of phenylsuccinate but not the *Z*-isomer. The authors hypothesized that an iridium photocatalyst or FMN could photochemically isomerize the more readily available *Z*-isomer to the *E*-isomer. After

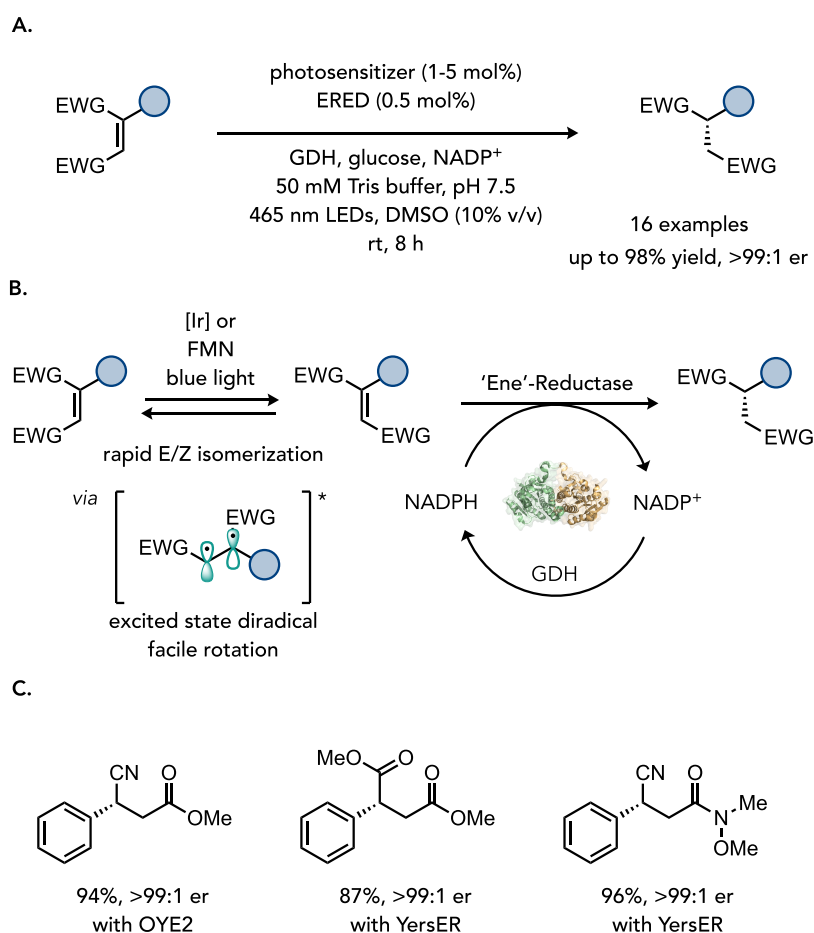


Figure 65. Photocatalytic alkene isomerization via an energy-transfer mechanism. (A) General reaction scheme. (B) Mechanism of the tandem reaction. (C) Representative substrate scope. Adapted with permission from *ACS Catalysis* 2022, 12, 8911. Copyright 2022 American Chemical Society.

developing the reaction, they found that 1–5 mol % of a photocatalyst with 0.5 mol % of an ERED enabled the desired transformation in high yield with excellent levels of enantioselectivity (Figure 65B). The reaction demonstrated good compatibility with various substrates and was modular to enable different EREDs to be used in the reaction (Figure 65C). This method consumes only a single olefin isomer, so the photocatalyst must reestablish the photostationary state required to achieve full conversions. This method nicely highlights the compatibility of nonimmobilized enzymes with photocatalysts.

Biocatalytic transformations are compatible with chemocatalytic methods in synergistic, dynamic one-pot reactions. However, many examples of chemoenzymatic catalysis comprise dynamic kinetic resolutions that typically involve the racemization of dynamic (i.e., chemically active) C–H stereocenters (e.g., α -keto, α -amino). In a collaboration between the Hyster and MacMillan groups, a strategy was developed to target traditionally static stereocenters and render them dynamic in a stereoconvergent transformation (Figure 66A).²⁰⁰ They developed a novel racemization targeting traditionally static β -keto C–H stereocenter racemization. There is a lack of methods targeting these stereocenters due to their inert nature. However, this racemization could be realized by merging photoredox, organo-, and hydrogen-atom-transfer (HAT) catalysis.²⁰¹ Mechanistically, the racemization operates through the initial condensation of an amine organocatalyst

onto the β -stereogenic ketone substrate to form the corresponding enamine intermediate. Oxidation of this intermediate via an excited state iridium photocatalyst forms an enamyl radical cation with a substantially acidified β position. Deprotonation at this position forms a key stereoablated α -enamyl radical species, which can undergo HAT with a thiol HAT catalyst to racemize the β stereocenter. The resulting racemic enamine can then undergo hydrolysis to the racemic ketone. Finally, thiol reduction by the reduced photoredox catalyst followed by protonation completes the photoredox and HAT catalytic cycles. Concurrent to this racemization, a kinetic resolution mediated by a ketoreductase forms enantio- and diastereoenriched 3-substituted alcohol products on only one enantiomer of the ketone (Figure 66B). During optimization the authors found that the amine organocatalyst needed to be hydrophobic to outcompete enamine hydrolysis in aqueous conditions and mitigate enzyme deactivation.

The success of this multicomponent process emphasizes the impressive compatibility and the promising future for combining photoredox and/or small molecule chemistries with biocatalytic transformations. This was highlighted foremost through the efficient operation of up to five separate catalytic cycles in the same pot. Various cyclic β -stereogenic ketones could be converted to their corresponding alcohols with good yields and selectivities, including an example, substantially expediting the synthesis of the pharmaceutical

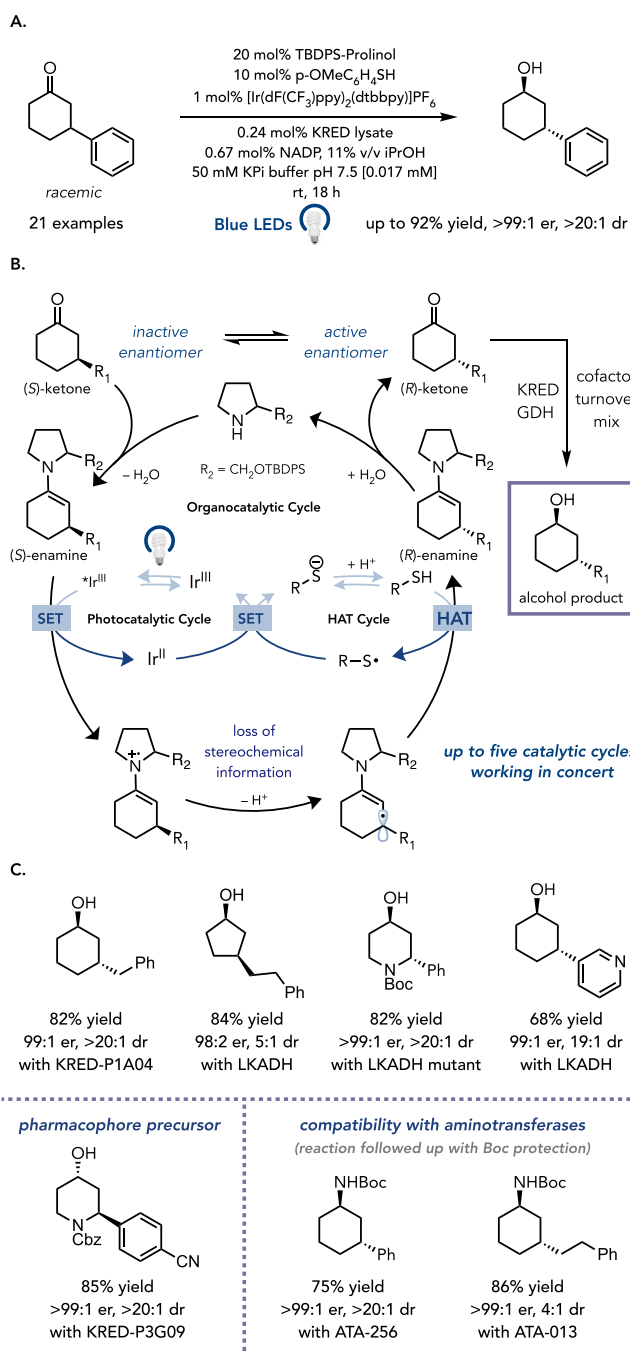


Figure 66. Organocatalytic racemization of β -stereogenic ketones in a photobiocatalytic dynamic kinetic resolution. (A) General reaction scheme. (B) Overall reaction mechanism. (C) Representative substrate scope. Adapted with permission from ACS *Catalysis* **2022**, *12*, 8911. Copyright 2022 American Chemical Society.

LNP023 (Figure 63C). Additionally, the scope of this transformation benefited from compatibility with several ketoreductases. This was exemplified through the selective syntheses of each of the four alcohol stereoisomers of a model ketone substrate simply by combining the racemization conditions with different ketoreductases. Finally, the authors showed the racemization could be successfully combined with pyridoxal phosphate-dependent aminotransferases for the stereoconvergent synthesis of chiral 3-substituted primary amines. Overall, this dynamic kinetic resolution (DKR)

demonstrates the promise for future developments of dynamic radical-based chemoenzymatic transformations.

Castagnolo and co-workers demonstrated a one-pot/one-step cascade to prepare 1,3-mercaptoalcohols from thiols and Michael acceptors.²⁰² In the first step, Ru(bpy)₃Cl₂ catalyzes a thiol–ene reaction to afford a β -silyl ketone. Then a KRED was used to reduce the ketone. Cofactor turnover is enabled by *i*-PrOH. As the thiol–ene reaction occurs in less than 5 min, the conjugate addition outcompetes the reduction of the methyl vinyl ether, leading to product formation with high yield and excellent enantioselectivity (Figure 67).

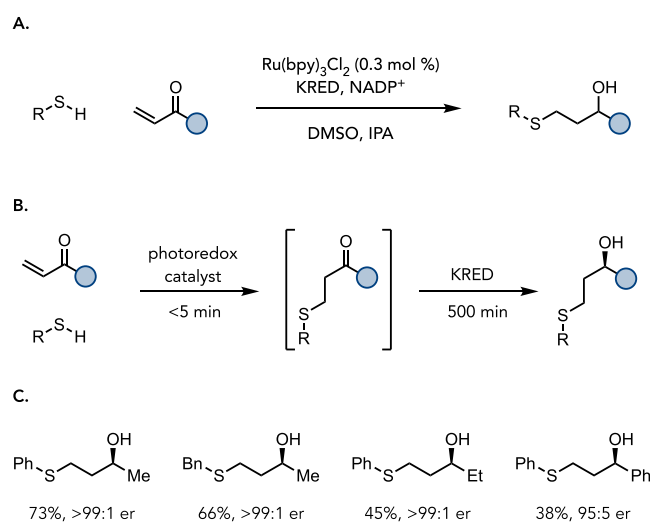


Figure 67. Conjugate addition ketone reduction.

Guan and He developed a photobiocatalytic cascade for synthesizing 2,2-disubstituted indol-3-ones using a photoredox catalyst and catalytically promiscuous lipase.²⁰³ In this reaction, the 2-substituted indole was photochemically oxidized by Ru(bpy)₃Cl₂ and O₂ to prepare an α -ketoimine *in situ*. This intermediate was then used as a substrate by wheat germ lipase for an asymmetric Mannich reaction with acetone. This promiscuous function by lipases was initially reported by Yu and co-workers using various lipases from different organisms.²⁰⁴ This reaction works for an array of different 2-aryl indoles, providing product in good yield with good to excellent levels of enantioselectivity. The reaction also accommodated cyclic and unsymmetric ketones, with functionalization occurring at the most substituted enol carbon. Reaction times were typically 48 to 74 h, presumably because the lipase was not optimized for this non-natural function. Control experiments confirmed that a properly folded lipase was essential for the observed reactivity (Figure 68).

Winkler and Glueck described a deracemization of chiral sulfoxides using a photobiocatalytic enzyme cascade (Figure 69A).²⁰⁵ Methionine sulfoxide reductase (SOR) can selectively reduce one enantiomer of the racemic sulfoxide using a conserved cysteine within the protein active site coupled with dithiothreitol as a terminal reductant (Figure 69B).²⁰⁶ They found that the SOR from *Pseudomonas montelii* (paMsr) could catalyze the stereoselective reduction of methyl aryl sulfoxides. For methyl thioether oxidation, the researchers found that an analog of chlorophyll cleanly provided the sulfoxide with no overoxidation to the sulfone. When these two steps were combined, an efficient and selective deracemization of sulfoxides was achieved, providing between 43% and 91% of

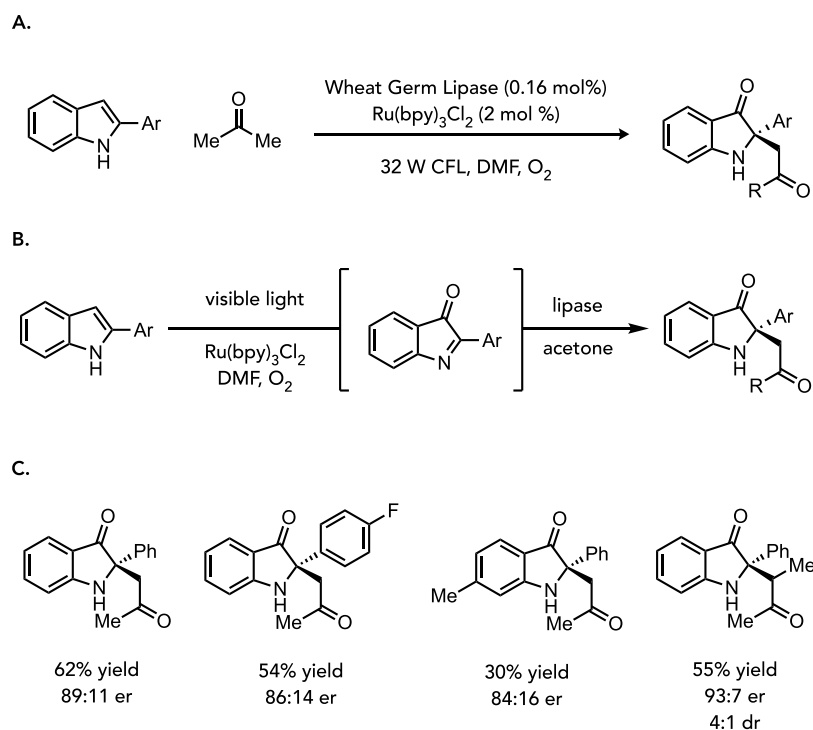


Figure 68. Photobiocatalytic conversion of 2-aryl indoles to indolones. (A) Photocatalyst/lipase tandem cascade. (B) Steps in the cascade. (C) Representative substrate scope.

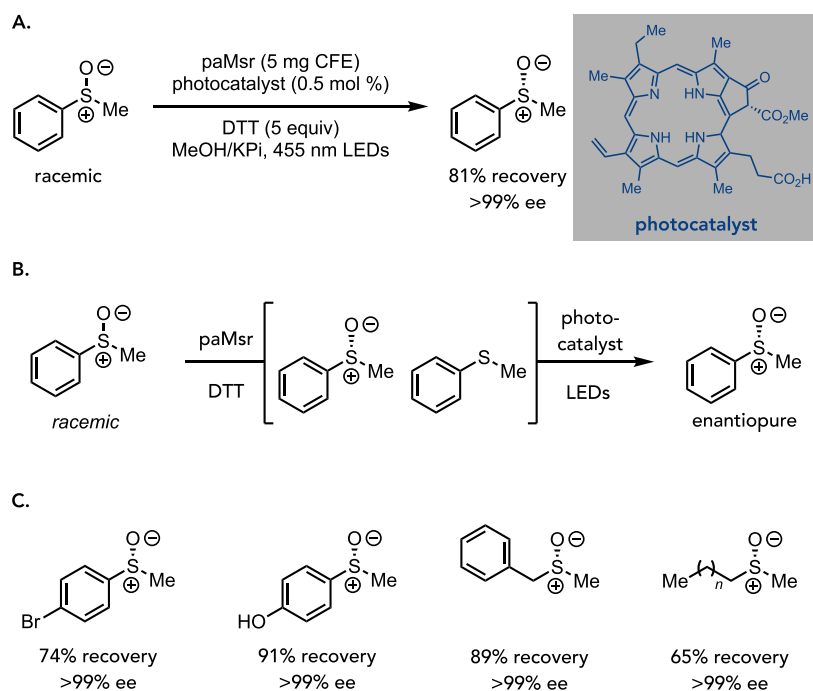


Figure 69. Deracemization of sulfoxides using a photobiocatalytic cascade. (A) Tandem photocatalyst/enzyme cascade for sulfoxide deracemization. (B) Steps of the cascade. (C) Representative substrate scope.

recovered starting material with >99% ee. The reaction was effective for methyl-aryl sulfoxides and dialkyl sulfoxides, highlighting the generality of this approach (Figure 69C).

Beyond using enzymes for stereoselective transformations, researchers have used enzymes in combination with photocatalysts to facilitate the synthesis of achiral molecules. For instance, Xie, Le, and Zhu used Cal-B to saponify *N*-aryl glycine methyl ester to afford the corresponding carboxylic

acid.²⁰⁷ This acid can then react with an enaminone using methylene blue as a photocatalyst to afford 3-substituted chromones in good yield. In a contemporary report, Wang and Yu demonstrated that lipase from *Candida rugosa* can catalyze a Friedel–Crafts reaction in the photobiocatalytic C3-formylation of indole.²⁰⁸ In this reaction, aqueous formaldehyde reacts with aniline to afford an imine, which can alkylate the C3-position of *N*-methylindole under the aegis of

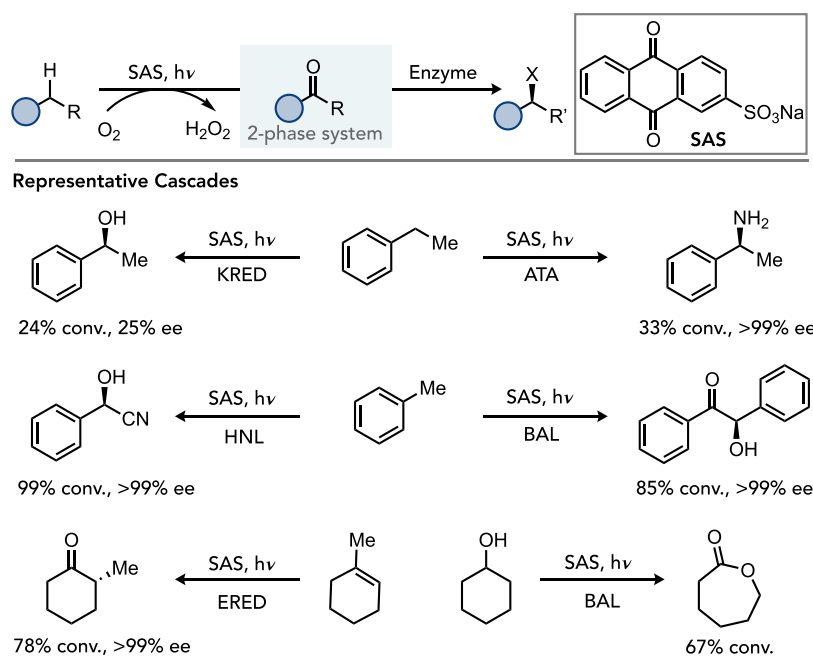


Figure 70. Asymmetric C–H functionalization of alkanes via photoredox catalysis and enzyme catalysis.

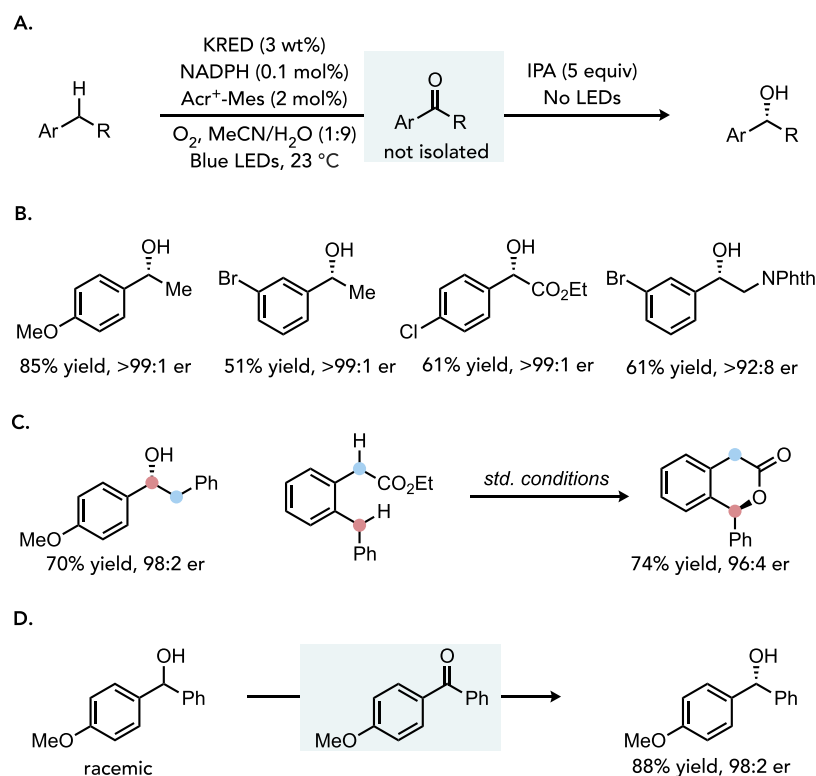


Figure 71. Asymmetric benzylic C–H hydroxylation via photoredox catalysis and KRED cascade. (A) Two-step approach for benzylic oxidation followed by ketone reduction by a KRED. (B) Representative substrate scope. (C) Site selective hydroxylation. (D) Deracemization.

the lipase. A histidine within the protein active site is proposed to serve as a hydrogen bond donor to activate the imine for the Friedel–Crafts reactions. In a concurrent photoredox reaction, the alkylated indole product is oxidized by 4CzIPN to the corresponding iminium and hydrolyzed to afford the 3-acyl indole product.

4.2.2. One-Pot/Two-Step Photobiocatalytic Cascades.

Recently, photocatalyzed *sp*³ C–H functionalization via single-

electron-transfer (SET) processes has witnessed rapid development. However, the enantioselective *sp*³ C–H functionalization via SET remains challenging. Very recently, chemists developed a series of enantioselective transformations using a photocatalyzed C–H functionalization followed by an enzyme-catalyzed asymmetric transformation. In 2019, Schmidt, Höhne, and co-workers developed an asymmetric C–H oxyfunctionalization of alkanes through a combination of

organophotocatalysis and enzyme catalysis (Figure 70).²⁰⁹ In this case, the alkanes could be oxidized to alkyl aldehydes and alkyl ketones by the organophotocatalyst sodium anthraquinone sulfate (SAS) under light irradiation. Then, the alkyl aldehydes and ketones could be selectively converted to chiral alcohols, amines, hydroxynitriles, acylolins, and achiral ketones in one-pot with high enantioselectivity (up to 99% ee) catalyzed by several enzymes, such as KREDs, transaminases (ATAs), hydroxynitrile lyase (HNL), benzaldehyde lyase (BAL), and EREDs (Figure 70). However, most cascade transformations provided lower conversion due to catalyst inhibition/deactivation, which reaction participants, cosolvent, or the formation of reactive oxygen or radical species in the reaction caused. The authors carried out a two-phase approach and a stepwise reaction to solve these problems. Finally, the authors pointed out that protein engineering can be applied to improve the activity and stability of the enzyme to increase catalyst compatibility in photobiocatalytic cascades. In 2019, Hollmann and co-workers used SAS to photo-oxidize alcohol starting materials in a one-pot/two-step cascade with transaminases to produce the corresponding chiral amine.²¹⁰ In 2020, Wu and co-workers extended this methodology by using enantiodivergent KREDs to access both stereoisomers of the chiral alcohol.²¹¹

Scheidt and co-workers developed an enantioselective benzylic C–H hydroxylation using a photoredox and enzymatic cascade reaction (Figure 71A).²¹² In this case, 9-mesityl-10-methylacridinium ion (Acr^+ -Mes ClO_4^-) ($E_{1/2} = 2.06$ V vs SCE) was applied as a photocatalyst for selective benzylic C–H oxidation under light irradiation in the presence of O_2 . Then a KRED was added to the pot to form enantioenriched benzyl alcohols. This light-driven oxidation and enzymatic reduction cascade worked on a broad range of substrates with excellent chemo-, regio-, and enantioselectivity (Figure 71B). Particularly interesting is the high regioselectivity for the most electron-rich C–H bond in substrates containing multiple benzylic C–H bonds (Figure 71C).

The authors carried out a series of mechanistic experiments to investigate the mechanism of this one-pot oxidation/reduction cascade reaction (Figure 71). A radical clock experiment used 1-(cyclopropylmethyl)-4-methoxybenzene. The ring-opened product was obtained in 61% yield, indicating radical formation occurred. Additionally, no desired product was found when adding either (2,2,6,6-tetramethylpiperidin-1-yl)oxyl (TEMPO) or butylated hydroxytoluene (BHT) under standard conditions, further suggesting a radical intermediate is formed in the reaction. Additionally, high yield and enantioselectivity were obtained (88% yield and 98:2 er) when the authors submitted racemic benzylic alcohol into the reaction, indicating that this oxidation/reduction cascade process can deracemize benzyl alcohols.

4.2.3. Outlook. The compatibility of photocatalysts and enzymes make them attractive for tandem photochemistry/enzyme cascades. In the first section, we summarized how enzymes can be used with photocatalysts for dynamic kinetic resolutions. While these reactions highlight the compatibility of these catalysts, future directions should be focused on developing new types of cascades that target challenges at the frontier of selective chemical synthesis. Reactions in the second half are focused on one-pot/two-step reactions. The development of immobilization systems that enable both reactions to operate simultaneously would enhance the simplicity and synthetic utility of this work.

5. ENZYMATIC REACTIONS COUPLED TO NATURAL PHOTOSYNTHESIS

Oxidoreductases, such as alcohol dehydrogenases, ene-reductases, amine dehydrogenases, and oxygenases, are among organic synthesis's most widely used enzymes.²¹³ All these reactions require stoichiometric amounts of reductants such as glucose, formate, or 2-propanol and form equimolar amounts of byproduct, gluconic acid, CO_2 , and acetone during the processes.²¹⁴ The poor atom efficiency of cofactor regeneration systems becomes one of the main bottlenecks for applying these enzymes on an industrial scale. A strategy that couples the enzymatic redox processes to the photosystem in photosynthetic cells has recently been developed to solve this problem. In these reactions, the cyanobacteria produce NADPH in a water oxidation reaction. Biocatalysts can use these reducing equivalents to facilitate transformations.²¹⁵ This section will be organized based on how the biocatalyst interfaces with the cyanobacterium. In the first section, we will focus on systems that use enzymes natively expressed by the cyanobacterium. The second section will focus on cyanobacterium heterologously expressing a biocatalyst. The final section will focus on reactions where reducing equivalents are shuttled across the cyanobacterium membrane to enable biocatalytic transformations outside the cell.

5.1. Biocatalysts Native to Cyanobacteria

Early efforts to use cyanobacteria for biocatalysis relied on natively expressed enzymes for the desired function. In 2000, Nakamura and co-workers reported the asymmetric reduction of aryl methyl ketones using a cyanobacterium, *Synechococcus* sp. PCC 7942, via a photosynthetic whole-cell-catalyzed reaction (Figure 72).²¹⁶ Pentafluoroacetophenone can be

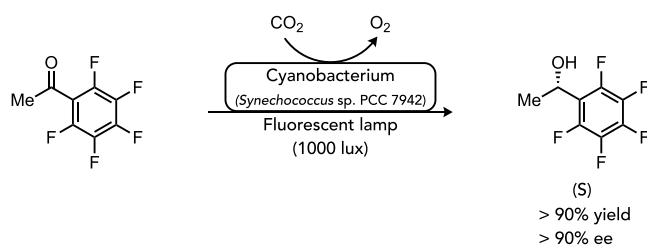


Figure 72. Reduction of acetophenone derivatives by cyanobacterium.

transformed to the corresponding (S)-alcohol using this strategy in over 90% yield and 99% ee after 3 days (Figure 72). The authors used 37 mg of cyanobacterium to achieve this reactivity to reduce 120 mg of the substrate. This approach is amenable to ketones with different aromatic substituents, providing products with high enantioselectivity but modest yield. A subsequent study found that ketone reduction occurred roughly four times faster when irradiated with light than when run in the dark, presumably due to increased NAD(P)H production.²¹⁷

In a follow-up study, the Nakamura group explored the role that light plays in influencing the enantioselectivity of the reduction of α,α -difluoroacetophenone by *Cyanobacterium*.²¹⁸ In the dark, the (R)-alcohol is produced with only 27–31% ee, while irradiation of the bacterium increases the enantioselectivity to 68–70% (Figure 73). A photosynthesis inhibitor, 3-(3,4-dichlorophenyl)-1,1-dimethylurea (DCMU), was added to elucidate the mechanism, which diminishes enantioselectivity

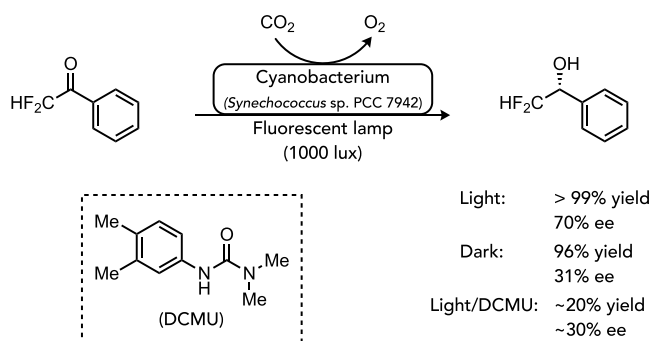


Figure 73. Influence of light on ketone reduction by cyanobacterium.

ity under irradiation to that observed in the dark reaction. The authors propose that multiple enzymes in the whole cell can catalyze the reduction—under light, NADPH is generated photosynthetically and is used by an (*R*)-selective oxidoreductase, while the (*S*)-selective oxidoreductase is primarily NADH-dependent. While the presence of multiple reactive enzymes complicates this overall strategy, it highlights an opportunity to use light to change the product outcome.

In 2015, Yamanak and co-workers reported the selective reduction of cinnamaldehyde to cinnamyl alcohol via cyanobacterial photobiocatalysis (Figure 74).²¹⁹ The authors explored this reaction using seven strains of cyanobacteria. They found that three different species, *Synechocystis* sp. PCC 6803, *Synechocystis* sp. PCC 6714, and *Fischerella musicola* UTEX, provide cinnamyl alcohol as the sole product with increased conversion under irradiation. In contrast, *Anabaena* sp. PCC 7120 forms a mixture of cinnamyl alcohol, phenylpropanal, and phenylpropanol favoring cinnamyl alcohol. Finally, *Synechococcus* sp. forms mixtures of phenylpropanal and phenylpropanol, which convert exclusively to phenylpropanol with extended reaction times. Importantly, with all species tested, there is significantly improved conversion to product when the cells are irradiated with light compared to dark reactions.

Cyanobacterial catalysis has also been used to synthesize chiral phosphonates, as demonstrated by Zymańczyk-Duda and Górak in 2015.²²⁰ Cyanobacteria from *Arthrospira maxima*, *Nostoc cf-muscorum*, and *Nodularia sphaerocarpa* were studied to reduce 2-oxoalkylphosphonates bearing aryl or alkyl groups (Figure 75). It was found that the substrate with an aryl group adjacent to the carbonyl functionality can be reduced to the diethyl (*S*)-2-hydroxy-2-phenyl ethyl phosphonate with high conversion and enantioselectivity. In contrast, substrates with methyl or ethyl groups showed lower enantioselectivities and significantly lower yield. Another promising aspect is that the cyanobacteria can tolerate high

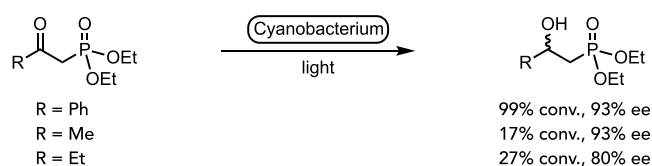


Figure 75. Reduction of 2-oxoalkylphosphonates using cyanobacterium and light.

substrate concentrations (up to 10 mM), which shows potential for preparative scale synthetic applications.

The cyanobacterium *Nostoc muscorum* PTCC 1636, isolated from paddy fields north of Iran, was reported to catalyze site-selective and regioselective bioconversion of hydrocortisone into androstane and pregnane derivatives, giving 11 β ,17 α ,20 β ,21-tetrahydroxypregn-4-en-3-one as the major product (Figure 76).²²¹

5.2. Heterologously Expressed Biocatalysts in Cyanobacteria

Since native cyanobacteria have multiple oxidoreductases, competing reactions can lead to mixtures of products with poor selectivity. Synthetic biologists have developed methods to heterologously express proteins within cyanobacteria, enabling the preparation of whole-cell biocatalysts which favor one product outcome. In 2017, a whole-cell catalyst of the recombinant bacterium *Rhodobacter sphaeroides* was used for a photobiocatalytic ketone reduction (Figure 77).²²² Several inducible expression plasmids are available for this organism, enabling heterologous expression of desired proteins. The authors introduced a plasmid encoding for the alcohol dehydrogenase (ADH) from *Leifsonia* sp. that was used to reduce 3'-chloroacetophenone to (*R*)-1-(3-chlorophenyl)ethanol with light. An *n*-hexane/aqueous biphasic medium was developed to allow a 70 mM optimum substrate concentration, providing 30% yield with a rate of 7.85 mM⁻¹ h⁻¹ g⁻¹ wet cells and >99% ee. The biphasic reaction mixture helps sequester the organic substrates away from the cell to avoid cell death or toxicity.

Kroutil and co-workers developed a cyanobacterium to express hydroxyisocaproate dehydrogenase to prepare α -hydroxyl acids from α -ketoacids.²²³ The dehydrogenase genes from *Lactobacillus confusus* (L-HicDH) and *Lactobacillus paracasei* (D-HicDH) were expressed in cyanobacterium *Synechocystis* sp. PCC 6803. L-HicDH expressed poorly in the cyanobacterium, providing low starting material conversion. However, D-HicDH expressed well, providing product in 53% yield with >99% ee.

Kourist and co-workers reported coupling an “ene”-reductase with cyanobacteria for a light-promoted enantioselective reduction of C=C bonds.²²⁴ The “ene”-reductase

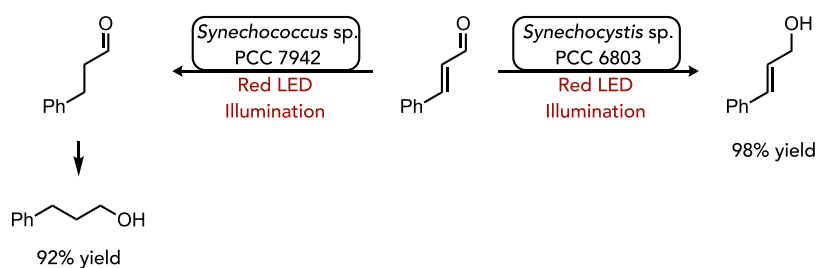


Figure 74. Cyanobacterial reduction of cinnamaldehyde with divergent product outcomes.

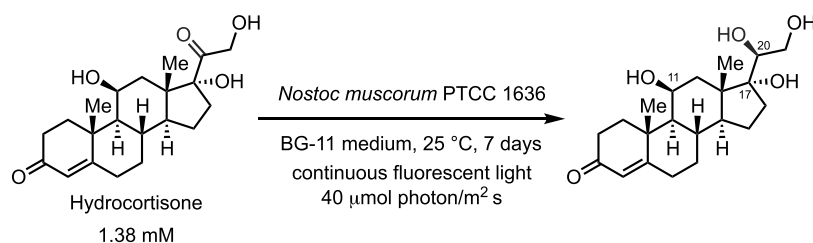


Figure 76. Cyanobacterial reduction of hydrocortisone.

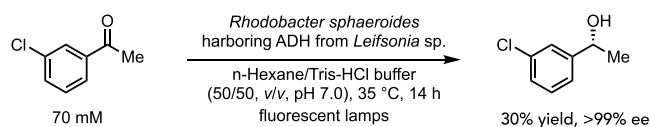


Figure 77. Ketoreductase using cyanobacteria.

YqjM from *Bacillus subtilis* was integrated into the cyanobacterium *Synechocystis* sp. PCC 6803 under the control of the light-induced promoter psbA2. The promoter allowed high expression levels and can be activated by a high-intensity light.²²⁵ The system was tested on a few substrates, and good conversions were observed (Figure 78). On a semipreparative scale (100 mg), (*R*)-naproxen was formed in 80% yield with >99:1 er.

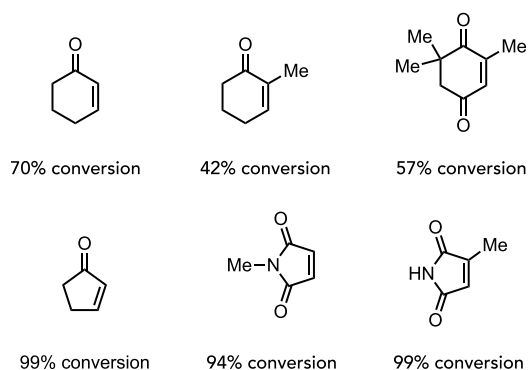
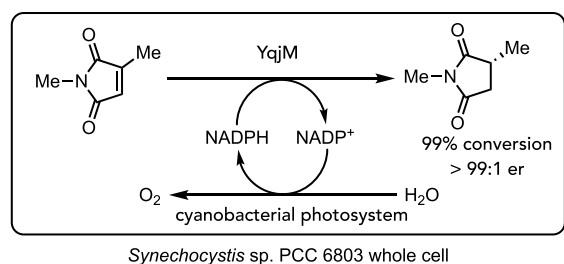


Figure 78. Ene-reductase activity using cyanobacteria.

By integrating an NADPH-dependent Baeyer–Villiger monooxygenase, cyclohexanone monooxygenase (CHMO) from *Acinetobacter calcoaceticus* NCIMB 9871, into the cyanobacterium *Synechocystis* sp. PCC6803, Kourist and co-workers developed a photosynthetic system that performed the oxyfunctionalization of cyclic ketones (Figure 79).²²⁶ The alcohol side products were observed, presumably due to endogenous alcohol dehydrogenases in the cyanobacteria.^{227,228} Interestingly, the ketone reduction proceeded faster in the *Synechocystis* wild-type than with the competing CHMO reaction (Figure 79), demonstrating the competing effect of both electron sinks.

In addition to utilizing the reduction system of cyanobacterial photosynthesis, the oxygen generated during the photosynthetic pathway can also be exploited in whole-cell biocatalysis to overcome the gas–liquid mass-transfer problem. Bühler and co-workers engineered the phototrophic cyanobacterium *Synechocystis* sp. PCC6803 to synthesize the alkane monooxygenase AlkBGT from *Pseudomonas putida* GPo1.²²⁹ Under anaerobic conditions with light irradiation, the system performed the regiospecific oxy functionalization of nonanoic acid methyl ester to ω -hydroxynonanoic acid methyl ester (Figure 80). Both the *in situ*-generated oxygen and cofactor were efficiently utilized. Kinetic studies indicated that the photosynthetically generated oxygen is concentrated within the microbial cell and captured *in situ* by the monooxygenase before diffusing out of the cell.

Using the same approach outlined above, Bühler and co-workers heterologously expressed the cytochrome P450 from *Acidovorax* sp. CHX100 to hydroxylate cyclohexane in high yield. The reaction rate was determined to be light-dependent. Using a two-phase system to slowly introduce substrate to the cell and remove cyclohexanol from the cell to avoid toxicity, the authors formed 4.5 g of cyclohexanol from 1 g of cells. This reaction could also be run on a 3 L scale using *in situ* O₂ generation using photosynthetic water oxidation.²³⁰

Kroutil and Kourist used a similar approach for imine reduction (Figure 81).²³¹ Using imine reductases (IREDs) previously reported to reduce cyclic imines, the authors introduced plasmids encoding these IREDs to the cyanobacteria. While initial attempts provided only modest yields, promoter engineering to decrease the toxicity of the enzyme led to cells that could reduce substrate with full conversion. Excellent enantioselectivities were observed in this reaction under the optimized reaction conditions.

Gröger and co-workers developed a microalgae-based photosynthetic formate production process and combined it with an amine dehydrogenase.²³² *Chlamydomonas reinhardtii* cells were first grown photoautotrophically in light and CO₂-enriched air, during which CO₂ was transformed into starch. The concentrated cell suspensions were transferred to darkness in airtight tubes, during which the starch was consumed and formate was excreted into the reaction medium. The formate-containing algal culture supernatants were combined with a formate dehydrogenase from *Candida boidinii* (cb-FDH)²³³ and an amine dehydrogenase EsLeuDH-DM²³⁴ to produce a variety of amines.

5.3. Transmembrane Shuttling

Winkler and Kroutil recognized that heterologous expression and substrate transport across the cyanobacteria wall presented a challenge in more broadly implementing photosynthetic organisms in biocatalytic reactions. To overcome this issue, they developed a shuttling strategy where acetone would shuttle reducing equivalents from a cyanobacterium to

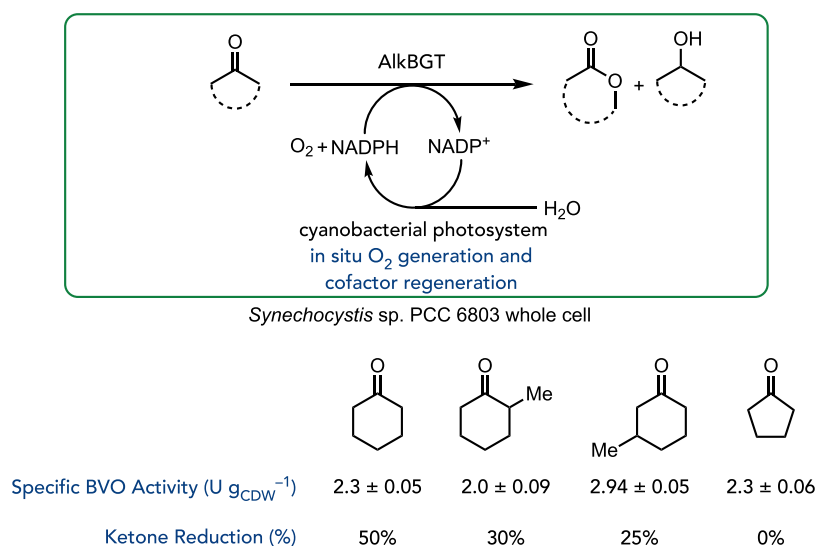


Figure 79. BVMO oxidation enabled by cyanobacteria.

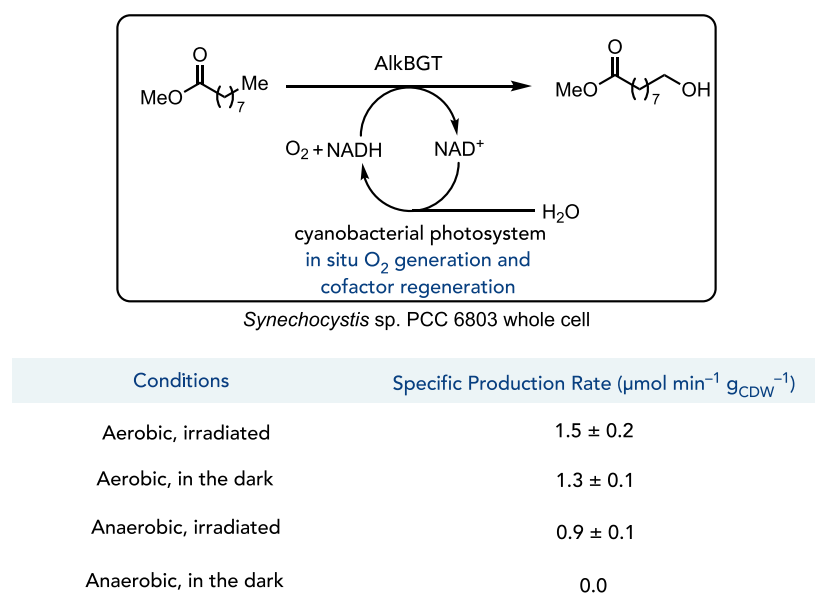


Figure 80. Cytochrome P450 oxidation.

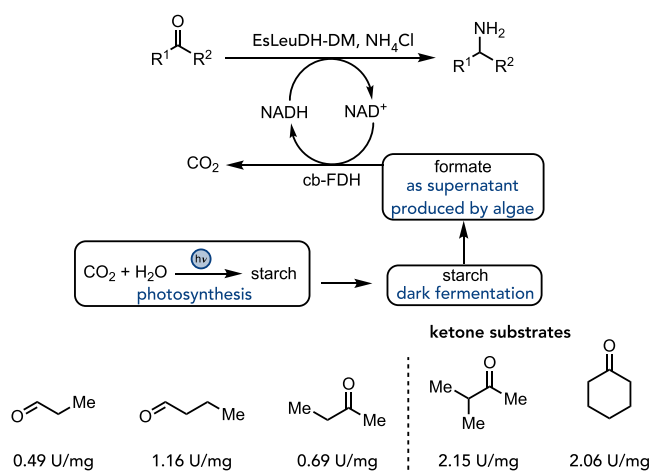


Figure 81. Photosynthesis to enable reductive amination.

biocatalysts in solution (Figure 82A).²³⁵ The cyanobacterium (*Synechococcus elongatus* PCC 7942) heterologously expressing the alcohol dehydrogenase from *Lactobacillus kefir* (Lk-ADH) reduces acetone to i-PrOH using photosynthetically produced NADPH (Module A). After passing through the cell membrane, i-PrOH is oxidized by the Lk-ADH to produce NADPH (Module B), which can be used by the enzyme of interest to modify a substrate (Module C). This highly modular approach enables a single cyanobacterium to drive many different types of biocatalytic reactions without requiring the cyanobacterium to express the biocatalyst of interest. In the initial report, the authors focus on systems where an “ene”-reductase is Module C (Figure 82B). They also demonstrate that alcohol dehydrogenases (Figure 82C), imine reductases (Figure 82D), and Baeyer–Villiger monooxygenases can serve as Module C.

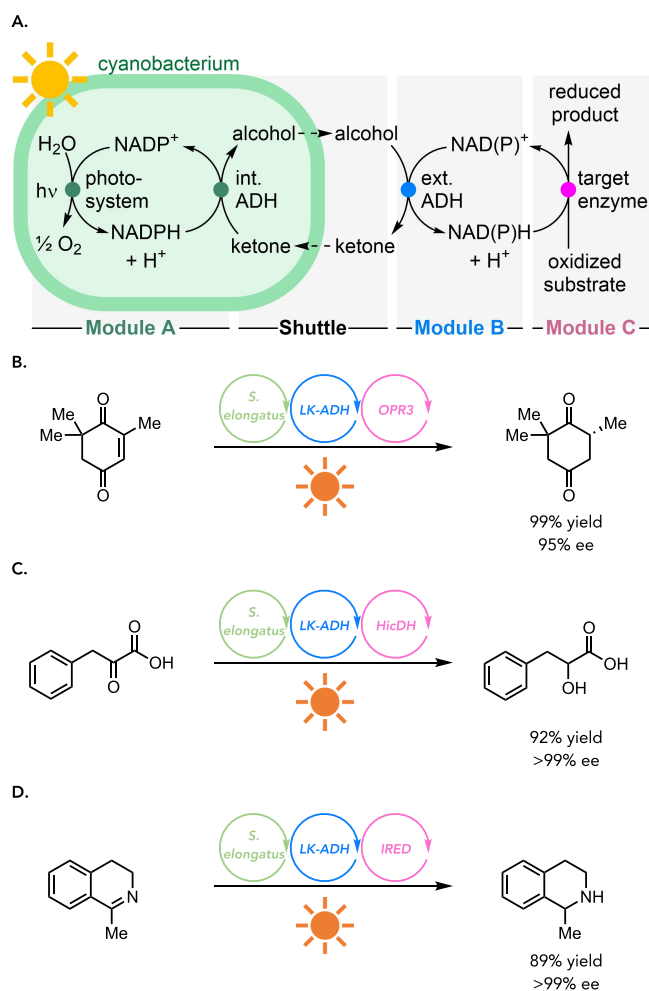


Figure 82. Redox shuttle for cyanobacteria. (A) General schematic for transmembrane shuttling of reducing equivalents. (B) Application of the shuttling cascade to alkene reduction via an ERED. (C) Application of the shuttling cascade for KREDs. (D) Application of the shuttling cascade for imine reduction via IREDs. Adapted with permission from *Angew. Chem. Int. Ed.* **2022**, *61*, e202207971. Copyright 2015 John Wiley & Sons.

6. CONCLUSION

The field of photobiocatalysis has blossomed exponentially over the past 20 years to the point where critical mechanistic differences have begun to surface, the most significant of which is how light promotes the transformation. As the field has grown, synthetic organic chemists have become more aware of the opportunities available to photocatalysis and how they can be used to solve synthetic challenges. By defining and delineating the activation modes, we aimed to provide a clear mechanistic understanding of how light enables the reported reactivity.

Despite tremendous progress, researchers have many opportunities to contribute significantly to the field. The issue of scalability is at the forefront of challenges in the area. Most photobiocatalytic reactions are run on an analytical or small preparative scale (<5 g). Moreover, the lighting setups' specific light intensity and wavelengths vary from group to group. Uniform lighting setups from commercial sources would help to facilitate reproducibility across the field. More broadly, it is essential to develop reactors that enable photobiocatalytic reactions to be run on large scales (>100

g). As biocatalysis is commonly used by the pharmaceutical industry, working with industrial researchers and engineers to develop new reactors that enable preparative scale reactions is essential to increase the adoption of this technology.

Beyond developing new reactors, we must also engineer proteins to use light more efficiently. Over the past decade, research efforts have been primarily focused on developing new photoenzymatic reactions. However, minimal effort has been focused on increasing the quantum yield, absorption profile, and overall activity. These metrics will need to be improved to decrease the enzyme loadings to the point where they can more easily be run at the catalyst loadings and substrate concentrations typically used in industrial biocatalytic reactions (<10 g/L enzyme lysate with >50 g/L substrate concentration). Directed evolution of existing proteins and introduction of new cofactors and chromophores into proteins can influence these parameters, leading to more valuable and efficient reactions.

Finally, we must develop new reactions that solve challenges plaguing modern organic chemistry. Selectivity is a hallmark of biocatalytic reactions. Given the breadth of selectivity challenges encountered by synthetic chemists, it is vital to target new photobiocatalytic reactions that solve these problems. The strategies for developing new reactions can vary significantly. Mining Nature for new photoenzymes will allow us to emulate Nature's synthetic strategies. Using mechanistic intuition, it should be possible to use existing enzymes in entirely new ways. Moreover, merging existing photocatalytic reactions with enzymes with an eye toward synthetic utility will make it possible to develop reactions that are more than the sum of their parts. Close collaborations with partitioner will be essential to make this area of research shine.

AUTHOR INFORMATION

Corresponding Author

Todd K. Hyster – Department of Chemistry and Chemical Biology, Cornell University, Ithaca, New York 14853, United States; orcid.org/0000-0003-3560-355X; Email: thyster@cornell.edu

Authors

Megan A. Emmanuel – Department of Chemistry, Princeton University, Princeton, New Jersey 08544, United States

Sophie G. Bender – Department of Chemistry and Chemical Biology, Cornell University, Ithaca, New York 14853, United States

Catherine Bilodeau – Department of Chemistry and Chemical Biology, Cornell University, Ithaca, New York 14853, United States

Jose M. Carceller – Department of Chemistry and Chemical Biology, Cornell University, Ithaca, New York 14853, United States; Institute of Chemical Technology (ITQ), Universitat Politècnica de València, Valencia 46022, Spain

Jacob S. DeHovitz – Department of Chemistry, Princeton University, Princeton, New Jersey 08544, United States

Haigen Fu – Department of Chemistry, Princeton University, Princeton, New Jersey 08544, United States

Yi Liu – Department of Chemistry, Princeton University, Princeton, New Jersey 08544, United States

Bryce T. Nicholls – Department of Chemistry, Princeton University, Princeton, New Jersey 08544, United States; Department of Chemistry and Chemical Biology, Cornell University, Ithaca, New York 14853, United States

Yao Ouyang – Department of Chemistry and Chemical Biology, Cornell University, Ithaca, New York 14853, United States

Claire G. Page – Department of Chemistry, Princeton University, Princeton, New Jersey 08544, United States; Department of Chemistry and Chemical Biology, Cornell University, Ithaca, New York 14853, United States

Tianzhang Qiao – Department of Chemistry and Chemical Biology, Cornell University, Ithaca, New York 14853, United States

Felix C. Raps – Department of Chemistry and Chemical Biology, Cornell University, Ithaca, New York 14853, United States

Damien R. Sorigué – Department of Chemistry and Chemical Biology, Cornell University, Ithaca, New York 14853, United States; Aix-Marseille University, CEA, CNRS, Institute of Biosciences and Biotechnologies, BLAM Cadarache, 13108 Saint-Paul-lez-Durance, France

Shang-Zheng Sun – Department of Chemistry and Chemical Biology, Cornell University, Ithaca, New York 14853, United States

Joshua Turek-Herman – Department of Chemistry, Princeton University, Princeton, New Jersey 08544, United States; Department of Chemistry and Chemical Biology, Cornell University, Ithaca, New York 14853, United States

Yuxuan Ye – Department of Chemistry and Chemical Biology, Cornell University, Ithaca, New York 14853, United States

Ariadna Rivas-Souchet – Department of Chemistry and Chemical Biology, Cornell University, Ithaca, New York 14853, United States

Jingzhe Cao – Department of Chemistry, Princeton University, Princeton, New Jersey 08544, United States; Department of Chemistry and Chemical Biology, Cornell University, Ithaca, New York 14853, United States

Complete contact information is available at:

<https://pubs.acs.org/10.1021/acs.chemrev.2c00767>

Author Contributions

Megan A Emmanuel writing-original draft, writing-review & editing; **Sophie G. Bender** writing-original draft, writing-review & editing; **Catherine Bilodeau** writing-original draft, writing-review & editing; **Jose M. Carceller** writing-original draft, writing-review & editing; **Jacob DeHovitz** writing-original draft, writing-review & editing; **Haigen Fu** writing-original draft, writing-review & editing; **Yi Liu** writing-original draft, writing-review & editing; **Bryce Nicholls** writing-original draft, writing-review & editing; **Yao Ouyang** writing-original draft, writing-review & editing; **Claire Page** writing-original draft, writing-review & editing; **Tianzhang Qiao** writing-original draft, writing-review & editing; **Felix C. Raps** writing-original draft, writing-review & editing; **Damien Sorigué** writing-original draft, writing-review & editing; **Shang-Zheng Sun** writing-original draft, writing-review & editing; **Joshua Turek-Herman** writing-original draft, writing-review & editing; **Yuxuan Ye** writing-original draft, writing-review & editing; **Ariadna Rivas-Souchet** writing-review & editing; **Jingzhe Cao** visualization, writing-review & editing; **Todd K. Hyster** visualization, writing-original draft, writing-review & editing.

Notes

The authors declare no competing financial interest.

Biographies

Megan A. Emmanuel was born and raised in Trinidad and Tobago. She did her undergraduate studies at New York University (NYU), where she did research with Prof. Marc Walters synthesizing organometallic nanomaterials for medical imaging. After completing her B.Sc., Megan did postbaccalaureate research at Weill Cornell Medical College with Prof. Stefano Rivella, looking into the antileukemic effects of proanthocyanidin natural products. She moved on to graduate studies at Princeton University in the lab of Prof. Todd Hyster, developing light-driven, non-natural enzymatic reactions. Megan is now a Senior Scientist in the Chemical Process Development group at Bristol Myers Squibb, where she develops and characterizes safe, robust processes for active pharmaceutical ingredients and drug intermediates.

Sophie G. Bender received her B.A. in Chemistry from Reed College in 2020, where she worked in the lab of Prof. Rebecca L. LaLonde on the development and synthesis of selective estrogen receptor modulators. She began her doctoral studies at Princeton University in the fall of 2020 under the supervision of Prof. Todd K. Hyster and transferred to Cornell University at the beginning of 2021 to continue her work in the Hyster group. Her research focuses on developing novel stereoselective carbon–carbon bond formations catalyzed by flavin-dependent “ene”-reductases.

Catherine Bilodeau received her B.S. in chemistry from Dickinson College in 2021, where she worked in the lab of Dr. Jason Gavenonis. During this time, she also interned at Curia Global, where she worked for Dr. Nasir Baig and Dr. Syed Mahmood. Currently, she is a second-year graduate student at Cornell University, working under the supervision of Dr. Todd K. Hyster.

Jose M. Carceller was born in Valencia, Spain, in 1991. He studied Chemistry at the Universidad de Valencia in 2014 and received his Ph.D. at the Universidad Politécnica de Valencia in 2019. Then he received a Margarita Salas grant and began his postdoctoral studies with Prof. Todd Hyster at Cornell University. His work focuses on the application of heterogeneous chemocatalysts and biocatalysts in the synthesis of fine chemicals and the use of visible light to expand the synthetic capabilities of enzymes.

Jacob S. DeHovitz is a postdoctoral researcher at the University of California, Berkeley, in the lab of Prof. Dean Toste in collaboration with Profs. Robert Bergman and Kenneth Raymond. Jacob completed his Ph.D. in 2021 under the guidance of Prof. Todd Hyster at Princeton University, where he developed asymmetric radical reactions involving biocatalysis and photochemistry. Jacob's postdoctoral research currently involves studying the mechanisms of supramolecular cluster-catalyzed reactions through structure–activity relationships.

Haigen Fu received his Ph.D. in 2019 from the University of Groningen, The Netherlands, under the supervision of Prof. Gerrit J. Poelarends. During his Ph.D., he developed asymmetric methods to synthesize noncanonical amino acids using C–N lyases. Afterward, he joined the group of Todd K. Hyster at Princeton University in 2020 and Cornell University in 2021 as a Postdoctoral Fellow. In Hyster lab, he evolved “ene”-reductases with photochemical strategies to unlock new reactivities to address challenges in organic synthesis.

Yi Liu completed her undergraduate studies in chemistry at Xiangtan University in 2013. She obtained her M.S. degree in 2016 from the Memorial University of Newfoundland in the group of Prof. Christopher M. Kozak, during which she studied organozinc complexes for ring-opening polymerizations. In 2021, she obtained her Ph.D. from McGill University under Prof. Bruce A. Arndtson in

studying palladium-catalyzed carbonylations for the generation of acylating electrophiles via ligand effects and/or visible light. She is currently a postdoc fellow in the lab of prof. Todd K. Hyster, where she mainly focuses on developing unnatural oxidative reactions with flavin-dependent enzymes.

Bryce T. Nicholls was born in Alberton, South Africa. He immigrated to the United States in 2014, and in 2018 he graduated with an A.B. in Biochemistry from Kenyon College in Gambier, OH. That same year, he began his Ph.D. studies at Princeton University, NJ, in the research group of Todd Hyster—now at Cornell University in Ithaca, NY. His research focuses on developing new photoenzymatic reactions.

Yao Ouyang received her B.S. degree (Pharmacy) in 2012 at China Pharmaceutical University, Nanjing, China. She completed a Ph.D. degree (Organic Chemistry) at the Shanghai Institute of Organic Chemistry in 2021 under the supervision of Prof. Feng-Ling Qing. In October 2021, she joined Prof. Todd Hyster as a postdoctoral fellow at Cornell University and is currently working on developing photoenzymatic reactions and protein engineering.

Claire G. Page obtained a B.Sc. in Chemistry from the University of California at Los Angeles in 2019. There she conducted research in the lab of Prof. Yi Tang. During her undergraduate studies, she also worked in the lab of Prof. Jorg Pietruszka at the IBOC of the University of Dusseldorf. In Fall 2019, she began her graduate studies at Princeton University under the guidance of Prof. Todd Hyster, where she is developing new methodology using flavoenzymes.

Tianzhang Qiao was born in Qinhuangdao, Hebei Province of P. R. China. He obtained his B.S. degree in Chemistry from Nankai University (NKU) in 2020 under the supervision of Prof. Shou-Fei Zhu. After working as a research assistant in Prof. Zhu's group for a year, he joined Prof. Todd Hyster's Lab at Cornell University to pursue his Ph.D. in organic chemistry. Tianzhang is interested in biocatalysis, and his current research focuses on ene-reductase-catalyzed non-natural photoenzymatic reactions.

Felix C. Raps was born and raised in southern Germany. After finishing his M.Sc. in 2017 and an internship at Actelion/Idorsia in 2018, he did his Ph.D. at the University of Basel in the lab of Christof Sparr, focusing on strategies for biomimetic polyketide synthesis and stereoselective synthesis of higher-order stereogenic elements. Currently, he is a postdoctoral researcher with Todd K. Hyster at Cornell, funded by the Swiss National Science Foundation (SNSF), developing novel photoenzymatic methodologies.

Damien Sorigué received his Ph.D. in 2016 from the University of Aix Marseille, France, under the supervision of Prof. Frederic Beisson. During his Ph.D. and his postdoctorat, he discovered and deciphered the mechanism of fatty acid photodecarboxylase. Afterward, he received a Marie Curie Skłodowska global fellowship and joined the group of Todd K. Hyster at Cornell University in 2022, where he tries to widen the scope of enzymatic chassis that can be used for photochemistry.

Shang-Zheng Sun obtained his Ph.D. from the Institute of Chemical Research of Catalonia (ICIQ) in 2020, working under the supervision of Prof. Ruben Martin. During his Ph.D., he focused on developing nickel-catalyzed reductive cross-couplings and remote sp^3 C–H functionalization of olefin feedstocks. In 2021, he joined the group of Prof. Todd Hyster at Cornell University as a postdoctoral fellow, where his research interest is developing new technologies to build up enantioenriched sp^3 C-linkages by photoenzymatic catalysis.

Joshua Turek-Herman obtained his B.A. in Chemistry from Swarthmore College in 2016. After his undergraduate studies, he performed postbaccalaureate research in the lab of Mikhail Kashlev at

the National Cancer Institute. He joined the lab of Prof. Todd Hyster as a Ph.D. student at Princeton University in 2018, where he studied biocatalytic approaches for radical C–C bond-forming reactions setting C–N stereocenters.

Yuxuan Ye obtained his B.S. in Chemistry from Peking University, where he did his undergraduate research with Prof. Jianbo Wang and Prof. Yan Zhang. During his undergraduate studies, he also conducted summer research at the University of California, Los Angeles, with Prof. Neil Garg. Yuxuan received his Ph.D. in Organic Chemistry from the Massachusetts Institute of Technology under the guidance of Prof. Stephen Buchwald. He then worked as a postdoctoral researcher with Prof. Todd Hyster at Princeton University and Cornell University. In August 2022, he joined the faculty at Westlake University as an Assistant Professor.

Ariadna Rivas-Souchet received her bachelor's degree in 2022 in Chemistry from Worcester Polytechnic Institute, where she worked under the supervision of Prof. Patricia Z. Musacchio developing new hydrogen atom abstractors for photoredox catalysis. Afterward, she joined the group of Todd K. Hyster at Cornell University in 2022 as a graduate student, where she currently works on asymmetric catalytic transformations enabled by flavin-dependent “ene”-reductases.

Jingzhe (Bill) Cao was born and raised in Taiyuan, ShanXi in China. After he completed his high school diploma from the Webb school, Bell Buckle, he earned his B.A. in 2018 from Boston University under the supervision of Prof. James Panek, where he worked on the convergent synthesis of novel muramyl dipeptide analogues. Bill is currently pursuing his Ph.D. at Princeton University under the supervision of Prof. Todd K. Hyster. His research focuses on the development of the enzyme-catalyzed asymmetrical radical hydroamination reaction.

Todd K. Hyster is an Associate Professor of Chemistry and Chemical Biology at Cornell University. He received his B.S. in Chemistry from the University of Minnesota. He did his Ph.D. studies with Tomislav Rovis at Colorado State University. As part of his Ph.D., he was a Marie Curie Fellow with Thomas Ward at the University of Basel. He was an NIH Postdoctoral Fellow with Prof. Frances Arnold at Caltech. He started his independent career at Princeton University in 2015. His group has developed new methods in photoenzymatic catalysis.

ACKNOWLEDGMENTS

The authors thank the National Institutes of Health National Institute of General Medical Sciences (R01GM127703). J.M.C. acknowledges the Margarita Salas grant from the Ministerio de Universidades, Universitat Politècnica de Valencia, Spain, funded by the European Union-Next Generation EU (2021–2023). Y.O. thanks the Shanghai Institute of Organic Chemistry for a postdoctoral fellowship. C.G.P. thanks the NSF GRFP for support. F.R. thanks the Swiss National Science Foundation (SNSF) for funding via its Postdoc Mobility Program. D.R.S.'s work was supported by a Marie Skłodowska-Curie Actions global fellowship (Project 101063280 - EXPERIMENTAL).

REFERENCES

- (1) Bell, E. L.; Finnigan, W.; France, S. P.; Green, A. P.; Hayes, M. A.; Hepworth, L. J.; Lovelock, S. L.; Niihura, H.; Osuna, S.; Romero; et al. *Biocatalysis*. *Nat. Rev. Method. Primers*. **2021**, *1*, 46.
- (2) Bornscheuer, U. T.; Buchholz, K. Highlights in Biocatalysis – Historical Landmarks and Current Trends. *Eng. Life. Sci.* **2005**, *5*, 309–323.

- (3) Bornscheuer, U. T.; Huisman, G. W.; Kazlauskas, R. J.; Lutz, S.; Moore, J. C.; Robins, K. Engineering the Third Wave of Biocatalysis. *Nature* **2012**, *485*, 185–194.
- (4) Hughes, D. L. Highlights of the Recent Patent Literature—Focus on Biocatalysis Innovation. *Org. Process Res. Dev.* **2022**, *26*, 1878–1899.
- (5) Junhua, Zhao, L.; Ran, N. Recent Advances in Developing Chemoenzymatic Process for Active Pharmaceutical Ingredients. *Org. Process Res. Dev.* **2007**, *11*, 259–267.
- (6) Savile, C. K.; Janey, J. M.; Mundorff, E. C.; Moore, J. C.; Tam, S.; Jarvis, W. R.; Colbeck, J. C.; Krebber, A.; Fleitz, F. J.; Brands, J.; et al. Biocatalytic Asymmetric Synthesis of Chiral Amines from Ketones Applied to Sitagliptin Manufacture. *Science* **2010**, *329*, 305–309.
- (7) Schober, M.; MacDermaid, C.; Ollis, A. A.; Chang, S.; Khan, D.; Hosford, J.; Latham, J.; Ihnken, L. A. F.; Brown, M. J. B.; Fuerst, D.; et al. Chiral Synthesis of LSD1 Inhibitor GSK2879552 Enabled by Directed Evolution of an Imine Reductase. *Nat. Catal.* **2019**, *2*, 909–915.
- (8) Kumar, R.; Karmilowicz, M. J.; Burke, D.; Burns, M. P.; Clark, L. A.; Connor, C. G.; Cordi, E.; Do, N. M.; Doyle, K. M.; Hoagland, S.; et al. Biocatalytic Reductive Amination from Discovery to Commercial Manufacturing Applied to Abrocitinib JAK1 Inhibitor. *Nat. Catal.* **2021**, *4*, 775–782.
- (9) Huffman, M. A.; Fryszkowska, A.; Alvizo, O.; Borra-Garske, M.; Campos, K. R.; Canada, K. A.; Devine, P. N.; Duan, D.; Forstater, J. H.; Grosser, S. T.; et al. Design of an In Vitro Biocatalytic Cascade for the Manufacture of Islatravir. *Science* **2019**, *366*, 1255–1259.
- (10) Simic, S.; Zukic, E.; Schmermund, L.; Faber, K.; Winkler, C. K.; Kroutil, W. Shortening Synthetic Routes to Small Molecule Active Pharmaceutical Ingredients Employing Biocatalytic Methods. *Chem. Rev.* **2022**, *122*, 1052–1126.
- (11) Renata, H.; Wang, Z. J.; Arnold, F. H. Expanding the Enzyme Universe: Accessing Non-Natural Reactions by Mechanism-Guided Directed Evolution. *Angew. Chem., Int. Ed.* **2015**, *54*, 3351–3367.
- (12) Hammer, S. C.; Knight, A. M.; Arnold, F. H. Design and Evolution of Enzymes for Non-Natural Chemistry. *Curr. Opin. Green. Sus. Chem.* **2017**, *7*, 23–30.
- (13) Siegel, J. B.; Zanghellini, A.; Lovick, H. M.; Kiss, G.; Lambert, A. R.; St.Clair, J. L.; Gallaher, J. L.; Hilvert, D.; Gelb, M. H.; Stoddard, B. L.; et al. Computational Design of an Enzyme Catalyst for a Stereoselective Biomolecular Diels-Alder Reaction. *Science* **2010**, *329*, 309–313.
- (14) Jiang, L.; Althoff, E. A.; Clemente, F. R.; Doyle, L.; Rothlisberger, D.; Zanghellini, A.; Gallaher, J. L.; Betker, J. L.; Tanaka, F.; Barbas, C. F.; et al. De Novo Computational Design of Retro-Aldol Enzymes. *Science* **2008**, *319*, 1387–1391.
- (15) Albin, A.; Fagnoni, M. Green Chemistry and Photochemistry were Born at the Same Time. *Green Chem.* **2004**, *6*, 1–6.
- (16) Candish, L.; Collins, K. D.; Cook, G. C.; Douglas, J. J.; Gómez-Suárez, A.; Jolit, A.; Keess, S. Photocatalysis in the Life Science Industry. *Chem. Rev.* **2022**, *122*, 2907–2980.
- (17) Holmberg-Douglas, N.; Nicewicz, D. A. Photoredox-Catalyzed C—H Functionalization Reactions. *Chem. Rev.* **2022**, *122*, 1925–2016.
- (18) Capaldo, L.; Ravelli, D.; Fagnoni, M. Direct Photocatalyzed Hydrogen Atom Transfer (HAT) for Aliphatic C—H Bonds Elaboration. *Chem. Rev.* **2022**, *122*, 1875–1924.
- (19) Sancar, A. Structure and Function of DNA Photolyase and Cryptochrome Blue-Light Photoreceptors. *Chem. Rev.* **2003**, *103*, 2203–2238.
- (20) Hedison, T. M.; Heyes, D. J.; Scrutton, N. S. Making Molecules with Photodecarboxylases: A Great Start or a False Dawn? *Current Research in Chemical Biology*. **2022**, *2*, 100017.
- (21) Vedalankar, P.; Tripathy, B. C. Evolution of Light-independent Protochlorophyllide Reductase. *Protoplasma*. **2019**, *256*, 293–312.
- (22) Harrison, W.; Huang, X.; Zhao, H. Photobiocatalysis for Abiological Transformations. *Acc. Chem. Res.* **2022**, *55*, 1087–1096.
- (23) Peng, Y.; Chen, Z.; Xu, J.; Wu, Q. Recent Advances in Photobiocatalysis for Selective Organic Synthesis. *Org. Process Res. Dev.* **2022**, *26*, 1900–1913.
- (24) Lee, S. H.; Choi, D. S.; Kuk, S. K.; Park, C. B. Photobiocatalysis: Activating Redox Enzymes by Direct or Indirect Transfer of Photoinduced Electrons. *Angew. Chem., Int. Ed.* **2018**, *57*, 7958–7985.
- (25) Schmermund, L.; Jurkas, V.; Özgen, F. F.; Barone, G. D.; Büchenschütz, H. C.; Winkler, C. K.; Schmidt, S.; Kourist, R.; Kroutil, W. Photo-Biocatalysis: Biotransformations in the Presence of Light. *ACS Catal.* **2019**, *9*, 4115–4144.
- (26) Begley, T.; Photoenzymes, P. A Novel Class of Biological Catalysts. *Acc. Chem. Res.* **1994**, *27*, 394–401.
- (27) Romero, N. A.; Nicewicz, D. A. Organic Photoredox Catalysis. *Chem. Rev.* **2016**, *116*, 10075–10166.
- (28) Prier, C. K.; Rankic, D. A.; MacMillan, D. W. C. Visible Light Photoredox Catalysis with Transition Metal Complexes: Applications in Organic Synthesis. *Chem. Rev.* **2013**, *113*, 5322–5363.
- (29) Zhang, M.; Wang, L.; Zhong, D. Photolyase: Dynamics and Electron-Transfer Mechanisms of DNA Repair. *Arch. Biochem. Biophys.* **2017**, *632*, 158–174.
- (30) Conrad, K. S.; Manahan, C. C.; Crane, B. R. Photochemistry of Flavoprotein Light Sensors. *Nat. Chem. Biol.* **2014**, *10*, 801–809.
- (31) Gabruk, M.; Mysliwa-Kurczel, B. Light-Dependent Protochlorophyllide Oxidoreductase: Phylogeny, Regulation, and Catalytic Properties. *Biochem.* **2015**, *54*, 5255–5262.
- (32) Zhang, S.; Heyes, D. J.; Feng, L.; Sun, W.; Johannissen, L. O.; Liu, H.; Levy, C. W.; Li, X.; Yu, X.; Lin, M.; Hardman, S. J. O.; Hoeven, R.; Sakuma, M.; Hay, S.; Leys, D.; Rao, Z.; Zhou, A.; Cheng, Q.; Scrutton, N. S. Structural Basis for Enzymatic Photocatalysis in Chlorophyll Biosynthesis. *Nature* **2019**, *574*, 722–725.
- (33) Sorigué, D.; Légeret, B.; Cuiné, S.; Blangy, S.; Moulin, S.; Billon, E.; Richaud, P.; Brugière, A.; Couté, Y.; Nurizzo, D.; et al. An Algal Photoenzyme Converts Fatty Acids to Hydrocarbons. *Science* **2017**, *357*, 903–907.
- (34) Rude, M. A.; Baron, T. S.; Brubaker, S.; Alibhai, M.; Del Cardayre, S. B.; Schirmer, A. Terminal Olefin (1-Alkene) Biosynthesis by a Novel P450 Fatty Acid Decarboxylase from *Jeotgalicoccus* Species. *Appl. Environ. Microbiol.* **2011**, *77*, 1718–1727.
- (35) Rui, Z.; Li, X.; Zhu, X.; Liu, J.; Domigan, B.; Barr, I.; Cate, J. H. D.; Zhang, W. Microbial Biosynthesis of Medium Chain 1-alkenes by a Nonheme Iron Oxidase. *Proc. Natl. Acad. Sci. U. S. A.* **2014**, *111*, 18237–18242.
- (36) Moulin, S. L. Y.; Beyly-Adriano, A.; Cuiné, S.; Blangy, S.; Légeret, B.; Floriani, M.; Burlacot, A.; Sorigué, D.; Samire, P.-P.; Li-Beisson, Y.; Peltier, G.; Beisson, F. Fatty Acid Photodecarboxylase is an Ancient Photoenzyme That Forms Hydrocarbons in the Thylakoids of Algae. *Plant Physiol.* **2021**, *186*, 1455–1472.
- (37) Sorigué, D.; Hadjidemetriou, K.; Blangy, S.; Gotthard, G.; Bonvalet, A.; Coquelle, N.; Samire, P.; Aleksandrov, A.; Antonucci, L.; Benachir, A.; et al. Mechanism and Dynamics of Fatty Acid Photodecarboxylase. *Science* **2021**, *372*, eabd5687.
- (38) Heyes, D. J.; Lakavath, B.; Hardman, S. J. O.; Sakuma, M.; Hedison, T. M.; Scrutton, N. S. Photochemical Mechanism of Light-Driven Fatty Acid Photodecarboxylase. *ACS Catal.* **2020**, *10*, 6691–6696.
- (39) Lakavath, B.; Hedison, T. M.; Heyes, D. J.; Shanmugam, M.; Sakuma, M.; Hoeven, R.; Tilakaratna, V.; Scrutton, N. S. Radical-Based Photoinactivation of Fatty Acid Photodecarboxylases. *Anal. Biochem.* **2020**, *600*, 113749.
- (40) Huijbers, M. M. E.; Zhang, W. Y.; Tonin, F.; Hollmann, F. Light-Driven Enzymatic Decarboxylation of Fatty Acids. *Angew. Chem., Int. Ed.* **2018**, *57*, 13648–13651.
- (41) Zeng, Y. Y.; Liu, L.; Chen, B. S.; Zhang, W. Y. Light-Driven Enzymatic Decarboxylation of Dicarboxylic Acids. *ChemistryOpen* **2021**, *10*, 553–559.
- (42) Chanquia, S. N.; Benfeldt, F. V.; Petrovai, N.; Santner, P.; Hollmann, F.; Eser, B. E.; Kara, S. Immobilization and Application of

Fatty Acid Photodecarboxylase in Deep Eutectic Solvents. *ChemBioChem*. **2022**, *23*, e202200482.

(43) Simić, S.; Jakšaitė; Huck, W. T. S.; Winkler, C. K.; Kroutil, W. Strategies from Transferring Photobiocatalysis to Contrunous Flow Exemplified by Photodecarboxylation of Fatty Acids. *ACS Catal*. **2022**, *12*, 14040–14049.

(44) Zhang, W.; Ma, M.; Huijbers, M. M. E.; Filonenko, G. A.; Pidko, E. A.; van Schie, M.; de Boer, S.; Burek, B. O.; Bloh, J. Z.; van Berkel, W. J. H.; et al. Hydrocarbon Synthesis via Photoenzymatic Decarboxylation of Carboxylic Acids. *J. Am. Chem. Soc.* **2019**, *141*, 3116–3120.

(45) Zhang, X.; Ma, Y.; Qin, X.; Hollmann, F.; Wang, Y. A New Deacidification Strategy for Crude Vegetable Oil: Removal of Free Fatty Acids via Photobiocatalytic Decarboxylation. *Authorea* **2022**, DOI: 10.22541/au.164736455.58070076/v1.

(46) Aselmeyer, C.; Légeret, B.; Bénarouche, A.; Sorigué, D.; Parsiegla, G.; Beisson, F.; Cerrière, F. Fatty Acid Photodecarboxylase is an Interfacial Enzyme That Binds to Lipid-Water Interfaces to Access Its Insoluble Substrate. *Biochem*. **2021**, *60*, 3200–3212.

(47) Cha, H. J.; Hwang, H. Y.; Lee, D. S.; Kumar, A. R.; Kwon, Y. U.; Voß, M.; Schuiten, E.; Bornscheuer, U. T.; Hollmann, F.; Oh, D. K.; et al. Whole-Cell Photoenzymatic Cascades to Synthesize Long-Chain Aliphatic Amines and Esters from Renewable Fatty Acids. *Angew. Chem., Int. Ed.* **2020**, *59*, 7024–7028.

(48) Zhang, W. Y.; Lee, J. H.; Younes, H. H. S.; Tonin, F.; Hagedoorn, P. L.; Pichler, H.; Baeg, Y.; Park, J. B.; Kourist, R.; Hollmann, F. Photobiocatalytic Synthesis of Chiral Secondary Fatty Alcohols from Renewable Unsaturated Fatty Acids. *Nat. Commun.* **2020**, *11*, 2258.

(49) Moulin, S.; Légeret, B.; Blangy, S.; Soriqúé, D.; Burlacot, A.; Auroy, P.; Li-Beisson, Y.; Peltier, G.; Beisson, F. Continuous Photoproduction of Hydrocarbon Drop-in Fuel by Microbial Cell Factories. *Sci. Reports*. **2019**, *9*, 13719.

(50) Bruder, S.; Moldenhauer, E. J.; Lemke, R. D.; Ledesma-Amaro, R.; Kabisch, J. Drop-in Biofuel Production Using Fatty Acid Photodecarboxylase from *Chlorella variabilis* in the Oleaginous yeast *Yarrowia lipolytica*. *Biotechnol. Biofuel* **2019**, *12*, 202.

(51) Li, J.; Ma, Y.; Liu, N.; Eser, B. E.; Guo, Z.; Jensen, P. R.; Stephanopoulos, G. Synthesis of High-Titer Alka(e)nes in *Yarrowia lipolytica* in Enabled by the Discovered Mechanism. *Nat. Commun.* **2020**, *11*, 6198.

(52) Yunus, I. S.; Wichmann, J.; Wördenweber, R.; Lauersen, K. J.; Kruse, O.; Jones, P. R. Synthetic Metabolic Pathways for Photo-biological Conversion of CO₂ into Hydrocarbon Fuel. *Metabolic Eng.* **2018**, *49*, 201–211.

(53) Yunus, I. S.; Anfelt, J.; Sporre, E.; Miao, R.; Hudson, E. P.; Jones, P. R. Synthetic Metabolic Pathways for Conversion of CO₂ Into Secreted Short-to Medium-Chain Hydrocarbons Using Cyanobacteria. *Metabolic Eng.* **2022**, *72*, 14–23.

(54) Guo, X.; Xia, A.; Li, F.; Huang, Y.; Zhu, X.; Zhang, W.; Zhu, X.; Liao, Q. Photoenzymatic Decarboxylation to Produce Renewable Hydrocarbon Fuels: A Comparison Between Whole-Cell and Broken-Cell Biocatalysis. *Energy Conv. Manag.* **2022**, *255*, 115311.

(55) Sun, Y.; Calderini, E.; Kourist, R. A. Reconstructed Common Ancestor of the Fatty Acid Photo-decarboxylase Calde Shows Photodecarboxylation Activity and Increased Thermostability. *ChemBioChem*. **2021**, *22*, 1833–1840.

(56) Santner, P.; Szabo, L. K.; Chanquia, S. N.; Merrill, A. H.; Hollmann, F.; Kara, S.; Eser, B. E. Optimization and Engineering of Fatty Acid Photodecarboxylase for Substrate Specificity. *ChemCatChem*. **2021**, *13*, 4038–4046.

(57) Li, D.; Han, T.; Xue, J.; Xu, W.; Xu, J.; Wu, Q. Engineering Fatty Acid Photodecarboxylase to Enable the Decarboxylation of *trans* Fatty Acids. *Angew. Chem., Int. Ed.* **2021**, *60*, 20695–20699.

(58) Xu, W.; Chen, Y.; Li, D.; Wang, Z.; Xu, J.; Wu, Q. Rational Design of Fatty Acid Photodecarboxylase Enables the Efficient Decarboxylation of Medium and Short-Chain Fatty Acids for the Production of Gasoline Bio-Alkanes. *Mol. Catal.* **2022**, *524*, 112261.

(59) Amer, M.; Wojcik, E. Z.; Sun, C.; Hoeven, R.; Hughes, J. M. X.; Faulkner, M.; Yunus, I. S.; Tait, S.; Johannissen, L. O.; Hardman, S. J. O.; Heyes, D. J.; Chen, G.-Q.; Smith, M. H.; Jones, P. R.; Toogood, H. S.; Scrutton, N. S. Low Carbon Strategies for Sustainable Bio-Alkane Gas Production and Renewable Energy. *Energy, Environ. Sci.* **2020**, *13*, 1818–1831.

(60) Xu, J.; Fan, J.; Lou, Y.; Xu, W.; Wang, Z.; Li, D.; Zhou, H.; Lin, X.; Wu, Q. Light-driven Decarboxylative Deuteration Enabled by a Divergently Engineered Photodecarboxylase. *Nature Commun.* **2021**, *12*, 3983.

(61) Xu, J.; Hu, Y.; Fan, J.; Arkin, M.; Li, D.; Peng, Y.; Xu, W.; Lin, X.; Wu, Q. Light-Driven Kinetic Resolution of α -Functionalized Carboxylic Acids Enabled by an Engineered Fatty Acid Photodecarboxylase. *Angew. Chem., Int. Ed.* **2019**, *58*, 8474–8478.

(62) Cheng, F.; Li, H.; Wu, D. Y.; Li, J. M.; Fan, Y.; Xue, Y. P.; Zheng, Y. G. Light-driven Deracemization of Phosphinothricin by Engineered Fatty Acid Photodecarboxylase on a Gram Scale. *Green Chem.* **2020**, *22*, 6815–6818.

(63) Amer, M.; Hoeven, R.; Kelly, P.; Faulkner, M.; Smith, M. H.; Toogood, H. S.; Scrutton, N. S. Renewable and Tuneable Bio-LPG Blends Derived from Amino Acids. *Biochemistry Biofuels* **2020**, *13*, 125.

(64) Park, H.; Toogood, H. S.; Chen, G.-Q.; Scrutton, N. S. Co-Production of Biofuels, Bioplastics and Biochemicals During Extended Fermentation of *Halomonas bluephagensis*. *Micro. Biotechnol.* **2023**, *16*, 307–321.

(65) Lévesque, F.; Di Maso, M. J.; Narsimhan, K.; Wismer, M. K.; Naber, J. R. Design of a Kilogram Scale, Plug Flow Photoreactor Enabled by High Power LEDs. *Org. Process Res. Dev.* **2020**, *24*, 2935–2940.

(66) Harper, K. C.; Moschetta, E. G.; Bordawekar, S. V.; Wittenberger, S. J. A Laser Driven Flow Chemistry Platform for Scale Photochemical Reactions with Visible Light. *ACS Cent. Sci.* **2019**, *5*, 109–115.

(67) Huisman, G. W.; Liang, J.; Krebber, A. Practical Chiral Alcohol Manufacture Using Ketoreductases. *Curr. Opin. Chem. Biol.* **2010**, *14*, 122–129.

(68) Ohnishi, Y.; Kagami, M.; Ohno, A. Reduction of a Model NAD(P)H. Photo-Activation of NADH and Its Model Compounds Toward the Reduction of Olefins. *Chem. Lett.* **1975**, *4*, 125–128.

(69) Fukuzumi, S.; Hironaka, K.; Tanaka, T. Photoreduction of Alkyl Halides by an NADH Model Compound. An Electron-transfer Chain Mechanism. *J. Am. Chem. Soc.* **1983**, *105*, 4722–4727.

(70) Emmanuel, M. A.; Greenberg, N. R.; Oblinsky, D. G.; Hyster, T. K. Accessing Non-natural Reactivity by Irradiating Nicotinamide-dependent Enzymes with Light. *Nature*. **2016**, *540*, 414–417.

(71) Noey, E. L.; Tibrewal, N.; Jiménez-Osés, G.; Osuna, S.; Park, J.; Bond, C. M.; Cascio, D.; Liang, J.; Zhang, X.; Huisman, G. W.; et al. Origins of Stereoselectivity in Evolved Ketoreductases. *Proc. Natl. Acad. Sci. U. S. A.* **2015**, *112*, E7065–E7072.

(72) Huang, X.; Feng, J.; Cui, J.; Jiang, G.; Harrison, W.; Zang, X.; Zhou, J.; Wang, B.; Zhao, H. Photoinduced Chemomimetic Biocatalysis for Enantioselective Intermolecular Radical Conjugate Addition. *Nat. Catal.* **2022**, *5*, 586–593.

(73) Toogood, H. S.; Scrutton, N. S. Discovery, Characterization, Engineering, and Applications of Ene-Reductases for Industrial Biocatalysis. *ACS Catal.* **2018**, *8*, 3532–3549.

(74) Warburg, O.; Christian, W. Ein zweites sauerstoffübertragendes Ferment und sein Absorptionsspektrum. *Naturwissenschaften*. **1932**, *20*, 688.

(75) Nizam, S.; Verma, S.; Borah, N. N.; Gazara, R. K.; Verma, P. K. Comprehensive Genome-wide Analysis Reveals Different Classes of Enigmatic Old Yellow Enzyme in Fungi. *Scientific Reports* **2014**, *4*, 4013.

(76) Schaller, F.; Biesgen, C.; Müssig, C.; Altmann, T.; Weiler, W. E. 12-oxophytodienoate Reductase 3 (OPR3) is an Isoenzyme Involved in Jasmonate Biosynthesis. *Planta*. **2000**, *210*, 979–984.

(77) Rider, L. W.; Ottosen, M. B.; Gattis, S. G.; Palfey, B. A. Mechanism of Dihydrouridine Synthase 2 from Yeast and the

Importance of Modifications for Efficient tRNA Reduction. *J. Biol. Chem.* **2009**, *284*, 10324–10333.

(78) Meah, Y.; Massey, V. Old Yellow Enzyme: Stepwise Reduction of Nitro-Olefins and Catalysis of Aci-nitro Tautomerization. *Proc. Natl. Acad. Sci. U.S.A.* **2000**, *97*, 10733–10738.

(79) Toogood, H. S.; Scrutton, N. S. Discovery, Characterization, Engineering, and Applications of Ene-Reductases for Industrial Biocatalysis. *ACS Catal.* **2018**, *8*, 3532–3549.

(80) Shultz, C. S.; Krska, S. W. Unlocking the Potential of Asymmetric Hydrogenation at Merck. *Acc. Chem. Res.* **2007**, *40*, 1320–1326.

(81) Massey, V.; Hemmerich, P.; Knappe, W. R.; Duchstein, H. J.; Fenner, H. Photoreduction of Flavoproteins and Other Biological Compounds Catalyzed by Deazaflavins. Appendix: Photochemical Formation of Deazaflavin Dimers. *Biochemistry* **1978**, *17*, 9–17.

(82) Stewart, R. C.; Massey, V. Potentiometric Studies of Native and Flavin-substituted Old Yellow Enzyme. *J. Biol. Chem.* **1985**, *260*, 13639–13647.

(83) Warren, J. J.; Tronic, T. A.; Mayer, J. M. Thermochemistry of Proton-Coupled Electron Transfer Reagents and its Implications. *Chem. Rev.* **2010**, *110*, 6961–7001.

(84) Sandoval, B. A.; Meichan, A. J.; Hyster, T. K. Enantioselective Hydrogen Atom Transfer: Discovery of Catalytic Promiscuity in Flavin-Dependent ‘Ene’-Reductases. *J. Am. Chem. Soc.* **2017**, *139*, 11313–11316.

(85) Biegasiewicz, K. F.; Cooper, S. J.; Gao, X.; Oblinsky, D. G.; Kim, J. H.; Garfinkle, S. E.; Joyce, L. A.; Sandoval, B. A.; Scholes, G. D.; Hyster, T. K. Photoexcitation of Flavoenzymes Enables a Stereoselective Radical Cyclization. *Science* **2019**, *364*, 1166–1169.

(86) Chen, K.; Arnold, F. H. Engineering New Catalytic Activities in Enzymes. *Nat. Catal.* **2020**, *3*, 203–213.

(87) Nicholls, B.; Oblinsky, D.; Kurtoic, S.; Grosheva, D.; Ye, Y.; Scholes, G.; Hyster, T. Engineering a Non-Natural Photoenzyme for Improved Photon Efficiency. *Angew. Chem., Int. Ed.* **2021**, e202113842.

(88) Ha, C.; Horner, J. H.; Newcomb, M.; Varick, T. R.; Arnold, B. R.; Luszyk, J. Kinetic Studies of the Cyclization of the 6,6-diphenyl-5-hexenyl Radical. A Test of the Accuracy of Rate Constants for Reactions of Hydrogen Transfer Agents. *J. Org. Chem.* **1993**, *58*, 1194–1198.

(89) Cesana, P. T.; Page, C. G.; Harris, D.; Emmanuel, M. A.; Hyster, T. K.; Schlau-Cohen, G. S. Photoenzymatic Catalysis in a New Light: *Gluconobacter* ‘Ene’-Reductase Conjugates Possessing High-Energy Reactivity with Tunable Low-Energy Excitation. *J. Am. Chem. Soc.* **2022**, *144*, 17516–17521.

(90) Page, C. G.; Cooper, S. J.; Dehovitz, J. S.; Oblinsky, D. G.; Biegasiewicz, K. F.; Antropow, A. H.; Armbrust, K. W.; Ellis, J. M.; Hamann, L. G.; Horn, E. J.; Oberg, K. M.; Scholes, G. D.; Hyster, T. K. Quaternary Charge-Transfer Complex Enables Photoenzymatic Intermolecular Hydroalkylation of Olefins. *J. Am. Chem. Soc.* **2021**, *143*, 97–102.

(91) Gao, X.; Turek-Herman, J. R.; Choi, Y. J.; Cohen, R. D.; Hyster, T. K. Photoenzymatic Synthesis of α -Tertiary Amines by Engineered Flavin-Dependent ‘Ene’-Reductases. *J. Am. Chem. Soc.* **2021**, *143*, 19643–19647.

(92) Gao, X.; Turek-Herman, J. R.; Choi, Y. J.; Cohen, R. D.; Hyster, T. K. Photoenzymatic Synthesis of α -Tertiary Amines by Engineered Flavin-Dependent ‘Ene’-Reductases. *J. Am. Chem. Soc.* **2021**, *143*, 19643–19647.

(93) Clayman, P. D.; Hyster, T. K. Photoenzymatic Generation of Unstabilized Alkyl Radicals: An Asymmetric Reductive Cyclization. *J. Am. Chem. Soc.* **2020**, *142*, 15673–15677.

(94) Huang, X.; Wang, B.; Wang, Y.; Jiang, G.; Feng, J.; Zhao, H. Photoenzymatic Enantioselective Intermolecular Radical Hydroalkylation. *Nature* **2020**, *584*, 69–74.

(95) Fu, H.; Lam, H.; Emmanuel, M. A.; Kim, J. H.; Sandoval, B. A.; Hyster, T. K. Ground-State Electron Transfer as an Initiation Mechanism for Biocatalytic C–C bond Forming Reactions. *J. Am. Chem. Soc.* **2021**, *143*, 9622–9629.

(96) Duan, X.; Cui, D.; Wang, Z.; Zheng, D.; Jiang, L.; Huang, W.-Y.; Jia, Y.-X.; Xu, J. A Photoenzymatic Strategy for Radical-Mediated Stereoselective Hydroalkylation with Diazo Compounds. *Angew. Chem., Int. Ed.* **2023**, *62*, e202214135.

(97) Laguerre, N.; Riehl, P. S.; Oblinsky, D. G.; Emmanuel, M. A.; Black, M. J.; Scholes, G. D.; Hyster, T. K. Radical Termination via β -Scission Enables Photoenzymatic Allylic Alkylation Using ‘Ene’-Reductases. *ACS Catal.* **2022**, *12*, 9801–9805.

(98) Everson, D. A.; Weix, D. J. Cross-Electrophile Coupling: Principles of Reactivity and Selectivity. *J. Org. Chem.* **2014**, *79*, 4793–4798.

(99) Lucas, E. L.; Jarvo, E. R. Stereospecific and Stereoconvergent Cross-couplings between Alkyl Electrophiles. *Nat. Rev. Chem.* **2017**, *1*, No. 0065.

(100) Fu, H.; Cao, J.; Qiao, T.; Qi, Y.; Charnock, S.; Garfinkle, S.; Hyster, T. An Asymmetric sp³–sp³ Cross-Electrophile Coupling Using Biocatalysis. *Nature* **2022**, *610*, 302–307.

(101) Sandoval, B. A.; Clayman, P. D.; Oblinsky, D. G.; Oh, S.; Nakano, Y.; Bird, M.; Scholes, G. D.; Hyster, T. K. Photoenzymatic Reductions Enabled by Direct Excitation of Flavin-Dependent ‘Ene’-Reductases. *J. Am. Chem. Soc.* **2021**, *143*, 1735–1739.

(102) Black, M. J.; Biegasiewicz, K. F.; Meichan, A. J.; Oblinsky, D. G.; Kudisch, B.; Scholes, G. D.; Hyster, T. K. Asymmetric Redox-neutral Radical Cyclization Catalysed by Flavin-dependent ‘Ene’-reductases. *Nat. Chem.* **2020**, *12*, 71–75.

(103) Peng, Y.; Wang, Z.; Chen, Y.; Xu, W.; Hu, Y.; Chen, Z.; Xu, J.; Wu, Q. Photoinduced Promiscuity of Cyclohexanone Monooxygenase for the Enantioselective Synthesis of α -fluoroketones. *Angew. Chem., Int. Ed.* **2022**, *61*, e202211199.

(104) Zhou, F.; Li, R.; Wang, X.; Du, S.; An, Z. Non-natural Photoenzymatic Controlled Radical Polymerization Inspired by DNA Photolysis. *Angew. Chem., Int. Ed.* **2019**, *58*, 9479–9484.

(105) Li, R.; An, Z. Achieving Ultrahigh Molecular Weights with Diverse Architectures for Unconjugated Monomers through Oxygen-Tolerant Photoenzymatic RAFT Polymerization. *Angew. Chem., Int. Ed.* **2020**, *59*, 22258–22264.

(106) Trimble, J. S.; Crawshaw, R.; Hardy, F. J.; Levy, C. W.; Brown, M. J. B.; Fuerst, D. E.; Heyes, D. J.; Obexer, R.; Green, A. P. A Designed Photoenzyme Promotes Enantioselective [2 + 2]-Cycloadditions via Triplet Energy Transfer. *Nature* **2022**, *611*, 709–714.

(107) Siegel, J. B.; Zanghellini, A.; Lovick, H. M.; Kiss, G.; Lambert, A. R.; St.Clair, J. L.; Gallaher, J. L.; Hilvert, D.; Gelb, M. H.; Stoddard, B. L.; et al. Computational Design of an Enzyme Catalyst for a Stereoselective Bimolecular Diels-Alder Reaction. *Science* **2010**, *329*, 309–313.

(108) Sun, N.; Huang, J.; Qian, J.; Zhou, T.; Guo, J.; Tang, L.; Zhang, W.; Deng, Y.; Zhao, W.; Wu, G.; et al. Enantioselective [2 + 2]-Cycloadditions with Triplet Photoenzymes. *Nature* **2022**, *611*, 715–720.

(109) Roelfes, G. LmrR: A Privileged Scaffold for Artificial Metalloenzymes. *Acc. Chem. Res.* **2019**, *52*, 545–556.

(110) Liu, X.; Kang, F.; Hu, C.; Wang, L.; Xu, Z.; Zheng, D.; Gong, W.; Lu, Y.; Ma, Y.; Wang, J. A Genetically Encoded Photosensitizer Protein Facilitates the Rational Design of a Miniature Photocatalytic CO₂-Reducing Enzyme. *Nat. Chem.* **2018**, *10*, 1201–1206.

(111) Fu, Y.; Huang, J.; Wu, Y.; Liu, X.; Zhong, F.; Wang, J. Biocatalytic Cross-Coupling of Aryl Halides with a Genetically Engineered Photosensitizer Artificial Dehalogenase. *J. Am. Chem. Soc.* **2021**, *143*, 617–622.

(112) Terrett, J. A.; Cuthbertson, J. D.; Shurtleff, V. W.; MacMillan, D. W. C. Switching on Elusive Organometallic Mechanisms with Photoredox Catalysis. *Nature* **2015**, *524*, 330–334.

(113) Welin, E. R.; Le, C.; Arias-Rotondo, D. M.; McCusker, J. K.; MacMillan, D. W. C. Photosensitized, Energy Transfer-Mediated Organometallic Catalysis Through Electronically Excited Nickel (II). *Science* **2017**, *355*, 380–385.

(114) Gu, Y.; Ellis-Guardiola, K.; Srivastava, P.; Lewis, J. C. Preparation, Characterization, and Oxygenase Activity of a Photocatalytic Artificial Enzyme. *ChemBioChem* **2015**, *16*, 1880–1883.

- (115) Schwochert, T. D.; Cruz, C. L.; Watters, J. W.; Reynolds, E. W.; Nicewicz, D. A.; Brustad, E. M. Design and Evaluation of Artificial Hybrid Photoredox Biocatalysts. *ChemBioChem*. **2020**, *21*, 3146–3150.
- (116) Zubi, Y. S.; Liu, B.; Gu, Y.; Sahoo, D.; Lewis, J. C. Controlling the Optical and Catalytic Properties of Artificial Metalloenzyme Photocatalysts Using Chemogenetic Engineering. *Chem. Sci.* **2022**, *13*, 1459–1468.
- (117) Whitehouse, C. J. C.; Bell, S. G.; Wong, L.-L. P450_{BM3} (CYP102A1): Connecting the Dots. *Chem. Soc. Rev.* **2012**, *41*, 1218–1260.
- (118) Gray, H. B.; Winkler, J. R. Long-Range Electron Transfer. *Proc. Nat. Acad. Sci.* **2005**, *102*, 3534–3539.
- (119) Reece, S. Y.; Seyedsayamdost, M. R.; Stubbe, J.; Nocera, D. G. Direct Observation of a Transient Tyrosine Radical Competent for Initiating Turnover in a Photochemical Ribonucleotide Reductase. *J. Am. Chem. Soc.* **2007**, *129*, 13828–13830.
- (120) Tran, N. H.; Nguyen, D.; Dwaraknath, S.; Mahadevan, S.; Chavez, G.; Nguyen, A.; Dao, T.; Mullen, S.; Nguyen, T. A.; Cheruzel, L. E. An Efficient Light-Driven P450 BM3 Biocatalyst. *J. Am. Chem. Soc.* **2013**, *135*, 14484–14487.
- (121) Tran, N. H.; Huynh, N.; Bui, T.; Nguyen, Y.; Huynh, P.; Cooper, M. E.; Cheruzel, L. E. Light-initiated Hydroxylation of Lauric Acid Using Hybrid P450 BM3 Enzymes. *Chem. Commun.* **2011**, *47*, 11936–11938.
- (122) Tran, N. H.; Huynh, N.; Chavez, G.; Nguyen, A.; Dwaraknath, S.; Nguyen, T. A.; Nguyen, M.; Cheruzel, L. A Series of Hybrid P450 BM3 Enzymes with Different Catalytic Activity in the Light-initiated Hydroxylation of Lauric Acid. *J. Inorg. Biochem.* **2012**, *115*, 50–56.
- (123) Kato, M.; Nguyen, D.; Gonzalez, M.; Cortez, A.; Mullen, S. E.; Cheruzel, L. E. Regio- and Stereoselective Hydroxylation of 10-Undecenoic Acid with a Light-Driven P450 BM3 Biocatalyst Yielding a Valuable Synthon for Natural Product Synthesis. *Bioorg. Med. Chem.* **2014**, *22*, 5687–5691.
- (124) Sosa, V.; Melkie, M.; Sulca, C.; Li, J.; Tang, L.; Li, J.; Faris, J.; Foley, B.; Banh, T.; Kato, M.; et al. Selective Light-Driven Chemoenzymatic Trifluoromethylation/Hydroxylation of Substituted Arenes. *ACS Catal.* **2018**, *8*, 2225–2229.
- (125) Beatty, J. W.; Douglas, J. J.; Cole, K. P.; Stephenson, C. R. A Scalable and Operationally Simple Radical Trifluoromethylation. *Nat. Commun.* **2015**, *6*, 7919–7925.
- (126) Lam, Q.; Cortez, A.; Nguyen, T. T.; Kato, M.; Cheruzel, L. Chromogenic Nitrophenolate-Based Substrates for Light-Driven Hybrid P450 BM3 Enzyme Assay. *J. Inorg. Biochem.* **2016**, *158*, 86–91.
- (127) Lentz, O.; Li, Q.-S.; Schwaneberg, U.; Lutz-Wahl, S.; Fischer, P.; Schmid, R. D. Modification of the Fatty Acid Specificity of Cytochrome P450 BM-3 from *Bacillus Megaterium* by Directed Evolution: A Validated Assay. *J. Mol. Catal. B: Enzymatic* **2001**, *15*, 123–133.
- (128) Farinas, E. T.; Schwaneberg, U.; Glieder, A.; Arnold, F. H. Directed Evolution of a Cytochrome P450 Monooxygenase for Alkane Oxidation. *Adv. Synth. Catal.* **2001**, *343*, 601–606.
- (129) Shalan, H.; Colbert, A.; Nguyen, T. T.; Kato, M.; Cheruzel, L. Correlating the Para-Substituent Effects on Ru(II)-Polypyridine Photophysical Properties and on the Corresponding Hybrid P450 BM3 Enzymes Photocatalytic Activity. *Inorg. Chem.* **2017**, *56*, 6558–6564.
- (130) Srivastava, V.; Singh, P. P. Eosin Y Catalysed Photoredox Synthesis: A Review. *RSC Adv.* **2017**, *7*, 31377–31392.
- (131) Lin, F.; Fan, W.; Wise, G. E. Eosin Y Staining of Proteins in Polyacrylamide Gels. *Anal. Biochem.* **1991**, *196*, 279–283.
- (132) Park, J. H.; Lee, S. H.; Cha, G. S.; Choi, D. S.; Nam, D. H.; Lee, J. H.; Lee, J. K.; Yun, C. H.; Jeong, K. J.; Park, C. B. Cofactor-Free Light-Driven Whole-Cell Cytochrome P450 Catalysis. *Angew. Chem., Int. Ed.* **2015**, *54*, 969–973.
- (133) Hu, W.-Y.; Li, K.; Weitz, A.; Wen, A.; Kim, H.; Murray, J. C.; Cheng, R.; Chen, B.; Naowarajna, N.; Grinstaff, M. W.; Elliott, S. J.; Chen, J.-S.; Liu, P. Light-Driven Oxidative Demethylation Reaction Catalyzed by a Rieske-Type Non-heme Iron Enzyme Stc2. *ACS Catal.* **2022**, *12*, 14559–14570.
- (134) Biegasiewicz, K. F.; Cooper, S. J.; Emmanuel, M. A.; Miller, D. C.; Hyster, T. K. Catalytic Promiscuity Enabled by Photoredox Catalysis in Nicotinamide-Dependent Oxidoreductases. *Nat. Chem.* **2018**, *10*, 770–775.
- (135) Romero, N. A.; Nicewicz, D. A. Organic Photoredox Catalysis. *Chem. Rev.* **2016**, *116*, 10075–10166.
- (136) Sandoval, B. A.; Kurtoic, S. I.; Chung, M. M.; Biegasiewicz, K. F.; Hyster, T. K. Photoenzymatic Catalysis Enables Radical-Mediated Ketone Reduction in Ene-Reductases. *Angew. Chem., Int. Ed.* **2019**, *131*, 8806–8810.
- (137) Prats Luján, A.; Bhat, M. F.; Saravanan, T.; Poelarends, G. J. Chemo- and Enantioselective Photoenzymatic Ketone Reductions Using a Promiscuous Flavin-dependent Nitroreductase. *ChemCatChem*. **2022**, *14*, e202200043.
- (138) Nakano, Y.; Black, M. J.; Meichan, A. J.; Sandoval, B. A.; Chung, M. M.; Biegasiewicz, K. F.; Zhu, T.; Hyster, T. K. Photoenzymatic Hydrogenation of Heteroaromatic Olefins Using 'Ene'-Reductases with Photoredox Catalysts. *Angew. Chem., Int. Ed.* **2020**, *59*, 10484–10488.
- (139) Ye, Y.; Cao, J.; Oblinsky, D. G.; Verma, D.; Prier, C. K.; Scholes, G. D.; Hyster, T. K. Using Enzymes to Tame Nitrogen-Centered Radicals for Enantioselective Hydroamination. *Nat. Chem.* **2023**, *15*, 206–212.
- (140) Hall, M.; Stuckler, C.; Ehammer, H.; Pointner, E.; Oberdorfer, G.; Gruber, K.; Hauer, B.; Sturmer, R.; Kroutil, W.; Macheroux, P.; et al. Asymmetric Bioreduction of C = C Bonds using Enoate Reductases OPR1, OPR3 and YqjM: Enzyme-Based Stereocontrol. *Adv. Synth. Catal.* **2008**, *350*, 411–418.
- (141) Grau, M. M.; van der Toorn, J. C.; Otten, L. G.; Macheroux, P.; Taglieber, A.; Zilly, F. E.; Arends, I. W. C. E.; Hollmann, F. Photoenzymatic Reduction of C = C Double Bonds. *Adv. Synth. Catal.* **2009**, *351*, 3279–3286.
- (142) Taglieber, A.; Schulz, F.; Hollmann, F.; Rusek, M.; Reetz, M. T. Light-Driven Biocatalytic Oxidation and Reduction Reactions: Scope and Limitations. *ChemBioChem*. **2008**, *9*, 565–572.
- (143) Massey, V. Activation of Molecular Oxygen by Flavins and Flavoproteins. *J. Biol. Chem.* **1994**, *269*, 22459–22462.
- (144) Peers, M. K.; Toogood, H. S.; Heyes, D. J.; Mansell, D.; Coe, B. J.; Scrutton, N. S. Light-driven Biocatalytic Reduction of α,β -unsaturated Compounds by Ene Reductases Employing Transition Metal Complexes as Photosensitizers. *Catal. Sci. Technol.* **2016**, *6*, 169–177.
- (145) Juris, A.; Balzani, V.; Barigelletti, F.; Campagna, S.; Belser, P.; von Zelewsky, A. Ru(II) Polypyridine Complexes: Photophysics, Photochemistry, Electrochemistry, and Chemiluminescence. *Coord. Chem. Rev.* **1988**, *84*, 85.
- (146) Lee, S. H.; Choi, D. S.; Pesic, M.; Lee, Y. W.; Paul, C. E.; Hollmann, F.; Park, C. B. Cofactor-Free, Direct Photoactivation of Enoate Reductases for the Asymmetric Reduction of C = C Bonds. *Angew. Chem., Int. Ed.* **2017**, *56*, 8681–8685.
- (147) Mifsud, M.; Gargiulo, S.; Iborra, S.; Arends, I. W. C. E.; Hollmann, F.; Corma, A. Photobiocatalytic Chemistry of Oxidoreductases Using Water as the Electron Donor. *Nat. Commun.* **2014**, *5*, 3145.
- (148) Opperman, D. J.; Piater, L. A.; van Heerden, E. A novel chromate reductase from *Thermus scotoductus* SA-01 Related to Old Yellow Enzyme. *J. Bacteriol.* **2008**, *190*, 3076–3082.
- (149) Gomes Silva, C. U.; Juárez, R.; Marino, T.; Molinari, R.; García, H. Influence of Excitation Wavelength (UV or visible light) on the Photocatalytic Activity of Titania Containing Gold Nanoparticles for the Generation of Hydrogen or Oxygen from Water. *J. Am. Chem. Soc.* **2011**, *133*, 595–602.
- (150) Fürst, M. J. L. J.; Gran-Scheuch, A.; Aalbers, F. S.; Fraaije, M. W. Baeyer–Villiger Monooxygenases: Tunable Oxidative Biocatalysts. *ACS Catal.* **2019**, *9*, 11207–11241.
- (151) Bocola, M.; Schulz, F.; Leca, F.; Vogel, A.; Fraaije, M. W.; Reetz, M. W. Converting Phenylacetone Monooxygenase into

- Phenylcyclohexanone Monooxygenase by Rational Design: Towards Practical Baeyer–Villiger Monooxygenases. *Adv. Synth. Catal.* **2005**, *347*, 979–986.
- (152) Schulz, F.; Leca, F.; Hollmann, F.; Reetz, T. M. Towards Practical Biocatalytic Baeyer–Villiger Reactions: Applying a Thermostable Enzyme in the Gram-scale Synthesis of Optically-active Lactones in a Two-liquid-phase System *Beilstein. J. Org. Chem.* **2005**, *1*, 10.
- (153) Schroeder, L.; Frese, M.; Müller, C.; Sewald, N.; Kottke, T. Photochemically Driven Biocatalysis of Halogenases for the Green Production of Chlorinated Compounds. *ChemCatChem.* **2018**, *10*, 3336–3341.
- (154) Carceller, J. M.; Mifsud, M.; Climent, M. J.; Iborra, S.; Corma, A. Production of Chiral Alcohols from Racemic Mixtures by Integrated Heterogeneous Chemoenzymatic Catalysis in Fixed Bed Continuous Operation. *Green Chem.* **2020**, *22*, 2767–2777.
- (155) Tschaen, D. M.; Abramson, L.; Cai, D.; Desmond, R.; Dolling, U. H.; Frey, L.; Karady, S.; Shi, Y. J.; Verhoeven, T. R. Asymmetric Synthesis of MK-0499. *J. Org. Chem.* **1995**, *60*, 4324–4330.
- (156) Cao, J.; Hyster, T. K. Pyridoxal-Catalyzed Racemization of α -Aminoketones Enables the Stereodivergent Synthesis of 1,2-Amino Alcohols Using Ketoreductases. *ACS Catal.* **2020**, *10*, 6171–6175.
- (157) Pietzke, M.; Burgos-Barragan, G.; Wit, N.; Tait-Mulder, J.; Sumpton, D.; Mackay, G. M.; Patel, K. J.; Vazquez, A. Amino acid dependent formaldehyde metabolism in mammals. *Commun. Chem.* **2020**, *3*, 78.
- (158) Wu, H.; Tian, C. Y.; Song, X. K.; Liu, C.; Yang, D.; Jiang, Z. Y. Methods for the Regeneration of Nicotinamide Coenzymes. *Green Chem.* **2013**, *15*, 1773–1789.
- (159) Chenault, H. K.; Simon, E. S.; Whitesides, G. M. Cofactor Regeneration for Enzyme-Catalysed Synthesis. *Biotechnol. Genet. Eng. Rev.* **1988**, *6*, 221–234.
- (160) Choudhury, S.; Baeg, J.; Park, N.; Yadav, R. K. A Solar Light-driven, Eco-friendly Protocol for Highly Enantioselective Synthesis of Chiral Alcohols via Photocatalytic/Biocatalytic Cascades. *Green Chem.* **2014**, *16*, 4389–4400.
- (161) Lo, H. C.; Fish, R. H. Biomimetic NAD⁺ Models for Tandem Cofactor Regeneration, Horse Liver Alcohol Dehydrogenase Recognition of 1,4-NADH Derivatives, and Chiral Synthesis. *Angew. Chem., Int. Ed.* **2002**, *41*, 478–481.
- (162) Yadav, R. K.; Baeg, J.-O.; Kumar, A.; Kong, K.-j.; Oh, G. H.; Park, N.-J. Graphene–BODIPY as a Photocatalyst in the Photocatalytic–Biocatalytic Coupled System for Solar Fuel Production from CO₂. *J. Mater. Chem. A* **2014**, *2*, 5068–5076.
- (163) Singh, C.; Chaubey, S.; Singh, P.; Sharma, K.; Shambhavi; Kumar, A.; Yadav, R. K.; Dwivedi, D. K.; Baeg, J.; Kumar, U.; Yadav, B. C.; Pandey, G. Self-assembled carbon nitride/cobalt (III) porphyrin photocatalyst for mimicking natural photosynthesis. *Diamond Relat. Mater.* **2020**, *101*, 107648.
- (164) Horváth, O.; Valicsek, Z.; Fodor, M. A.; Major, M. M.; Imran, M.; Grampp, G.; Wankmüller, A. Visible Light-driven Photophysics and Photochemistry of Water-soluble Metalloporphyrins. *Coord. Chem. Rev.* **2016**, *325*, 59–66.
- (165) Ahmadi, E.; Ramazani, A.; Hamdi, Z.; Mashhadi-Malekzadeh, A.; Mohamadnia, Z. 5,10,15,20-tetrakis(4-carboxyphenyl)porphyrin Covalently Bound to Nano-silica Surface: Preparation, Characterization and Chemosensor Application to Detect TNT. *Silicon.* **2015**, *7*, 323–332.
- (166) Moghadam, M.; Tangestaninejad, S.; Mirkhani, V.; Mohammadpour-Baltork, I.; Shaibani, R. Rapid and Efficient Acetylation of Alcohols and Phenols with Acetic Anhydride Catalyzed by Electron-deficient Tin(IV) Porphyrin. *J. Mol. Catal. A: Chem.* **2004**, *219*, 73–78.
- (167) Wang, Y.; Sun, J.; Zhang, H.; Zhao, Z.; Liu, W. Tetra(4-carboxyphenyl)porphyrin for Efficient Cofactor Regeneration under Visible Light and its Immobilization. *Catal. Sci. Technol.* **2018**, *8*, 2578–2587.
- (168) Lo, H. C.; Buriez, O.; Kerr, J. B.; Fish, R. H. Regioselective Reduction of NAD⁺ Models with [Cp*Rh(bpy)H]⁺: Structure–Activity Relationships and Mechanistic Aspects in the Formation of the 1,4-NADH Derivatives. *Angew. Chem., Int. Ed.* **1999**, *38*, 1429–1432.
- (169) Nam, D. H.; Lee, S. H.; Park, C. B. CdTe, CdSe, and CdS Nanocrystals for Highly Efficient Regeneration of Nicotinamide Cofactor Under Visible Light. *Small.* **2010**, *6* (8), 922–926.
- (170) Bhoware, S. S.; Kim, K. Y.; Kim, J. A.; Wu, Q.; Kim, J. Photocatalytic Activity of Pt Nanoparticles for Visible Light-Driven Production of NADH. *J. Phys. Chem. C* **2011**, *115* (5), 2553–2557.
- (171) Liu, J.; Antonietti, M. Bio-inspired NADH Regeneration by Carbon Nitride Photocatalysis Using Diatom Templates. *Energy Environ. Sci.* **2013**, *6*, 1486–1493.
- (172) Burai, T. N.; Panay, A. J.; Zhu, H.; Lian, T.; Lutz, S. Light-Driven, Quantum Dot-Mediated Regeneration of FMN To Drive Reduction of Ketosiphonone by Old Yellow Enzyme. *ACS Catal.* **2012**, *2*, 667–670.
- (173) Brown, K. A.; Wilker, M. B.; Boehm, M.; Hamby, H.; Dukovic, G.; King, P. W. Photocatalytic Regeneration of Nicotinamide Cofactors by Quantum Dot–Enzyme Biohybrid Complexes. *ACS Catal.* **2016**, *6*, 2201–2204.
- (174) Kurisu, G.; Kusunoki, M.; Katoh, E.; Yamazaki, T.; Teshima, K.; Onda, Y.; Kimata-Arigo, Y.; Hase, T. Structure of the Electron Transfer Complex between Ferredoxin and Ferredoxin-NADP(+) Reductase. *Nat. Struct. Biol.* **2001**, *8*, 117–121.
- (175) Lamed, R. J.; Zeikus, J. G. Thermostable, Ammonium-activated Malic Enzyme of *Clostridium thermocellum*. *Biochem. J.* **1981**, *195*, 183–190.
- (176) Brown, K. A.; Wilker, M. B.; Boehm, M.; Dukovic, G.; King, P. W. Characterization of Photochemical Processes for H₂ Production by CdS Nanorod–[FeFe] Hydrogenase Complexes. *J. Am. Chem. Soc.* **2012**, *134*, 5627–5636.
- (177) Grzyb, J.; Bojko, M.; Waloszek, A.; Strzałka, K. Cadmium Inhibitory Action Leads to Changes in Structure of Ferredoxin:NADP + Oxidoreductase. *Phytochemistry.* **2011**, *72* (1), 14–20.
- (178) Lee, S. H.; Kwon, Y. C.; Kim, D. M.; Park, C. B. Cytochrome P450-Catalyzed O-Dealkylation Coupled With Photochemical NADPH Regeneration. *Biotechnol. Bioeng.* **2013**, *110*, 383–390.
- (179) Zachos, I.; Gaßmeyer, S. K.; Bauer, D.; Sieber, V.; Hollmann, F.; Kourist, R. Photobiocatalytic Decarboxylation for Olefin Synthesis. *Chem. Commun.* **2015**, *51*, 1918–1921.
- (180) Bojarra, S.; Reichert, D.; Grote, M.; Baraibar, Á. G.; Dennig, A.; Nidetzky, B.; Mügge, C.; Kourist, R. Bio-Based α,ω -Functionalized Hydrocarbons from Multistep Reaction Sequences with Bio- and Metallo-Catalysts Based on the Fatty Acid Decarboxylase OleT_{1E}. *ChemCatChem.* **2018**, *10*, 1192–1201.
- (181) Hobisch, M.; Holtmann, D.; de Santos, P. G.; Alcade, M.; Hollmann, F.; Kara, S. Recent Developments in the Use of Peroxygenases – Exploring their High Potential in Selective Oxyfunctionalisations. *Biotechnol. Adv.* **2021**, *51*, 107615.
- (182) Lutz, S.; Steckhan, E.; Liese, A. First Asymmetric Electroenzymatic Oxidation Catalyzed by a Peroxidase. *Electrochem. Commun.* **2004**, *6*, 583–587.
- (183) Ni, Y.; Fernández-Fueyo, E.; Baraibar, A. G.; Ullrich, R.; Hofrichter, M.; Yanase, H.; Alcalde, M.; van Berkel, W. J. H.; Hollmann, F. Peroxygenase-Catalyzed Oxyfunctionalization Reactions Promoted by the Complete Oxidation of Methanol. *Angew. Chem., Int. Ed.* **2016**, *55*, 798–801.
- (184) Priebe, J. B.; Radnik, J.; Lennox, A. J. J.; Pohl, M.-M.; Karnahl, M.; Hollmann, D.; Grabow, K.; Bentrup, U.; Junge, H.; Beller, M.; et al. Solar Hydrogen Production by Plasmonic Au–TiO₂ Catalysts: Impact of Synthesis Protocol and TiO₂ Phase on Charge Transfer Efficiency and H₂ Evolution Rates. *ACS Catal.* **2015**, *5*, 2137–2148.
- (185) Kofuji, Y.; Ohkita, S.; Shiraishi, Y.; Sakamoto, H.; Tanaka, S.; Ichikawa, S.; Hirai, T. Graphitic Carbon Nitride Doped with Biphenyl Diimide: Efficient Photocatalyst for Hydrogen Peroxide Production from Water and Molecular Oxygen by Sunlight. *ACS Catal.* **2016**, *6*, 7021–7029.
- (186) Hiraikawa, H.; Shiota, S.; Shiraishi, Y.; Sakamoto, H.; Ichikawa, S.; Hirai, T. Au Nanoparticles Supported on BiVO₄: Effective

Inorganic Photocatalysts for H₂O₂ Production from Water and O₂ under Visible Light. *ACS Catal.* **2016**, *6*, 4976–4982.

(187) Zhang, W.; Fernández-Fueyo, E.; Ni, Y.; van Schie, M.; Gacs, J.; Renirie, R.; Wever, R.; Mutti, F. G.; Rother, D.; Alcalde, M.; Hollmann, F. Selective Aerobic Oxidation Reactions Using a Combination of Photocatalytic Water Oxidation and Enzymatic Oxyfunctionalizations. *Nat. Catal.* **2018**, *1*, 55–62.

(188) Popov, V. O.; Lamzin, V. S. NAD⁺ Dependent Formate Dehydrogenase. *Biochem. J.* **1994**, *301*, 625–643.

(189) Rauch, M.; Schmidt, S.; Arends, I. W. C. E.; Oppelt, K.; Kara, S.; Hollmann, F. Photobiocatalytic Alcohol Oxidation using LED Light Sources. *Green Chem.* **2017**, *19*, 376–379.

(190) Gargiulo, S.; Arends, I. W. C. E.; Hollmann, F. A Photoenzymatic System for Alcohol Oxidation. *ChemCatChem.* **2011**, *3*, 338–342.

(191) Kochius, S.; Ni, Y.; Kara, S.; Gargiulo, S.; Schrader, J.; Holtmann, D.; Hollmann, F. Light-Accelerated Biocatalytic Oxidation Reactions. *ChemPlusChem.* **2014**, *79*, 1554–1557.

(192) Gastaldi, S.; Escoubet, S.; Vanthuyne, N.; Gil, G.; Bertrand, M. P. Dynamic Kinetic Resolution of Amines Involving Biocatalysis and in Situ Free Radical Mediated Racemization. *Org. Lett.* **2007**, *9*, 837–839.

(193) Poulhes, F.; Vanthuyne, N.; Bertrand, M. P.; Gastaldi, S.; Gil, G. Chemoenzymatic Dynamic Kinetic Resolution of Primary Amines Catalyzed by CAL-B at 38–40 °C. *J. Org. Chem.* **2011**, *76*, 7281–7286.

(194) El Bliidi, L.; Vanthuyne, N.; Siri, D.; Gastaldi, S.; Bertrand, M. P.; Gil, G. Switching from (R)- to (S)-selective Chemoenzymatic DKR of Amines involving Sulfanyl Radical-mediated Racemization. *Org. Biomol. Chem.* **2010**, *8*, 4165–4168.

(195) El Bliidi, L.; Nechab, M.; Vanthuyne, N.; Gastaldi, S.; Bertrand, M. P.; Gil, G. En Route to (S)- Selective Chemoenzymatic Dynamic Kinetic Resolution of Aliphatic Amines. One-Pot KR/Racemization/KR Sequence Leading to (S)- Amides. *J. Org. Chem.* **2009**, *74*, 2901.

(196) Yang, Q.; Zhao, F.; Zhang, N.; Liu, M.; Hu, H.; Zhang, J.; Zhou, S. Mild Dynamic Kinetic Resolution of Amines by Coupled Visible-light Photoredox and Enzyme Catalysis. *Chem. Commun.* **2018**, *54*, 14065–14068.

(197) Guo, X.; Okamoto, Y.; Schreier, M. R.; Ward, T. R.; Wenger, O. S. Enantioselective Synthesis of Amines by Combining Photoredox and Enzymatic Catalysis in a Cyclic Reaction Network. *Chem. Sci.* **2018**, *9*, 5052–5056.

(198) Metternich, J. B.; Gilmour, R. A Bio-Inspired, Catalytic E→ Z Isomerization of Activated Olefins. *J. Am. Chem. Soc.* **2015**, *137*, 11254–11257.

(199) Litman, Z. C.; Wang, Y.; Zhao, H.; Hartwig, J. F. Cooperative Asymmetric Reactions Combining Photocatalysis and Enzymatic Catalysis. *Nature.* **2018**, *560*, 355–359.

(200) DeHovitz, J. S.; Loh, Y. Y.; Kautzky, J. A.; Nagao, K.; Meichan, A. J.; Yamauchi, M.; MacMillan, D. W. C.; Hyster, T. K. Static to Inducibly Dynamic Stereocontrol: The Convergent Use of Racemic β-Substituted Ketones. *Science.* **2020**, *369*, 1113–1118.

(201) Pirnot, M. T.; Rankic, D. A.; Martin, D. B. C.; MacMillan, D. W. C. Photoredox Activation for the Direct β-Arylation of Ketones and Aldehydes. *Science* **2013**, *339*, 1593–1596.

(202) Lauder, K.; Toscani, A.; Qi, Y.; Lim, J.; Charnock, S. J.; Korah, K.; Castagnolo, D. Photo-biocatalytic One-pot Cascades for the Enantioselective Synthesis of 1,3-Mercaptoalkanol Volatile Sulfur Compounds. *Angew. Chem., Int. Ed.* **2018**, *57*, 5803–5807.

(203) Ding, X.; Dong, C.-L.; Guan, Z.; He, Y.-H. Concurrent Asymmetric Reactions Combining Photocatalysis and Enzyme Catalysis: Direct Enantioselective Synthesis of 2,2-disubstituted indol-3-ones from 2-arylindoles. *Angew. Chem. Int. Ed.* **2019**, *58*, 118–124.

(204) Li, K.; He, T.; Li, C.; Feng, X.-W.; Yu, X.-Q. Lipase-Catalyzed Direct Mannich Reaction in Water: Utilization of Catalytic Promiscuity for C–C bond Formation in a “One-pot” Synthesis. *Green Chem.* **2009**, *11*, 777–779.

(205) Bierbaumer, S.; Schermund, L.; List, A.; Winkler, C. K.; Glueck, S. M.; Kroutil, W. Synthesis of Enantiopure Sulfoxides by Concurrent Photocatalytic Oxidation and Biocatalytic Reduction. *Angew. Chem., Int. Ed.* **2022**, *61*, e202117103.

(206) Lim, J. C.; You, Z.; Kim, G.; Levine, R. L. Methionine Sulfoxide Reductase A is a Stereospecific Methionine Oxidase. *Proc. Natl. Acad. Sci. U.S.A.* **2011**, *108*, 10472–10477.

(207) Hu, J.-Y.; Xie, Z.-B.; Tang, J.; Le, Z.-G.; Zhu, Z.-Q. Combining Enzyme and Photoredox Catalysis for the Construction of 3-aminoalkyl Chromones. *J. Org. Chem.* **2022**, *87*, 14965–14969.

(208) Yu, Y.; Lin, R.-D.; Yao, Y.; Shi, M.-L.; Lu, W.-F.; Wang, N.; Yu, X.-Q. Development of a Metal and Oxidant-Free Enzyme–Photocatalyst Hybrid System for Highly Efficient C-3 Acylation Reaction of Indoles. *ACS Catal.* **2022**, *12*, 12543–12554.

(209) Zhang, W.; Fueyo, E. F.; Hollmann, F.; Martin, L. L.; Pesic, M.; Wardenga, R.; Höhne, M.; Schmidt, S. Combining Photo-Organic Redox- and Enzyme Catalysis Facilitates Asymmetric C-H Bond Functionalization. *Eur. J. Org. Chem.* **2019**, *2019*, 80–84.

(210) Gacs, J.; Zhang, W.; Knaus, T.; Mutti, F. G.; Arends, I. W. C. E.; Hollmann, F. A Photo-Enzymatic Cascade to Transform Racemic Alcohols to Enantiomerically Pure Amines. *Catalysts.* **2019**, *9* (4), 305.

(211) Peng, Y.; Li, D.; Fan, J.; Xu, W.; Xu, J.; Yu, H.; Lin, X.; Wu, Q. Enantiocomplementary C-H Bond Hydroxylation Combining Photocatalysis and Whole-Cell Biocatalysis in a One-Pot Cascade Process. *Eur. J. Org. Chem.* **2020**, *2020*, 821–825.

(212) Betori, R. C.; May, C. M.; Scheidt, K. A. Combined Photoredox/Enzymatic C-H Benzylic Hydroxylations. *Angew. Chem., Int. Ed.* **2019**, *58*, 16490–16494.

(213) Hollmann, F.; Arends, I. W. C. E.; Buehler, K.; Schallmeyer, A.; Bühler, B. Enzyme-Mediated Oxidations for the Chemist. *Green Chem.* **2011**, *13*, 226–265.

(214) Ni, Y.; Holtmann, D.; Hollmann, F. How Green is Biocatalysis? To Calculate is to Know. *ChemCatChem* **2014**, *6*, 930–943.

(215) Abed, R. M. M.; Dobretsov, S.; Sudesh, K. Applications of Cyanobacteria in Biotechnology. *J. Appl. Microbiol.* **2009**, *106*, 1–12.

(216) Nakamura, K.; Yamanaka, R.; Tohi, K.; Hamada, H. Cyanobacterium-catalyzed Asymmetric Reduction of Ketones. *Tetrahedron Lett.* **2000**, *41*, 6799–6802.

(217) Nakamura, K.; Yamanaka, R. Light Mediated Cofactor Recycling System in Biocatalytic Asymmetric Reduction of Ketones. *Chem. Commun.* **2002**, *2*, 1782–1783.

(218) Nakamura, K.; Yamanaka, R. Light-mediated Regulation of Asymmetric Reduction of Ketones by a Cyanobacterium. *Tetrahedron: Asymmetry* **2002**, *13*, 2529–2533.

(219) Yamanaka, R.; Nakamura, K.; Murakami, M.; Murakami, A. Selective Synthesis of Cinnamyl Alcohol by Cyanobacterial Photobiocatalysts. *Tetrahedron Lett.* **2015**, *56*, 1089–1091.

(220) Górak, M.; Żyłańczyk-Duda, E. Application of Cyanobacteria for Chiral Phosphonate Synthesis. *Green Chem.* **2015**, *17*, 4570–4578.

(221) Yazdi, M. T.; Arabi, H.; Faramarzi, M. A.; Ghasemi, Y.; Amini, M.; Shokravi, S.; Mohseni, F. A. Biotransformation of Hydrocortisone by a Natural Isolate of *Nostoc Muscorum*. *Phytochemistry.* **2004**, *65*, 2205–2209.

(222) Ma, X.; Liang, H.; Ning, C.; Deng, S.; Su, E. Integrating a Light-Driven Coenzyme Regeneration System by Expression of an Alcohol Dehydrogenase in Phototrophic Bacteria for Synthesis of Chiral Alcohol. *J. Biotechnol.* **2017**, *259*, 120–125.

(223) Jurkaš, V.; Winkler, C. K.; Poschenrieder, S.; Oliveira, P.; Pacheco, C. C.; Ferreira, E. A.; Weissensteiner, F.; De Santis, P.; Kara, S.; Kourist, R.; et al. Expression and Activity of Heterologous Hydroxyisocaproate Dehydrogenase in *Synechocystis* sp. PCC 6803 Δ*hoxYH*. *Eng. Microbio.* **2022**, *2*, 100008.

(224) Köninger, K.; Gómez-Baraibar, A.; Mügge, C.; Paul, C. E.; Hollmann, F.; Nowaczyk, M. M.; Kourist, R. Recombinant Cyanobacteria for the Asymmetric Reduction of C = C Bonds Fueled by the Biocatalytic Oxidation of Water. *Angew. Chem., Int. Ed.* **2016**, *55*, 5582–5585.

(225) Bartsch, M.; Gassmeyer, S. K.; Köninger, K.; Igarashi, K.; Liauw, P.; Dyczmons-Nowaczyk, N.; Miyamoto, K.; Nowaczyk, M.; Kourist, R. Photosynthetic Production of Enantioselective Biocatalysts. *Microb. Cell Fact.* **2015**, *14*, 53.

(226) Böhmer, S.; Köninger, K.; Gómez-Baraibar, Á.; Bojarra, S.; Mügge, C.; Schmidt, S.; Nowaczyk, M. M.; Kourist, R. Enzymatic Oxyfunctionalization Driven by Photosynthetic Water-Splitting in the Cyanobacterium *Synechocystis* sp. PCC6803. *Catalysts*. **2017**, *7*, 240.

(227) Nakamura, K.; Yamanaka, R. Light Mediated Cofactor Recycling System in Biocatalytic Asymmetric Reduction of Ketone. *Chem. Commun.* **2002**, 1782–1783.

(228) Nakamura, K.; Yamanaka, R. Light-Mediated Regulation of Asymmetric Reduction of Ketones by a Cyanobacterium. *Tetrahedron Asymmetry*. **2002**, *13*, 2529–2533.

(229) Hoschek, A.; Bühler, B.; Schmid, A. Overcoming the Gas-Liquid Mass Transfer of Oxygen by Coupling Photosynthetic Water Oxidation with Biocatalytic Oxyfunctionalization. *Angew. Chem., Int. Ed.* **2017**, *56*, 15146–15149.

(230) Hoschek, A.; Toepel, J.; Hochkeppel, A.; Karande, R.; Bühler, B.; Schmid, A. Light-dependent and Aeration-Independent Gram-scale Hydroxylation of Cyclohexane to Cyclohexanol by CYP450 Harboring *Synechocystis* sp. 6803. *Biotechnol. J.* **2019**, *14*, 1800724.

(231) Büchschütz, H. C.; Vidimce-Risteski, V.; Eggbauer, B.; Schmidt, S.; Winkler, C. K.; Schrittwieser, J. H.; Kroutil, W.; Kourist, R. Stereoselective Biotransformation of Cyclic Imines in Recombinant Cells of *Synechocystis* sp. PCC6803. *ChemCatChem*. **2020**, *12*, 726–730.

(232) Löwe, J.; Siewert, A.; Scholpp, A.-C.; Wobbe, L.; Gröger, H. Providing Reducing Power by Microalgal Photosynthesis: A Novel Perspective Towards Sustainable Biocatalytic Production of Bulk Chemicals Exemplified for Aliphatic Amines. *Sci. Rep.* **2018**, *8*, 10436.

(233) Tishkov, V. I.; Popov, V. O. Catalytic Mechanism and Application of Formate Dehydrogenase. *Biochemistry. Biokhimiia* **2004**, *69*, 1252–1267.

(234) Chen, F. F.; Liu, Y. Y.; Zheng, G. W.; Xu, J. H. Asymmetric Amination of Secondary Alcohols by using a Redox-Neutral Two-Enzyme Cascade. *ChemCatChem*. **2015**, *7*, 3838–3841.

(235) Jurkaš, V.; Weissensteiner, F.; De Santis, P.; Vrabl, S.; Sorgenfrei, F. A.; Bierbaumer, S.; Kara, S.; Kourist, R.; Wangikar, P. P.; Winkler, C. K.; et al. Transmembrane Shuttling of Photosynthetic Produced Electrons to Propel Extracellular Biocatalysis Redox Reactions in a Modular Fashion. *Angew. Chem., Int. Ed.* **2022**, *61*, e202207971.